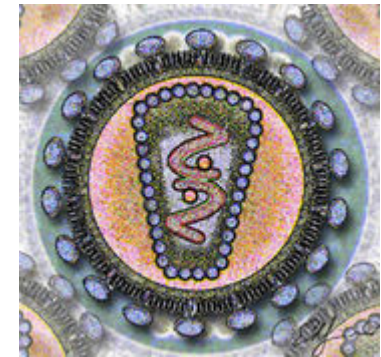
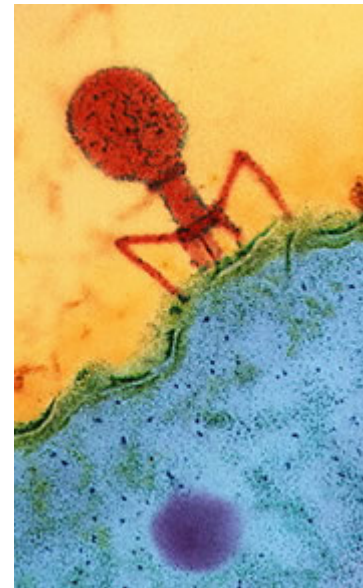
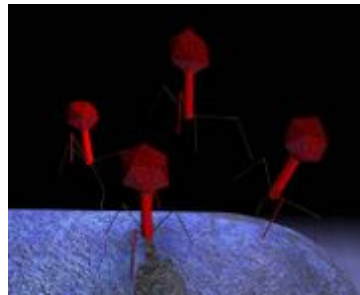
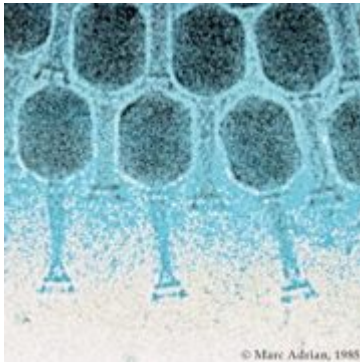
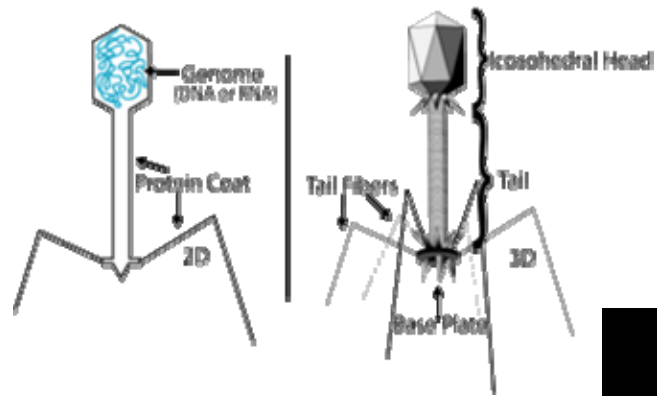
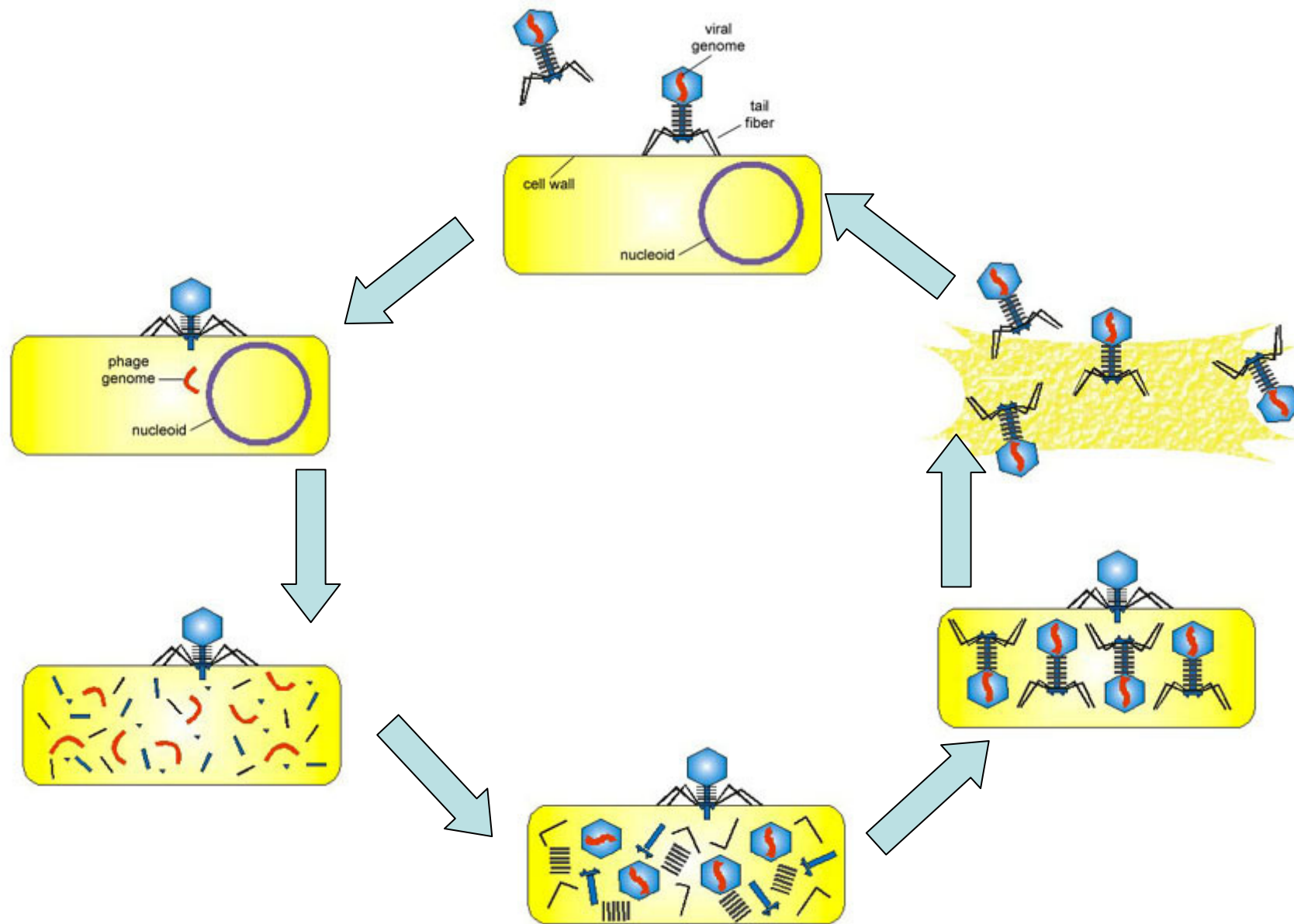


# Non-viral Transfection

# Virus



# Virus Reproduction



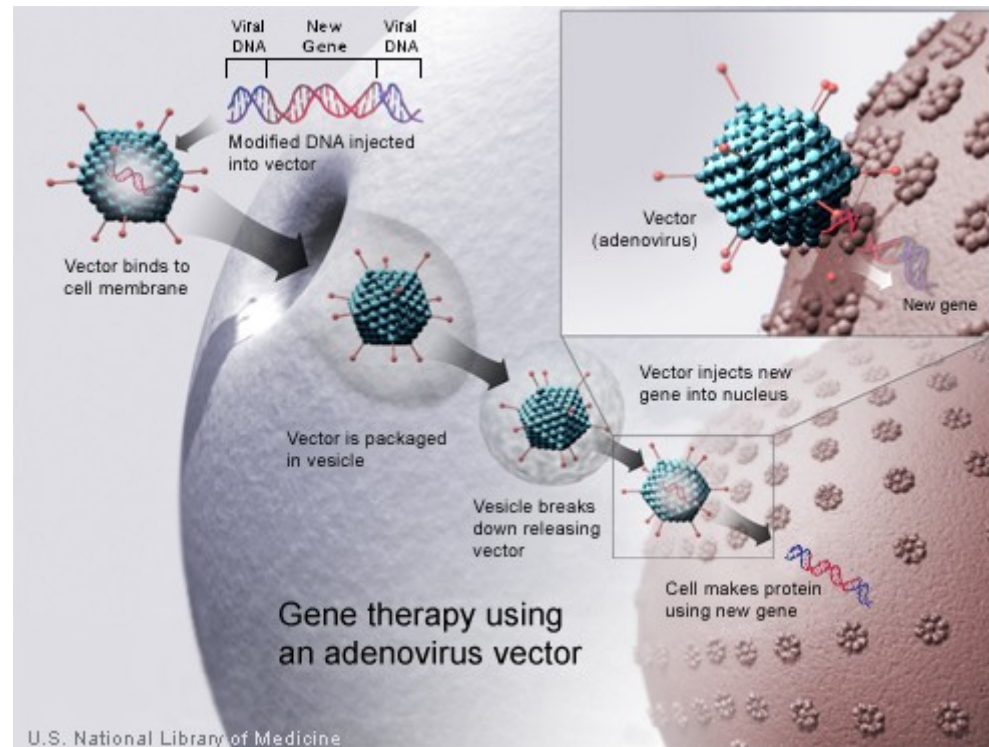
# Gene Therapy

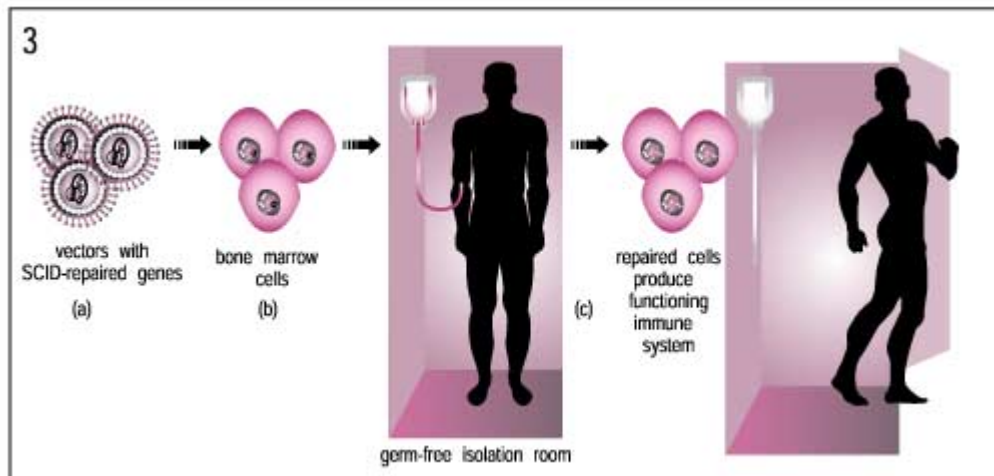
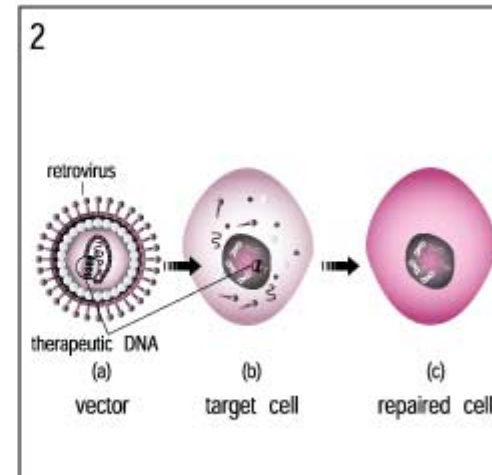
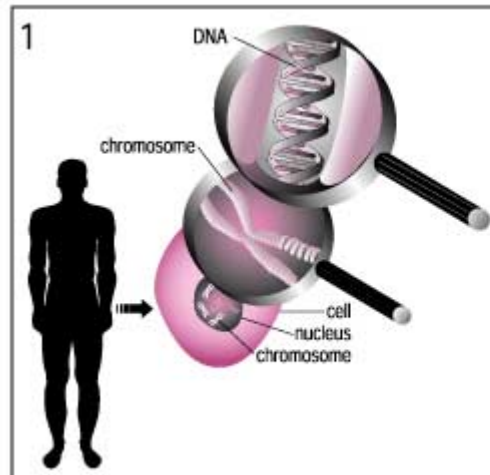
- Gene therapy is a technique for correcting defective genes responsible for disease development. Researchers may use one of several approaches for correcting faulty genes:
  - **A normal gene may be inserted into a nonspecific location within the genome to replace a nonfunctional gene. This approach is most common.**
  - **An abnormal gene could be swapped for a normal gene through homologous recombination.**
  - **The abnormal gene could be repaired through selective reverse mutation, which returns the gene to its normal function.**
  - **The regulation (the degree to which a gene is turned on or off) of a particular gene could be altered.**



# How Gene Therapy Works?

- In most gene therapy studies, a "normal" gene is inserted into the genome to replace an "abnormal," disease-causing gene. A carrier molecule called a vector must be used to deliver the therapeutic gene to the patient's target cells. Currently, the most common vector is a virus that has been genetically altered to carry normal human DNA. Viruses have evolved a way of encapsulating and delivering their genes to human cells in a pathogenic manner. Scientists have tried to take advantage of this capability and manipulate the virus genome to remove disease-causing genes and insert therapeutic genes.
- Target cells such as the patient's liver or lung cells are infected with the viral vector. The vector then unloads its genetic material containing the therapeutic human gene into the target cell. The generation of a functional protein product from the therapeutic gene restores the target cell to a normal state.





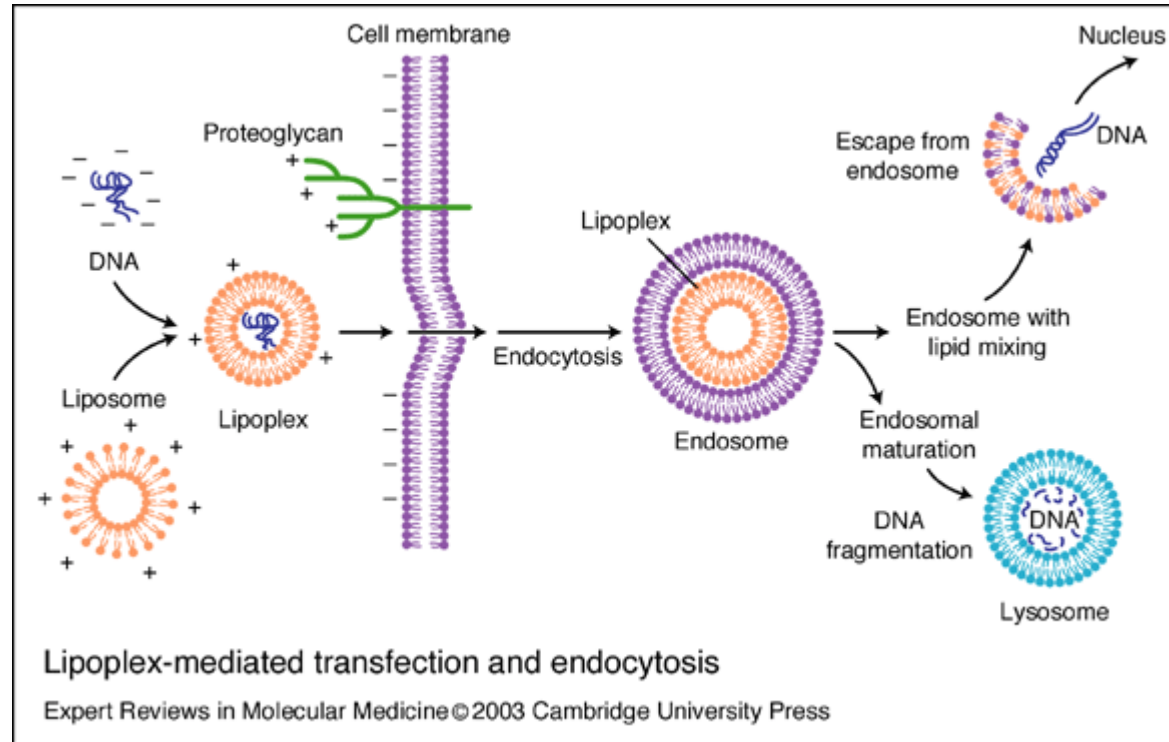
Infographic by Rene Gordon

<http://www.fda.gov/fdac/features/2000/gene.html>

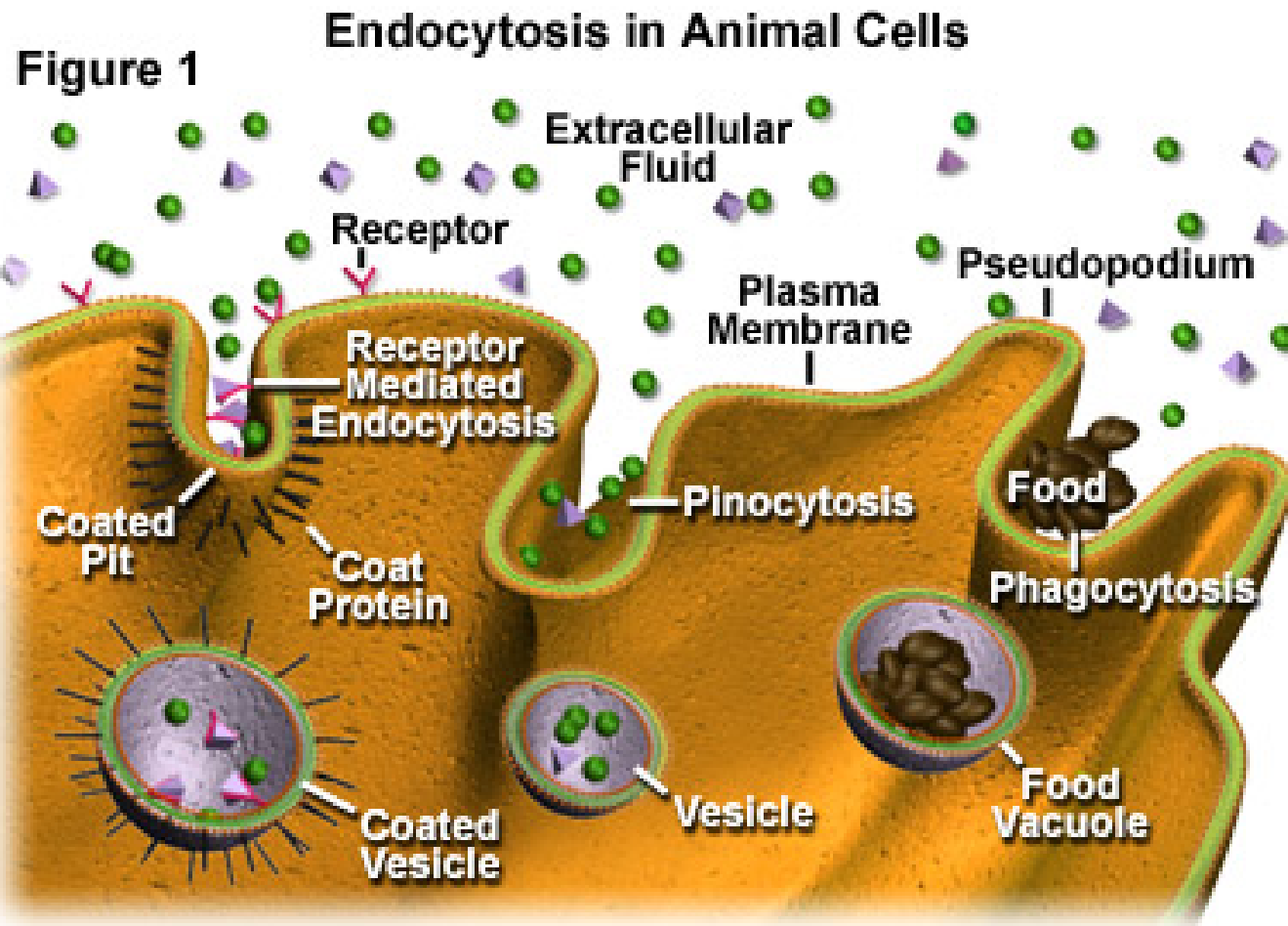
# Gene Delivery

- Transfection- the delivery of foreign molecules such as DNA and RNA into eukaryotic cells
- Naked DNA is not suitable for in-vivo transport of genetic materials-> degradation by serum nucleases
- Ideal gene delivery system
  - Biocompatible
  - Non-immunogenic
  - Stable in blood stream
  - Protect DNA during transport
  - Small enough to extravagate
  - Cell and tissue specific

# Transfection



# Endocytosis



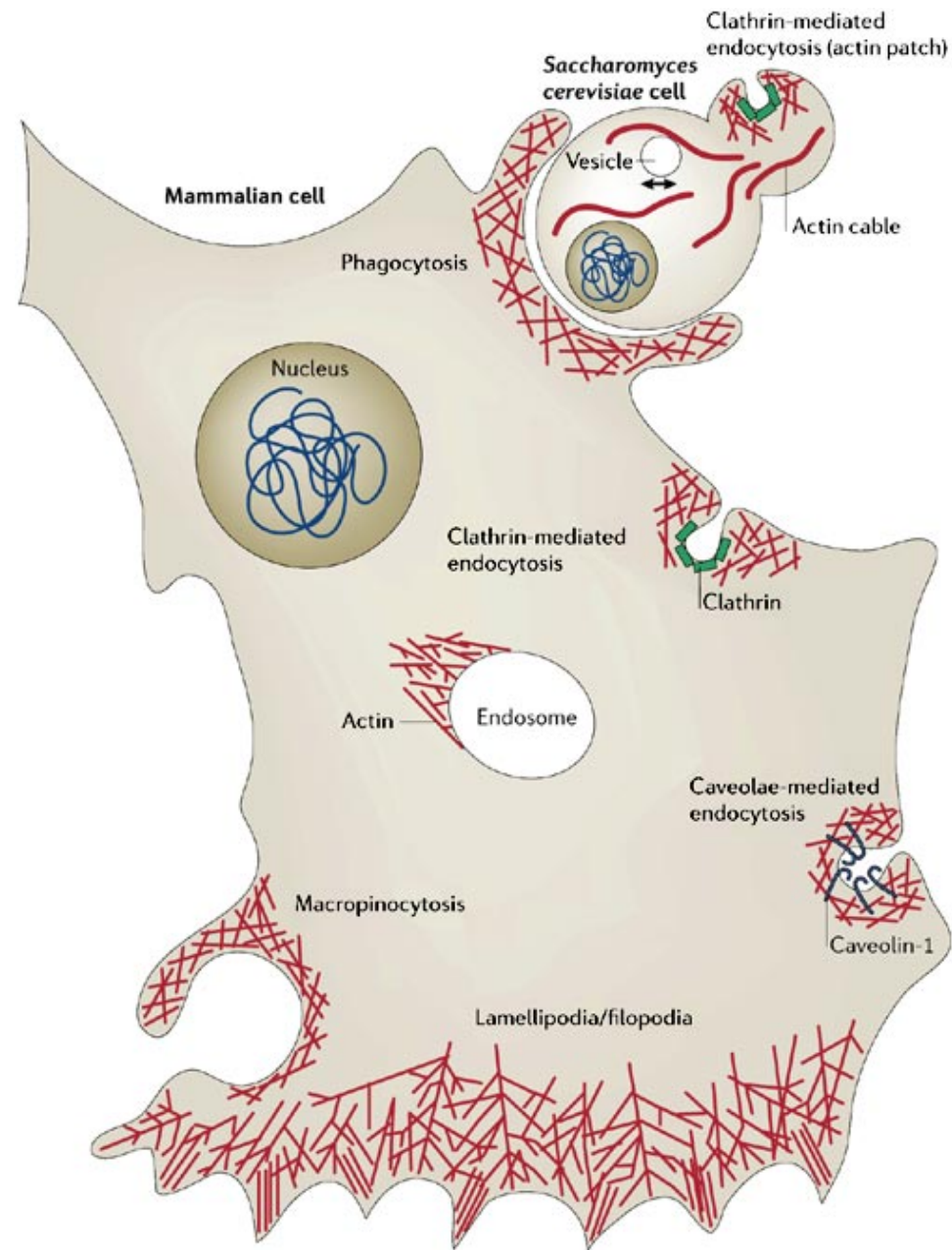
# Endocytosis

- Phagocytosis is the process by which cells ingest large objects, such as cells which have undergone apoptosis, bacteria, or viruses. The membrane folds around the object, and the object is sealed off into a large vacuole known as a phagosome.
- Pinocytosis is a synonym for endocytosis. This process is concerned with the uptake of solutes and single molecules such as proteins.
- Receptor-mediated endocytosis is a more specific active event where the cytoplasm membrane folds inward to form coated pits. These inward budding vesicles bud to form cytoplasmic vesicles.

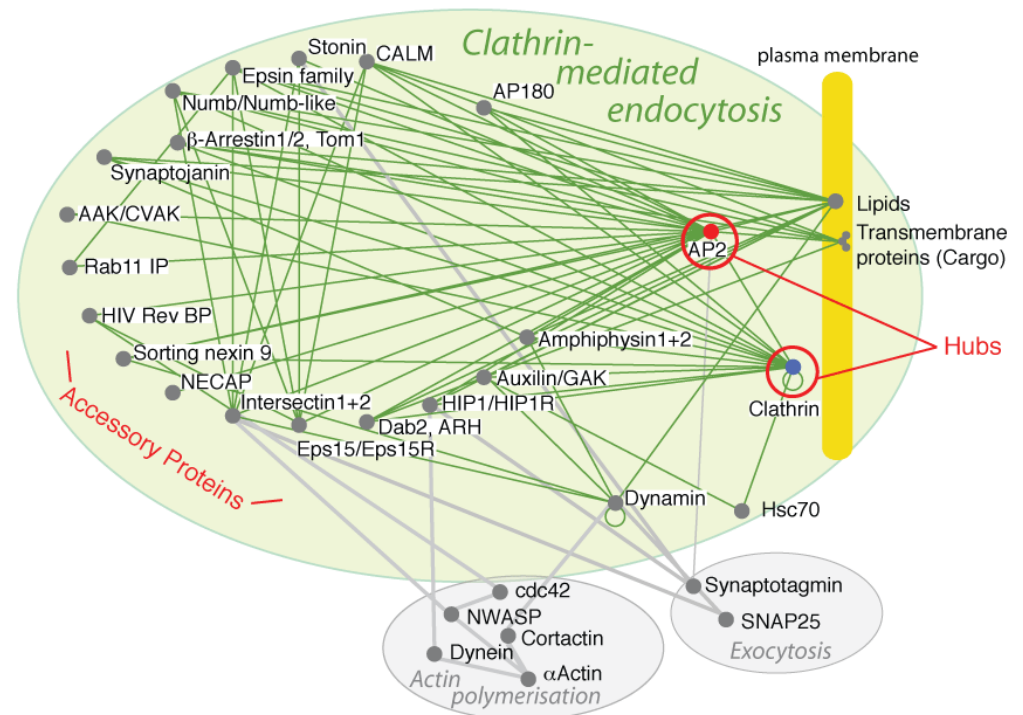
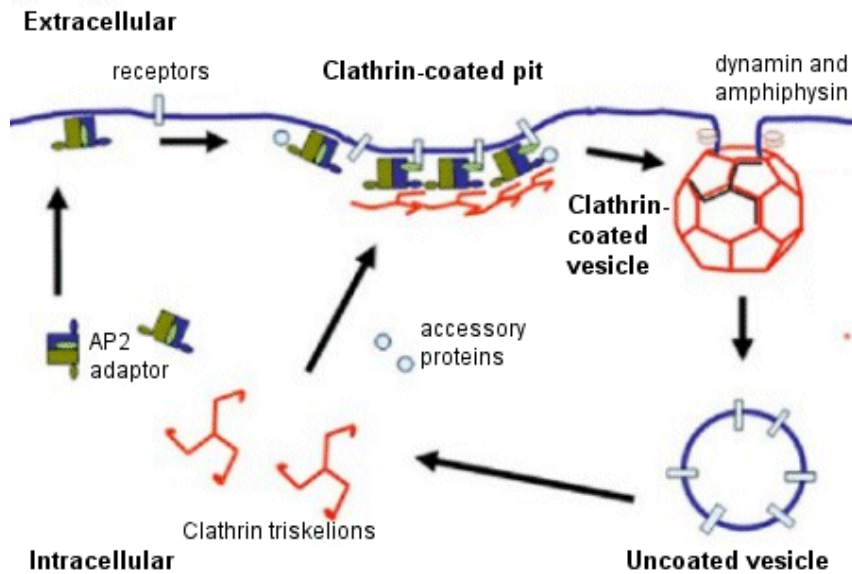
# Endocytosis pathways

- Macropinocytosis is the invagination of the cell membrane to form a pocket which then pinches off into the cell to form a vesicle filled with extracellular fluid (and molecules within it). The filling of the pocket occurs in a non-specific manner. The vesicle then travels into the cytosol and fuses with other vesicles such as endosomes and lysosomes.
- Clathrin-mediated endocytosis is the specific uptake of large extracellular molecules such as proteins, membrane localized receptors and ion-channels. These receptors are associated with the cytosolic protein clathrin which initiates the formation of a vesicle by forming a crystalline coat on the inner surface of the cell's membrane.
- Caveolae consist of the protein caveolin-1 with a bilayer enriched in cholesterol and glycosphingolipids. Caveolae are flask shaped pits in the membrane that resemble the shape of a cave (hence the name caveolae). Uptake of extracellular molecules are also believed to be specifically mediated via receptors in caveolae.

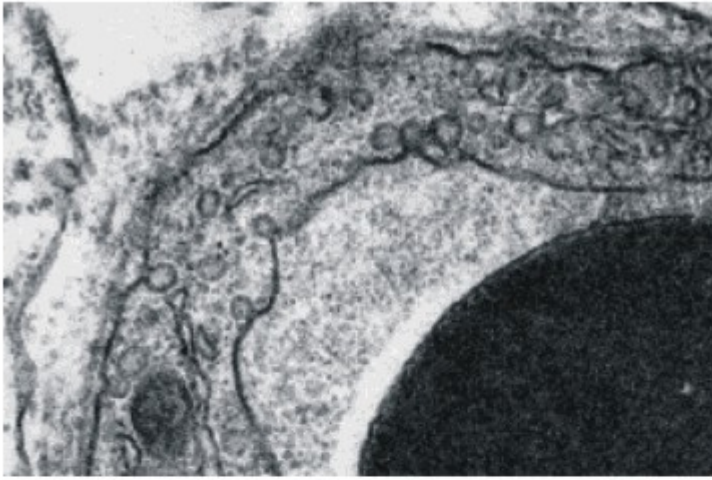




# Clathrin-mediated endocytosis

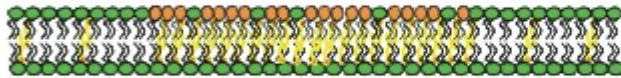


A

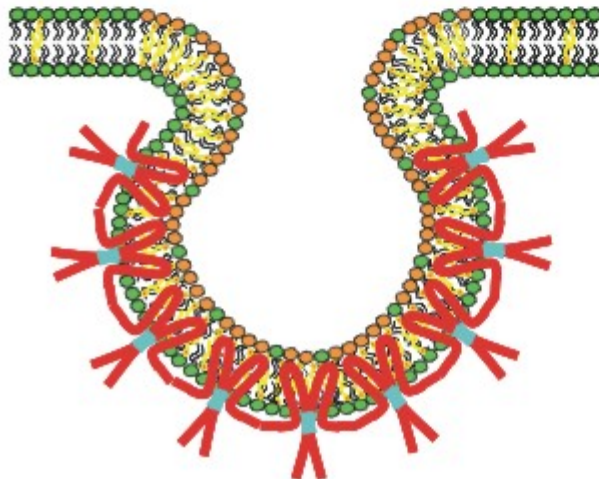


B

Lipid Rafts



Caveolae



Caveolin



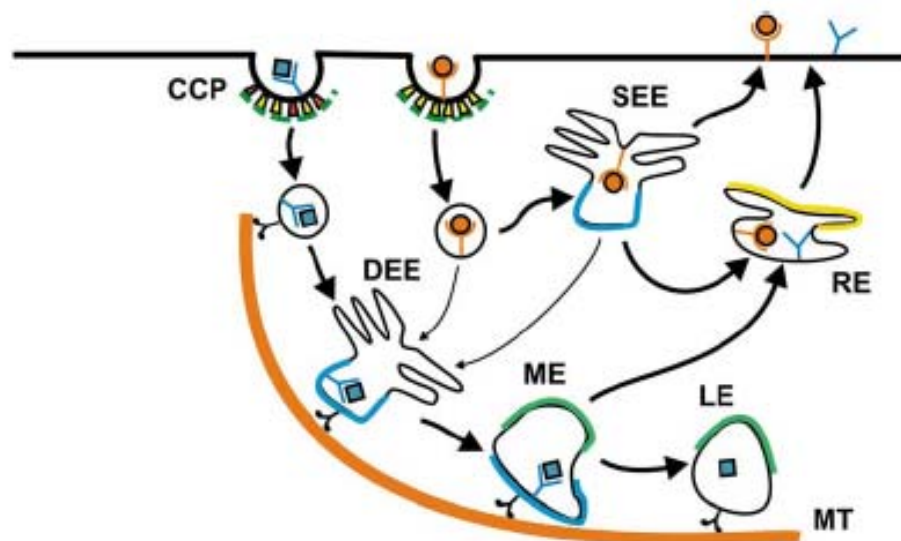
Phospholipid



Sphingolipid



Cholesterol



**CCP** Clathrin-coated pit

**DEE** Dynamic early endosome

**SEE** Static early endosome


**ME** Maturing endosome

**LE** Late endosome

**RE** Recycling endosome

**MT** Microtubule

 Non Ap-2 adaptor

 Ap-2

 Clathrin coat

 LDL receptor

 Tfn receptor

 LDL

 Tfn

 Rab 5

 Rab 7

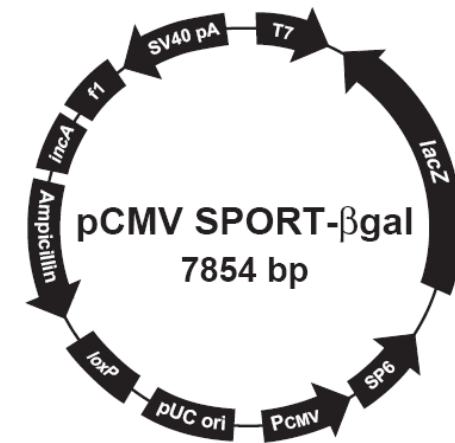
 Rab 11

**Figure 7. A Proposed Model for Pre-Early Endosome Sorting that Differentially Targets Endocytic Cargos into Distinct Populations of Coated Vesicles and Early Endosomes**

Early endosomes are comprised of a dynamic population that matures quickly towards late endosomes and a relatively static population that matures much more slowly. Cargos destined for degradation, including LDL, EGF, and influenza virus, are internalized by a sub-population(s) of clathrin-coated vesicles, which likely contain alternative adaptors in addition to AP-2. These vesicles rapidly engage microtubules and are consequently targeted to the dynamic population of early endosomes, which are also moving on microtubules. The recycling ligand transferrin is indiscriminately recruited to all clathrin-coated vesicles and thus delivered to both populations of early endosomes nonselectively, effectively being enriched in the larger, static population.

# Transient and Stable Transfection

- Transient
  - No chromosome integration
  - Expression 24-96 Hr
  - Super-coiled plasmid
- Stable
  - Chromosome integration
  - Linear DNA
  - 1 in  $10^4$
  - Selection



# Challenges

- Cell targeting
- Transport through the cell membrane
- Uptake and degradation in endolysosome
- Intracellular trafficking of plasmid to nucleus

# Transfection Technology

- DEAE dextran
- Calcium phosphate
- Electroporation
- Microinjection
- Biolistic particle
- Nanoparticles
  - Cationic liposome
  - Cationic polymer
  - Activated dendrimer
  - Gold nanoparticles
  - Chitosan



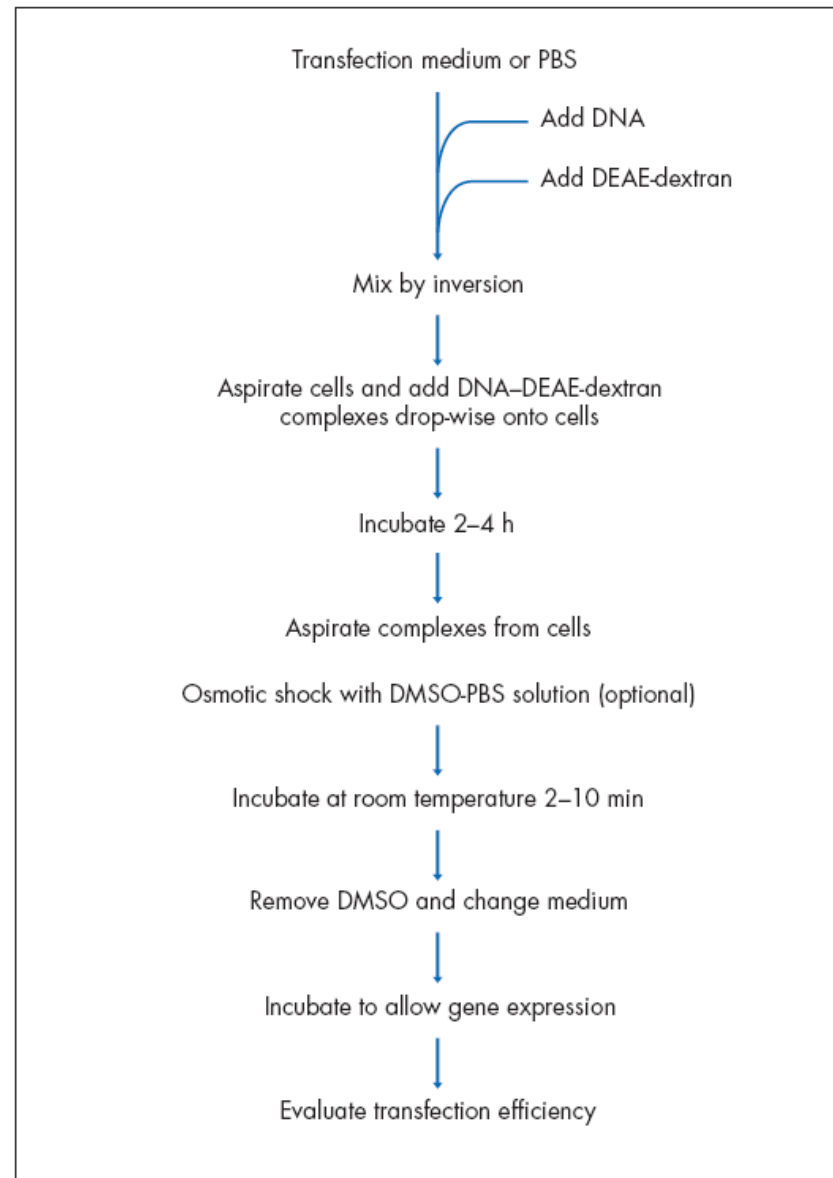
# DEAE-dextran

- Diethylaminoethyl (DEAE)-dextran was introduced in 1965 (5) and is one of the oldest methods for introducing nucleic acids into cultured mammalian cells. The positively charged DEAE-dextran molecule interacts with the negatively charged phosphate backbone of the nucleic acid. The DNA–DEAE-dextran complexes appear to adsorb onto the cell surface and be taken up by endocytosis. The advantages of this technique are its relative simplicity and reproducibility of results. Disadvantages include cytotoxic effects and the fact that the amount of serum in the culture medium must be temporarily reduced during the transfection procedure. In addition, the DEAE-dextran method is best suited for transient transfection only.

**Dextran** is a complex branched polysaccharide made of many glucose molecules joined into chains of varying lengths.



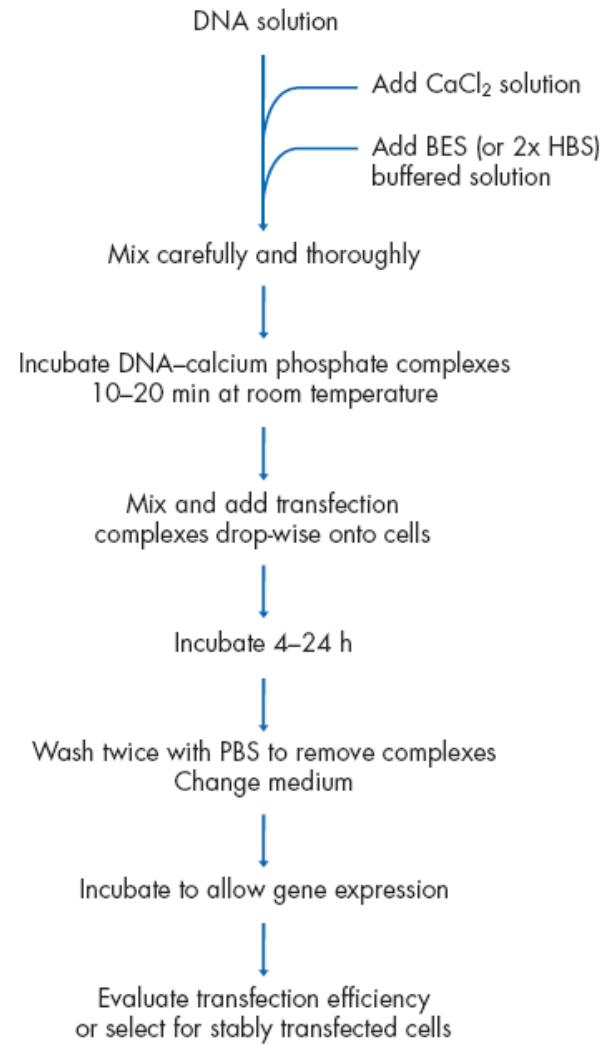
## DEAE-Dextran Method\*



# Calcium Phosphate

- The calcium-phosphate method was first used in 1973 to introduce adenovirus DNA into mammalian cells (6). The principle involves mixing DNA in a phosphate buffer with calcium chloride. The resulting calcium-phosphate–DNA complexes adhere to the cell membrane and enter the cytoplasm by endocytosis. Advantages of calcium-phosphate–based transfection are its easy handling and, compared with the DEAE-dextran method, its much higher suitability for stable transfections. However, a common disadvantage is low reproducibility, which is mainly caused by variation in transfection complex size and shape. These variations can be caused by minor changes in the pH of the solutions used for the transfection, as well as the manner in which these solutions are combined. A further drawback of the calcium-phosphate method is that some cell types, including primary cells, may resist this form of DNA transfer.

## Calcium-Phosphate Method\*



# Electroporation

The use of high-voltage pulses to introduce DNA into cultured cells was first established by Wong and Neumann using fibroblasts . Cells in a suitable cuvette are subjected to a short high-voltage pulse that causes the membrane potential of the cells to break down. As a result, pores are formed through which macromolecules such as DNA can enter. The main advantage of electroporation is its applicability for transient and stable transfection of all cell types. However, a disadvantage is that approximately 5-fold greater quantities of DNA and cells are needed than in either DEAE-dextran or calcium phosphate methods. A major drawback of electroporation is the high cell mortality that can result in the death of up to 50–70% of the cells. In addition, the optimal settings for voltage, capacitance, pulse length, and gap width are cell-type dependent, and it is necessary to repeat the electroporation experiment a number of times to optimize the electroporation efficiency and cell viability.

# Electroporator



Pulse voltage:	20-1.200 V
Pulse form:	Exponentially diminishing, electronically controlled
Time constant:	15-500 $\mu$ s, in increments 5 $\mu$ s
Multiple pulsing:	1-99, with 1 min. time interval

# Polymer Nanocontainers

# Nanocontainers

- Liposomes
- Dendrimers
- Layer by Layer Deposition
- Block Copolymer
- Shell Cross-Link

# Cationic Liposome

Liposomes were first introduced in 1987 by Felgner and coworkers (9). The liposomes currently in use typically contain a mixture of cationic and neutral lipids organized into lipid bilayer structures. Transfection-complex formation is based on the interaction of the positively charged liposome with the negatively charged phosphate groups of the nucleic acid. The uptake of the liposome–DNA complexes may be mediated by endocytosis. Compared to the DEAE-dextran and calciumphosphate methods, liposomes often offer higher transfection efficiency and better reproducibility. However, one drawback of liposome-mediated transfection is that the presence of serum during the transfection procedure often lowers the transfection efficiency. For this reason, serum is often omitted when transfecting with liposomes. In many cases, the absence of serum from the medium increases the cytotoxicity of the liposome. Another drawback of classical liposome-mediated transfection is that results



## - Stability

# Liposomes

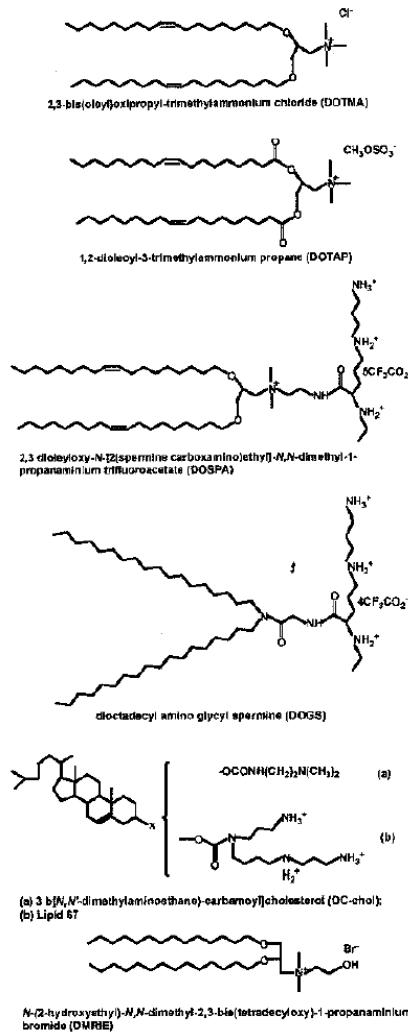


Figure 21.7 Structures of some cationic lipids commonly used in gene therapy.

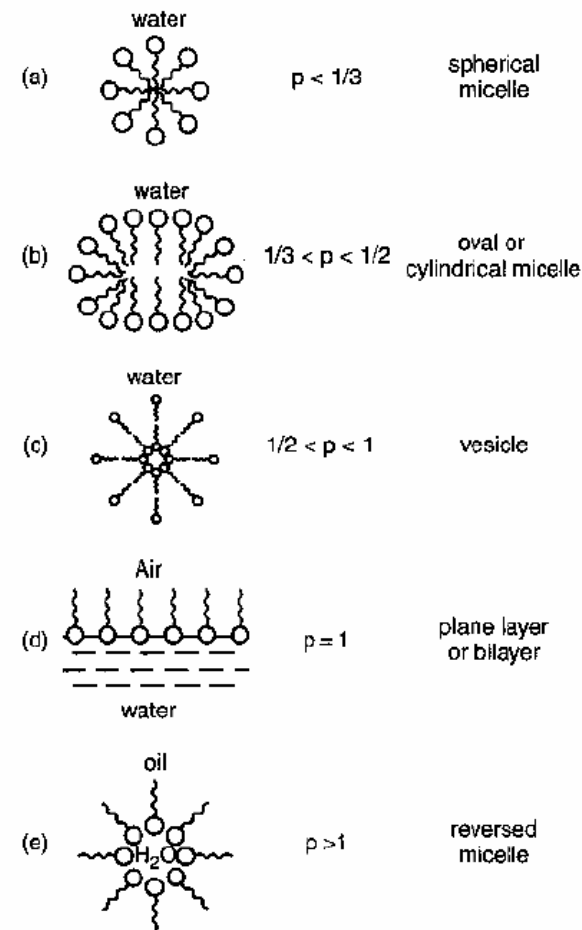
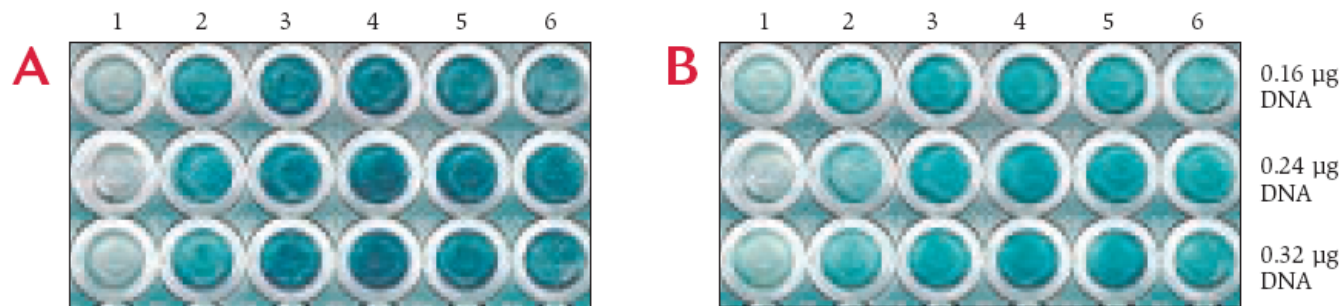
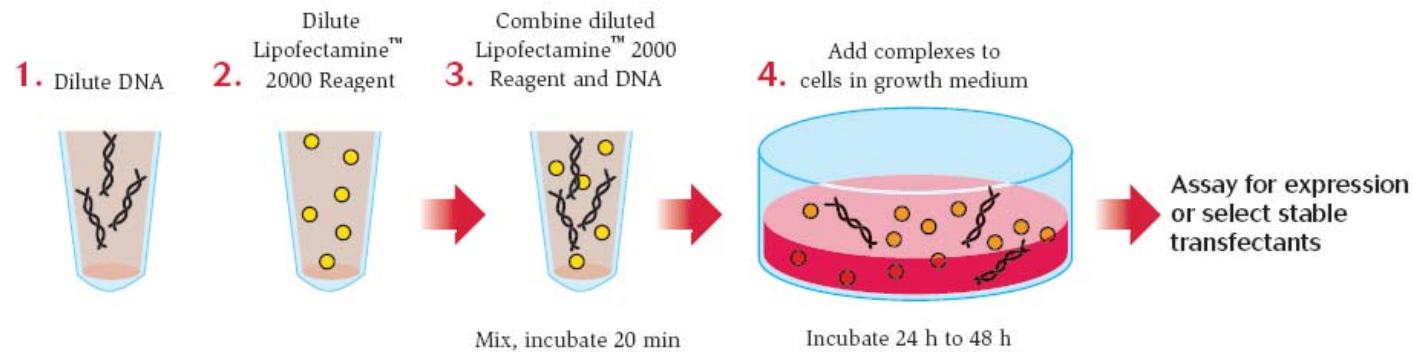


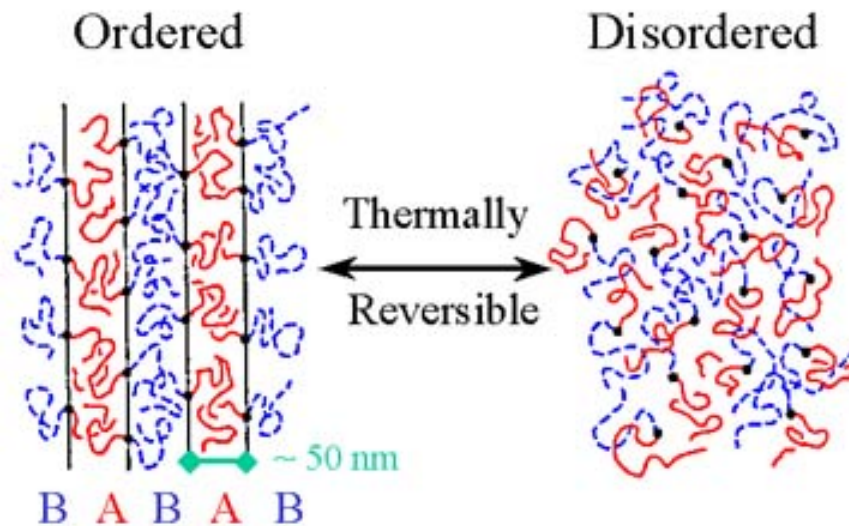
Figure 12.14. Sketch of structures formed by amphiphilic molecules at water-oil or water-air interfaces for various values of the packing parameter  $p$  of Eq. (12.6). [Adapted from E. Nakache et al., in Nalwa (2000), Vol. 5, Chapter 11, p. 580.]



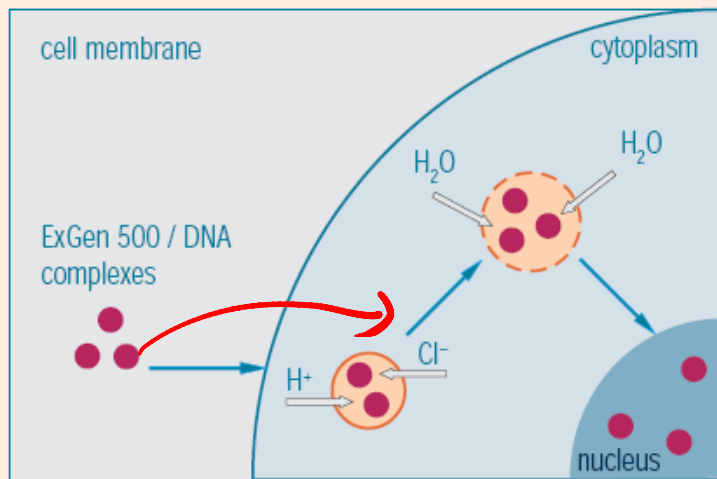
CHO-S cells were transfected with pCMV•SPORT-βgal DNA (0.16 µg to 0.32 µg) and Lipofectamine™ 2000 Reagent (0.2 µl to 1.2 µl, columns 1-6 respectively) in 96-well plates. After 24 hours, cells were stained with X-gal. **Panel A:** Cells ( $2 \times 10^4$ ) were plated the day before transfection in growth medium containing serum. **Panel B:** The day of transfection, cells were trypsinized, counted, and  $5 \times 10^4$  cells were added directly to the wells containing the complexes.

Cell Line	Cell Type	Transfection efficiency (%)
293-F	Human kidney	99
293-H	Human kidney	99
CHO-S	Hamster ovary	96
COS-7L	Monkey kidney	99
BE(2)C	Human neuroblastoma	77
SKBR3	Human breast cancer	49
MDCK	Dog kidney	43
HT1080	Human fibrosarcoma	81
Human fibroblasts	Primary passaged	48
HeLa	Human cervical carcinoma	94
CV-1	Monkey kidney	70
Vero	Monkey kidney	86
PC12	Rat pheochromocytoma	85
Murine ES	Mouse embryonic stem	75
Rat Hepatocytes	Primary liver	50
E18 Cortical Neurons	Rat primary	25
E18 Hippocampal Neurons	Rat primary	30

# Block Copolymers

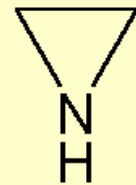


# Polymer

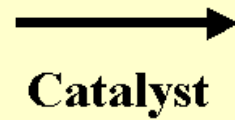


1. ExGen 500 interacts with DNA to form small, stable, highly diffusible complexes which are readily endocytosed.
2. "Proton-sponge" effect of ExGen 500 buffers endosomal pH by provoking massive proton accumulation and passive chloride influx.
3. Rapid osmotic swelling causes endosomal rupture, allowing translocation of DNA to the nucleus without DNA degradation.

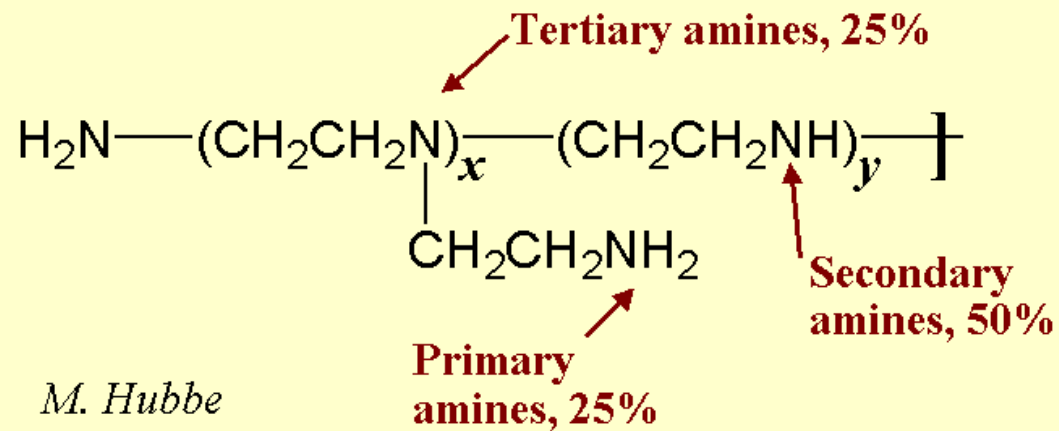
# Synthesis of Poly-ethylenimine



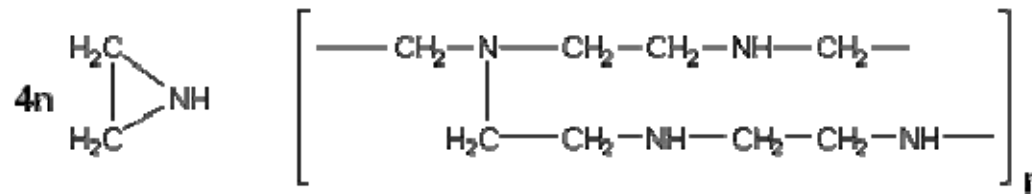
**Ethylene  
imine**



**PEI**



*M. Hubbe*



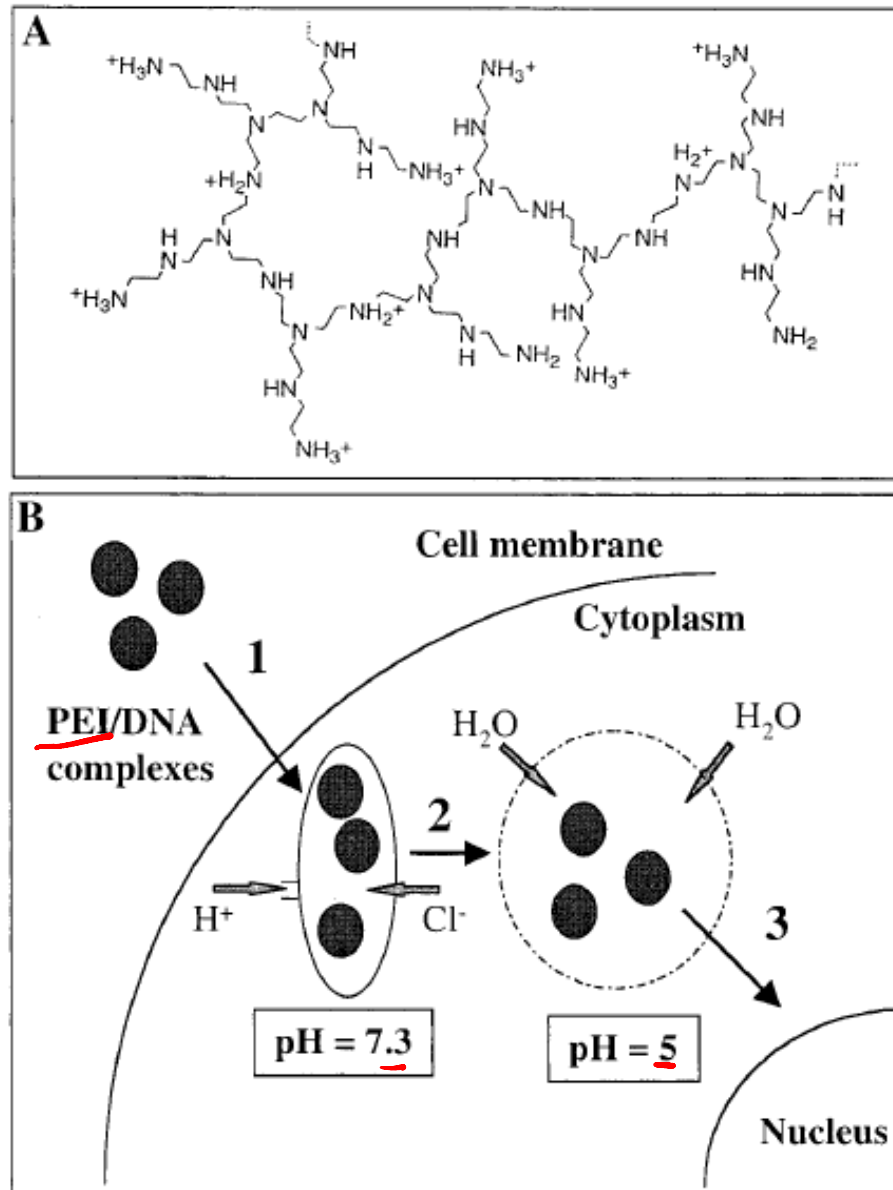
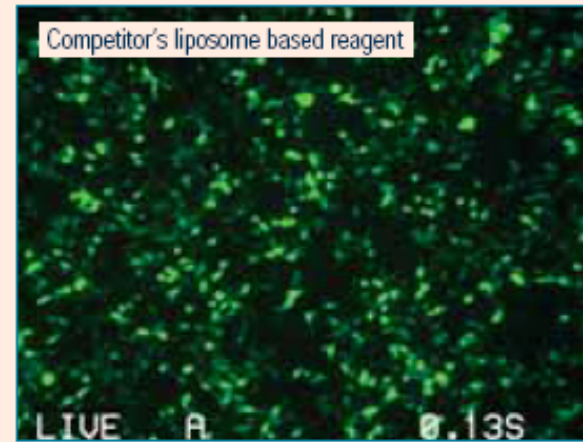
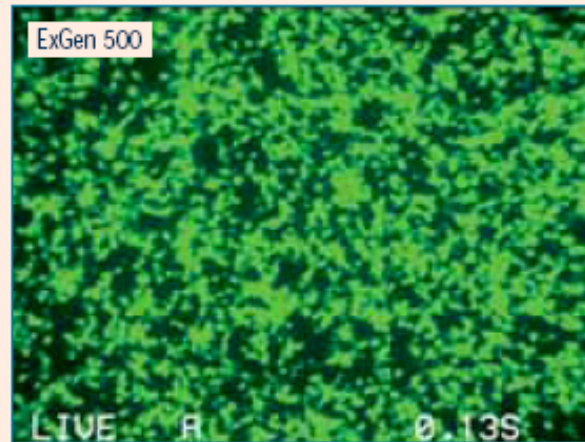


Figure 1. (A) Structure of PEI with a random topology. (B) The 'proton sponge effect': after endocytosis of the cationic complexes (1), acidic endosome buffering (2) leads to increased osmotic pressure and finally to lysis (3)

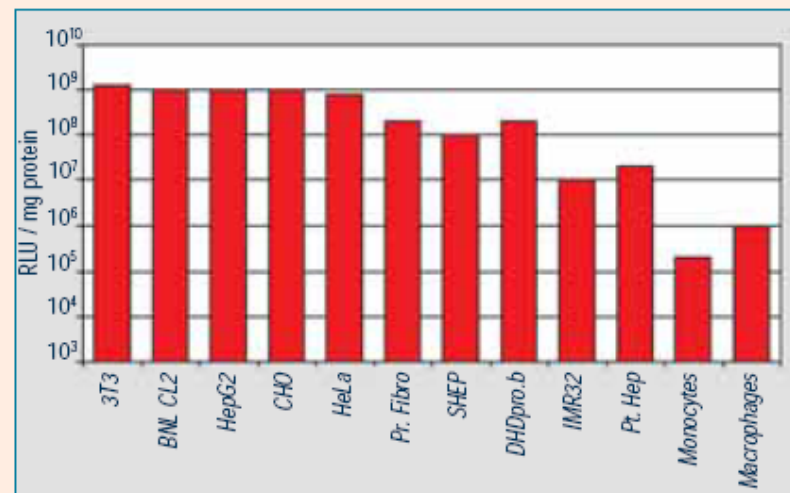
## ExGen 500 performs when other transfection reagents fail



### Expression of Green Fluorescent Protein (GFP) in 293 cells.

Cells were transfected with a vector containing the GFP coding sequence using ExGen 500 and competitor's liposome based reagent.

## ExGen 500 transfects a wide variety of cell types





# Dendrimers

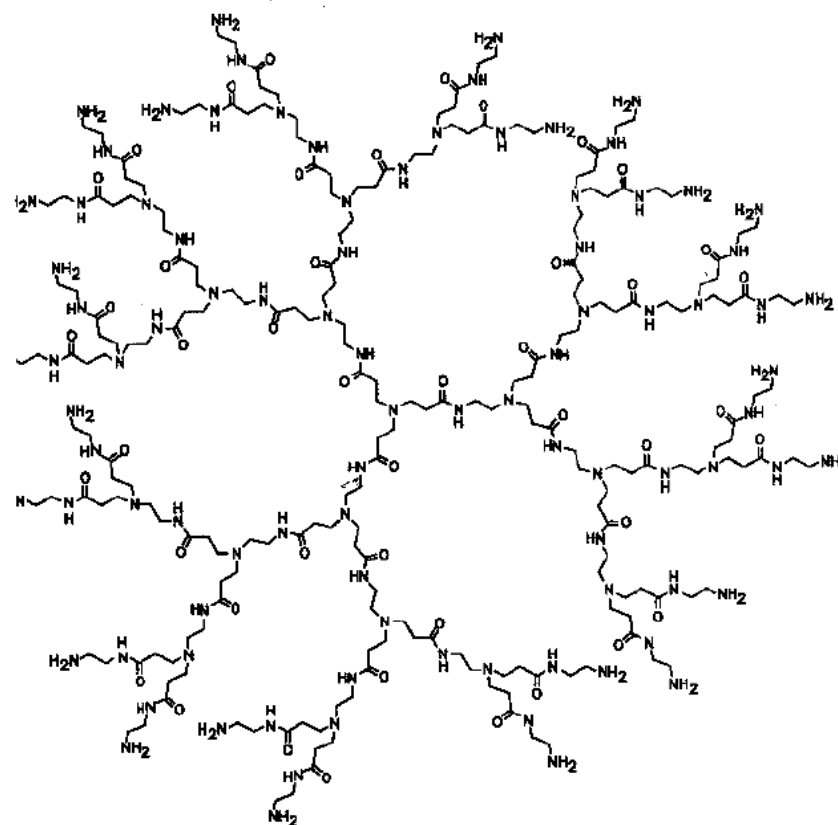


**Figure 11.16.** Fifth-generation polyaminoamine (PAMAM) dendrimer. [Prepared by D. A. Tomalia, H. Baker, J. R. Dewald, M. Hall, G. Kallos, S. Martin, J. Roeck, J. Ryder, and P. Smith, *Polym. J.* **17**, 117 (1985).]

# Dendrimer

## The Construction of Dendrimers — 1

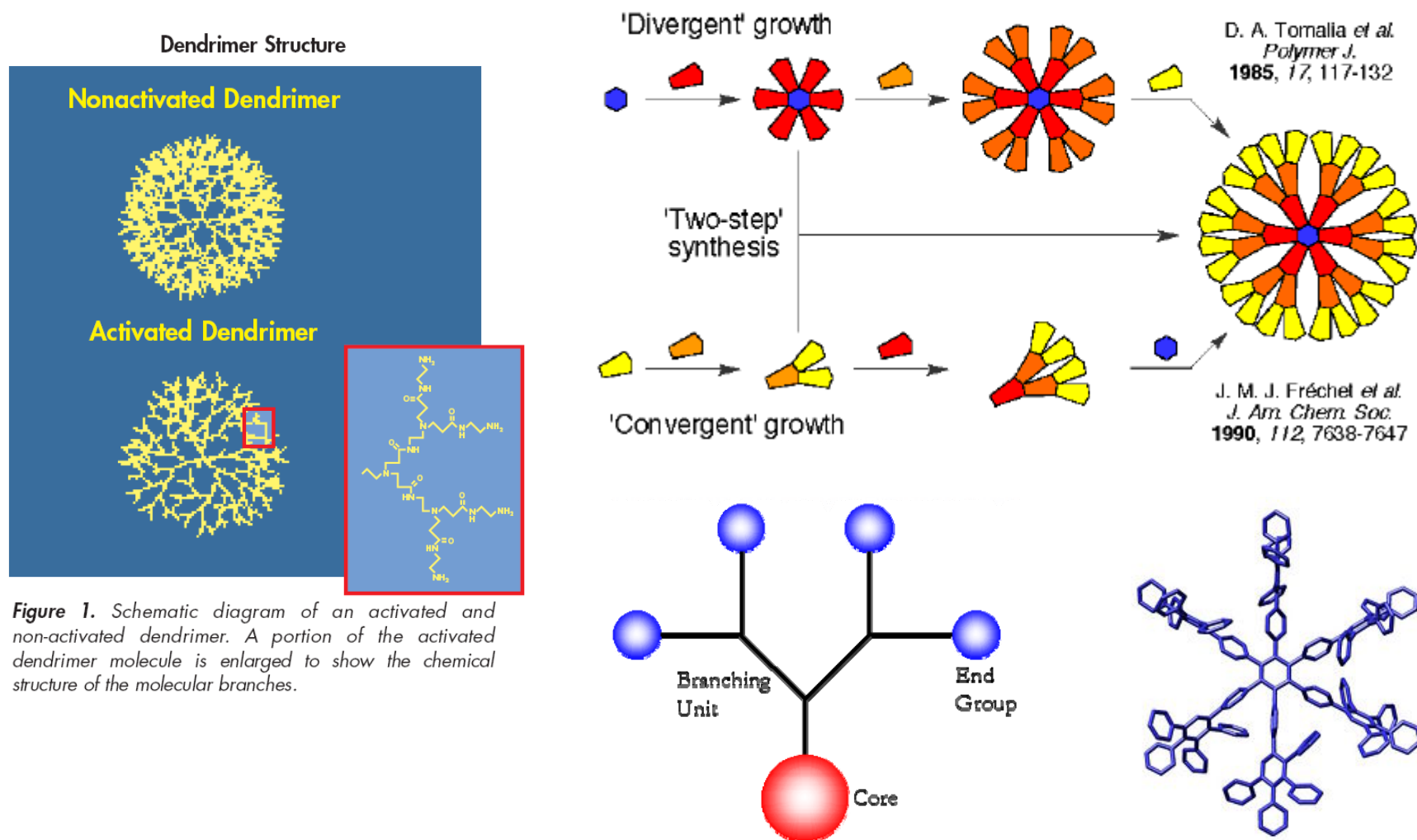


**Figure 1.** Schematic diagram of an activated and non-activated dendrimer. A portion of the activated dendrimer molecule is enlarged to show the chemical structure of the molecular branches.

### Activated-Dendrimer–DNA Interaction



**Figure 2.** Model of the activated-dendrimer–DNA complex. Activated dendrimers (purple spheres) interact with DNA (black) to form a ring-like (toroid-like) structure. The upper right section of the illustration shows naked DNA, the lower section shows the interaction between dendrimers and DNA inside the complex, and the upper left section shows the final complete coverage of DNA within the complex.

### PolyFect Reagent with HeLa Cells

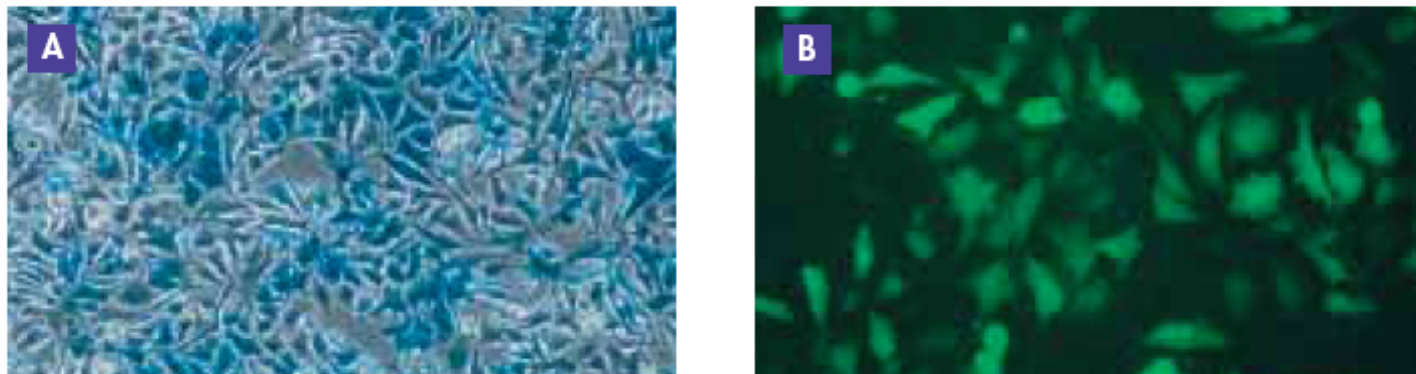


**Figure 8.** Expression of **A**  $\beta$ -galactosidase and **B** green fluorescent protein (GFP) in HeLa cells. Cells were cotransfected in 6-well plates with  $\beta$ -galactosidase and GFP reporter plasmids using PolyFect Transfection Reagent and the HeLa cell protocol. Expression was visualized by X-gal staining or fluorescence microscopy 2 days post-transfection.

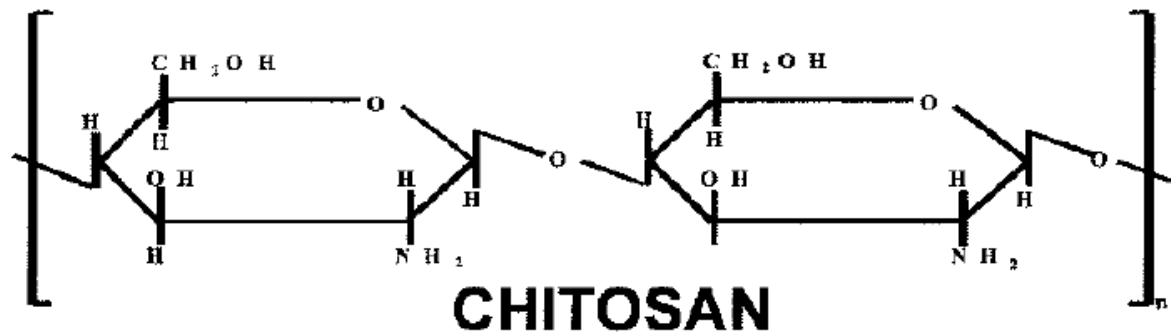
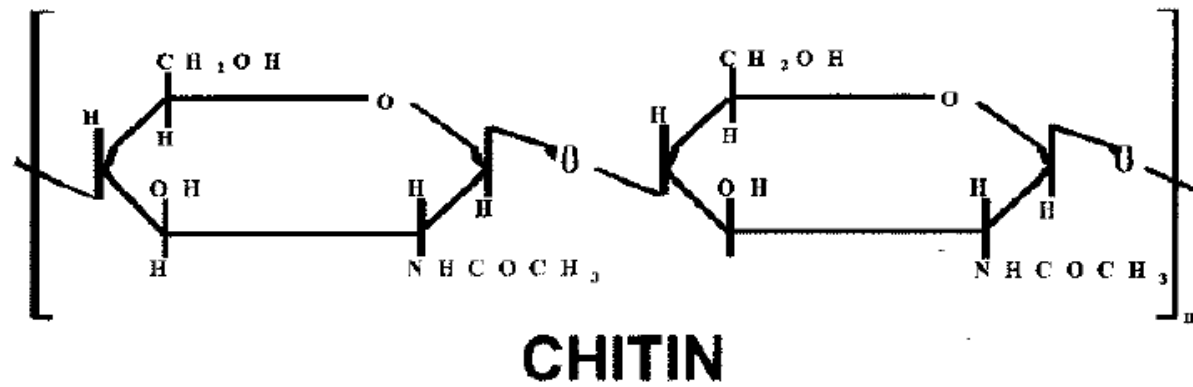
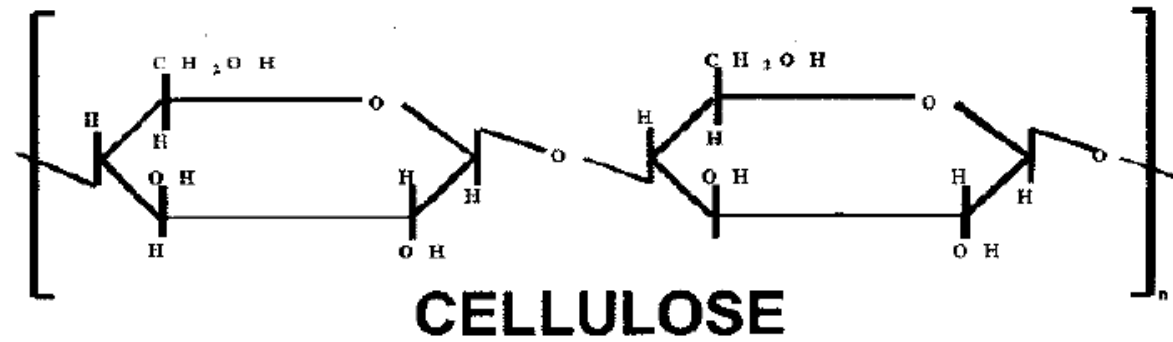


Figure 21.3 Structural similarities between cellulose, chitin, and chitosan.

# $\beta$ -Galactosidase Enzyme Assay

The Beta-Galactosidase Enzyme Assay System offers a direct and easy procedure for measuring Beta-galactosidase enzyme activity in cells transfected with the pSV-Beta-Galactosidase Control Vector. The pSV-Beta-Galactosidase Vector is designed to be used as a positive control vector for monitoring transfection efficiencies into mammalian cells. Cell extracts are incubated with the provided buffer and substrate ONPG (o-nitrophenyl-B-D-galactopyranoside). The optical density is measured spectrophotometrically or with an ELISA reader. The absorbance should be read at 420nm.

$$1 \text{ Miller Unit} = 1000 * (\text{Abs}_{420} - (1.75 * \text{Abs}_{550})) / (t * v * \text{Abs}_{600})$$

where:

Abs<sub>420</sub> is the absorbance of the yellow o-nitrophenol,

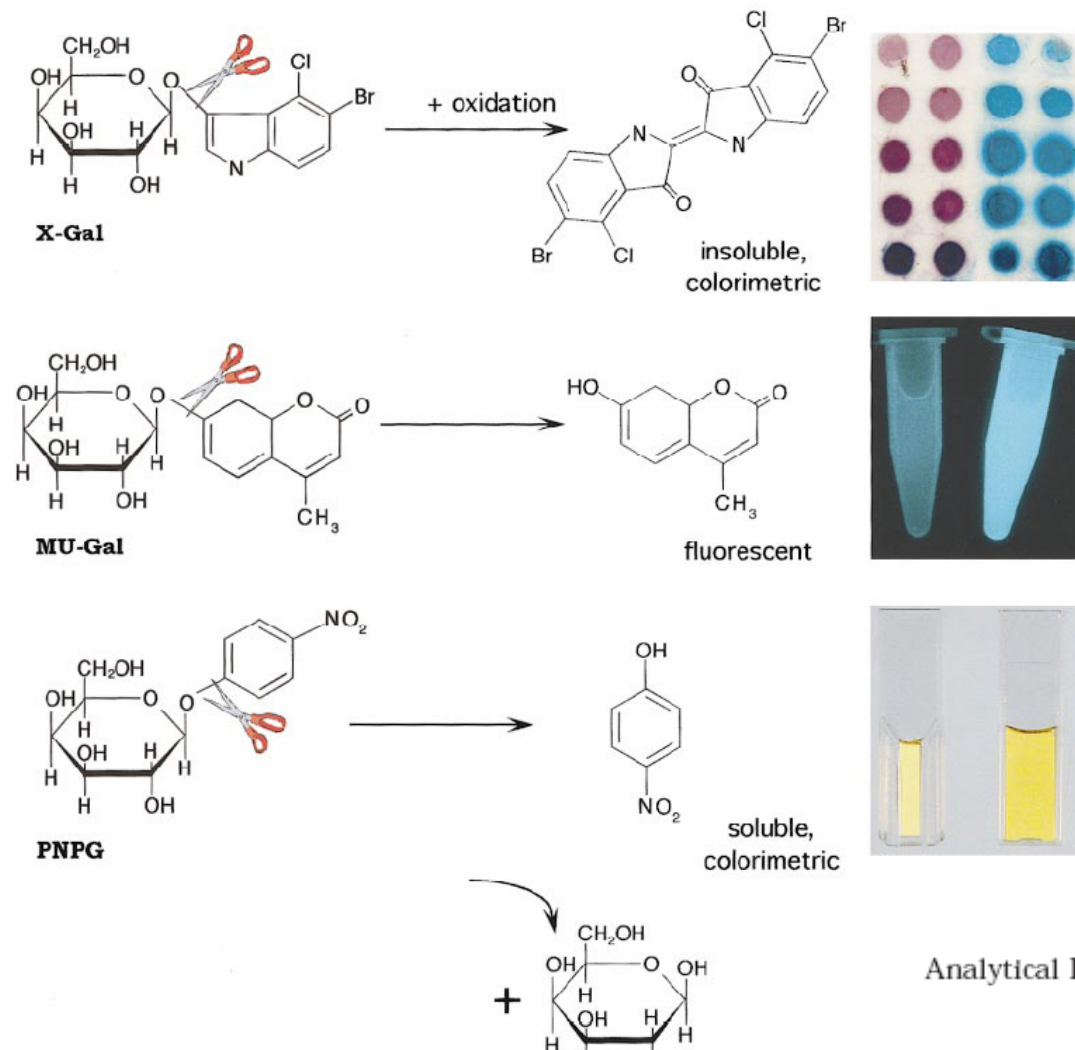
Abs<sub>550</sub> is the scatter from cell debris, which, when multiplied by 1.75

approximates the scatter observed at 420nm,

$t$  = reaction time in minutes,

$v$  = volume of culture assayed in milliliters,

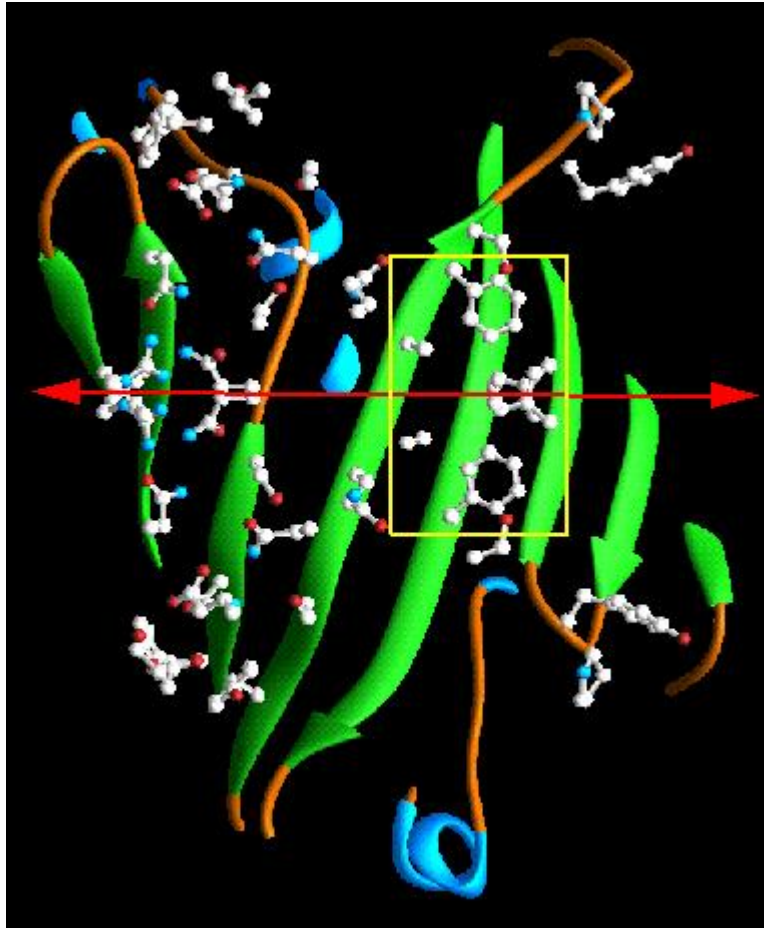
Abs<sub>600</sub>† reflects cell density.



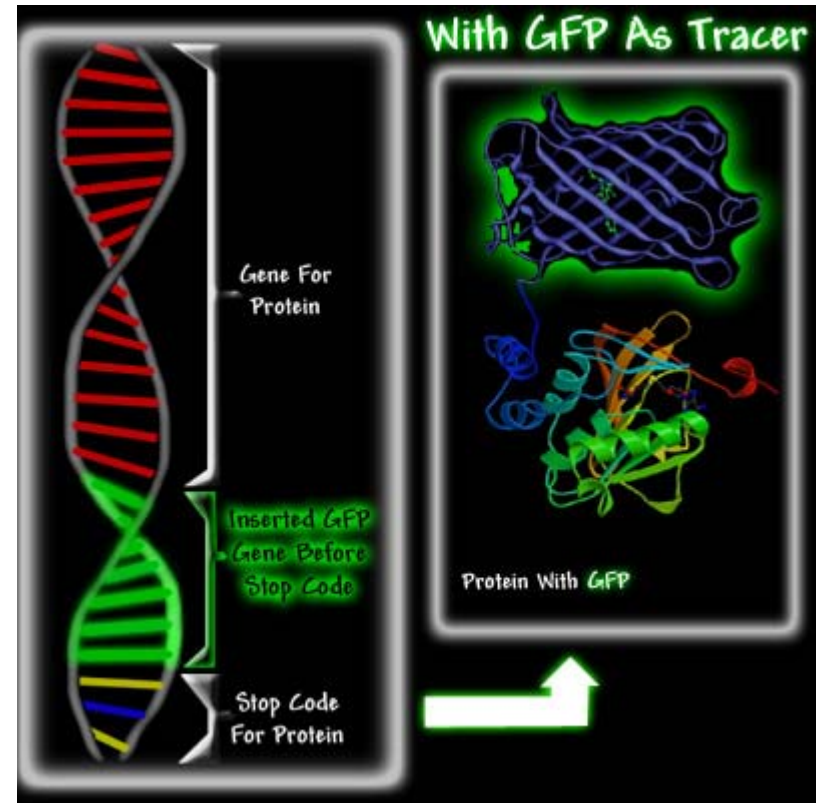
Analytical Biochemistry **285**, 1–15 (2000)

**FIG. 1.** Enzymatic function of  $\beta$ -galactosidase in cleaving indicator substrates.  $\beta$ -gal cleaves  $\beta$ -D-galactoside containing substrates with a diverse range of aglycone groups, targeting between the glycosyl oxygen and anomeric carbon as indicated (scissors). Substrates shown indicate commonly used indicators for assays on  $\beta$ -gal function on plates (X-Gal) or for liquid assay by measure of fluorescence (MU-Gal or MUG) or color (ONPG). Top left, X-Gal is 5-bromo-4-chloro-3-indolyl- $\beta$ -D-galactoside, and when cleaved and oxidized produces the insoluble dye 5-bromo-4-chloro-indigo, as described previously (22). Right panel, top, yeast colonies expressing  $\beta$ -gal and exposed to X-Gal (right half) or the closely related compound Magenta-Gal (left half, see Biosynth, Inc., or Diagnostic Chemicals Limited). Middle left, MUG is methylumbelliferyl- $\beta$ -D-galactoside, and when cleaved by  $\beta$ -gal produces the fluorescent product methylumbelliferone (first described in (102)). Right panel, middle, shows yeast lysates expressing  $\beta$ -gal exposed to MUG, under long-wave UV. Bottom left, PNPG and ONPG are closely related nitrophenol- $\beta$ -D-galactosides with similar assay properties, e.g., (103), whose cleavage releases the yellow product nitrophenol (right panel, bottom); PNPG is shown.

# Green Fluorescent Protein (GFP)



The **green fluorescent protein (GFP)** is a protein from the jellyfish *Aequorea victoria* that fluoresces green when exposed to blue light.





# GFP Rats





# Gold Nanoparticles

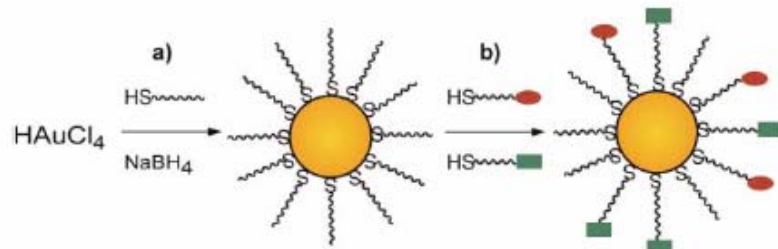
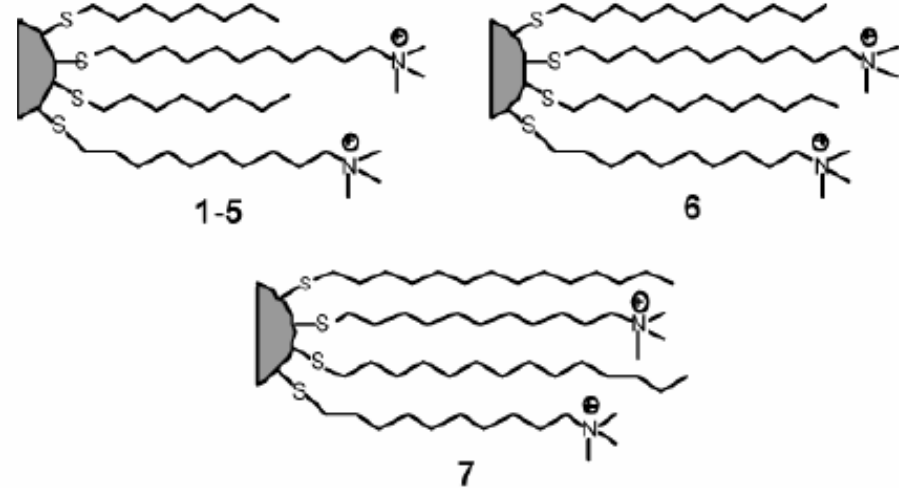
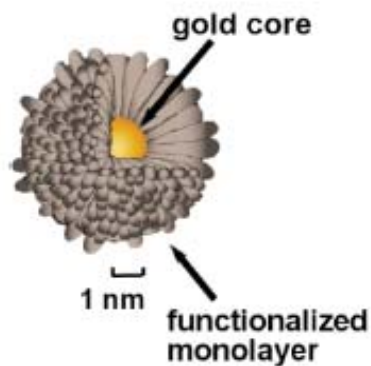
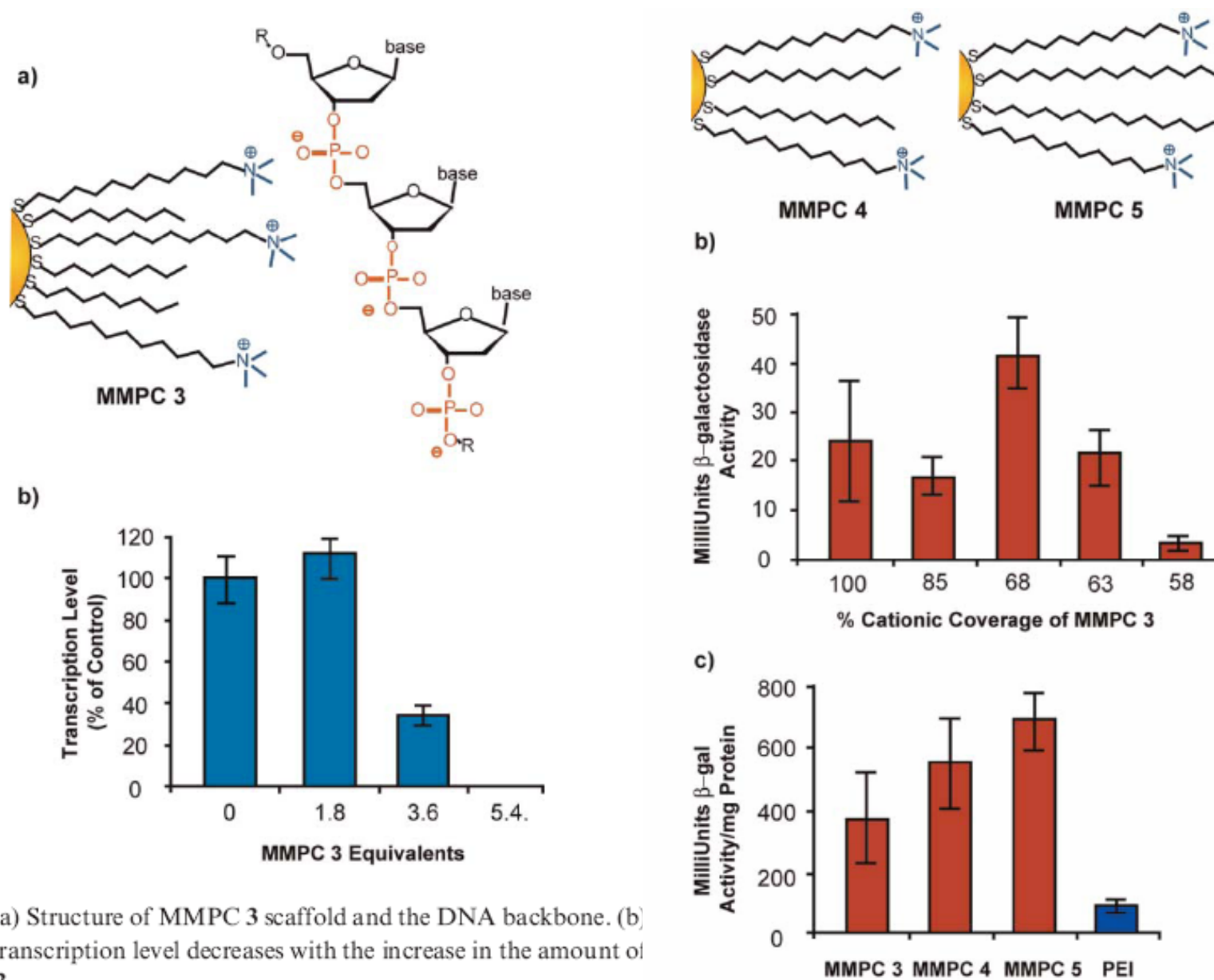


**Fig. 2** Synthesis of gold MPCs using (a) the Brust-Schiffrin reaction and MMPCs *via* (b) the Murray place-exchange method.

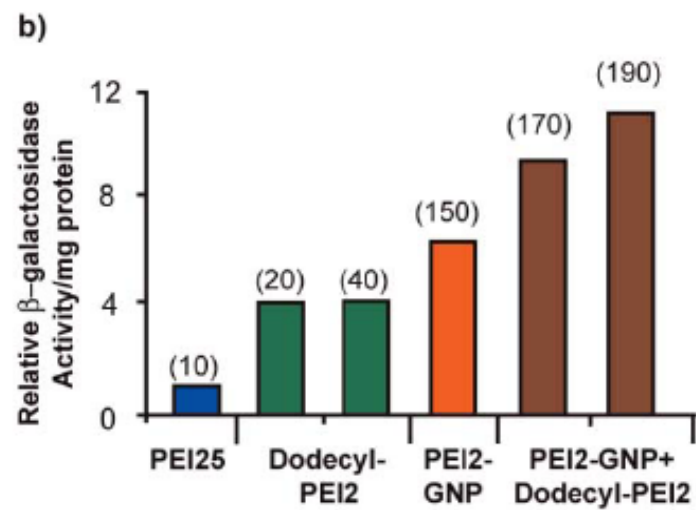
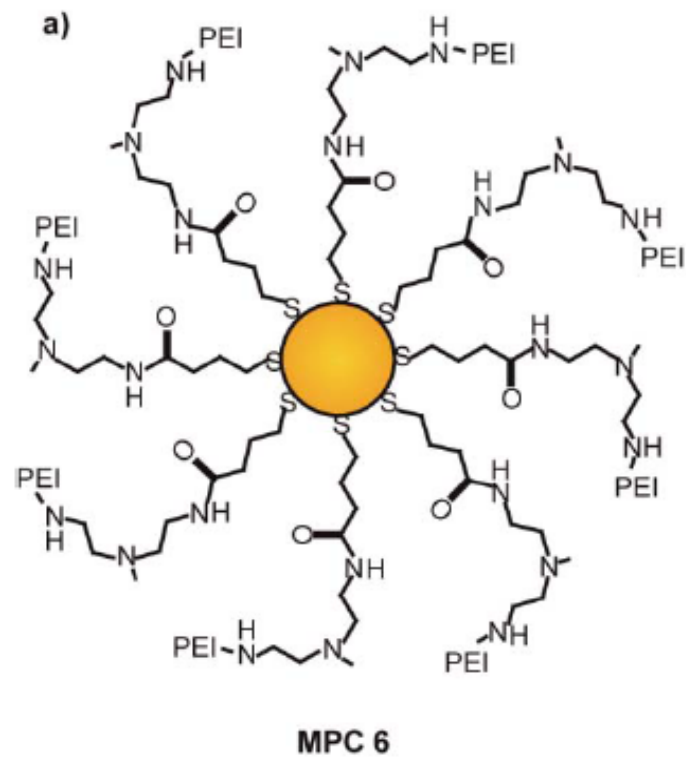


MMPC	1	2	3	4	5	6	7
% cationic coverage	100	85	68	63	58	77	89

**Figure 1.** MMPCs used for transfection.



**Fig. 5** (a) Structure of MMPC 3 scaffold and the DNA backbone. (b) Percent transcription level decreases with the increase in the amount of MMPC 3.



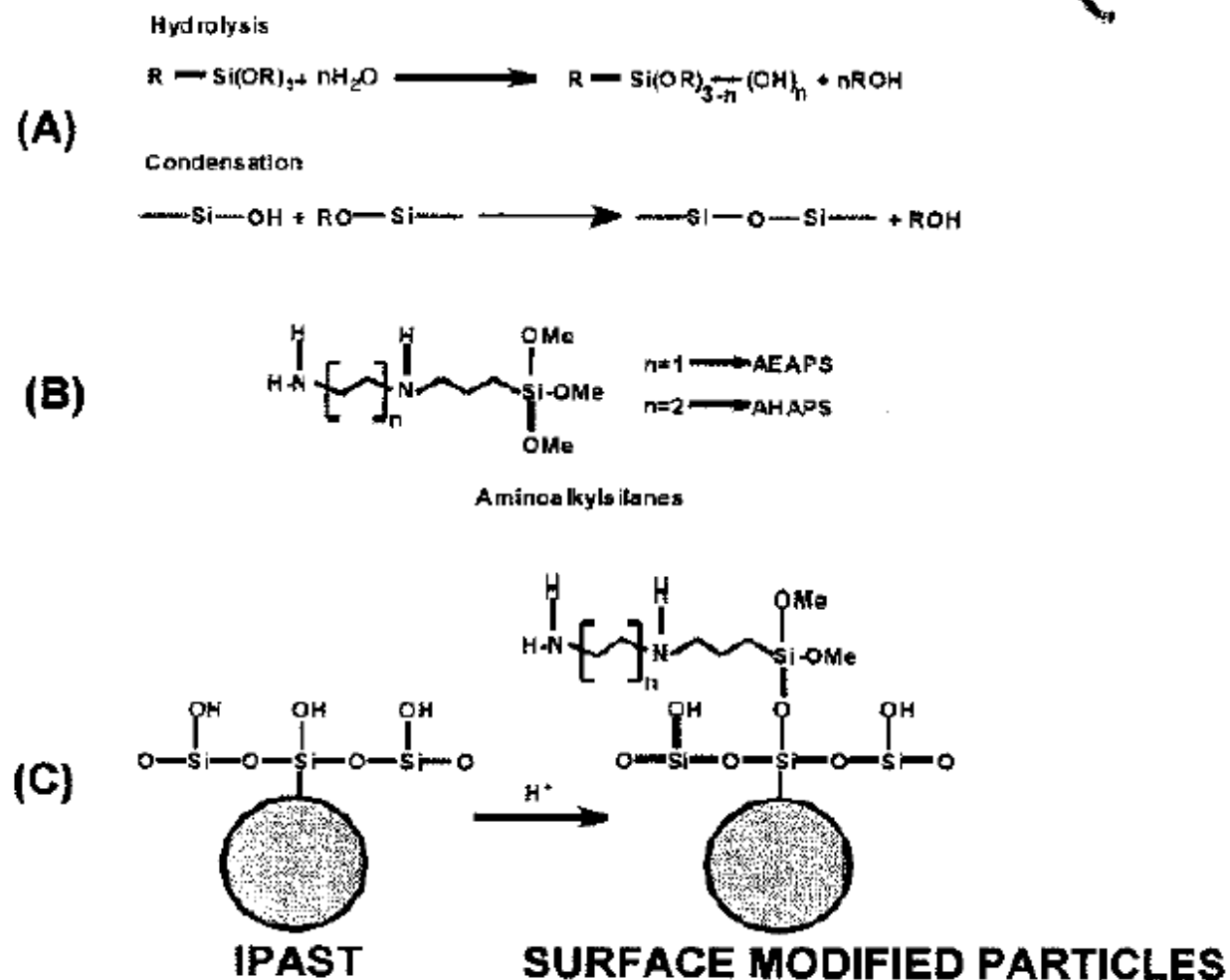
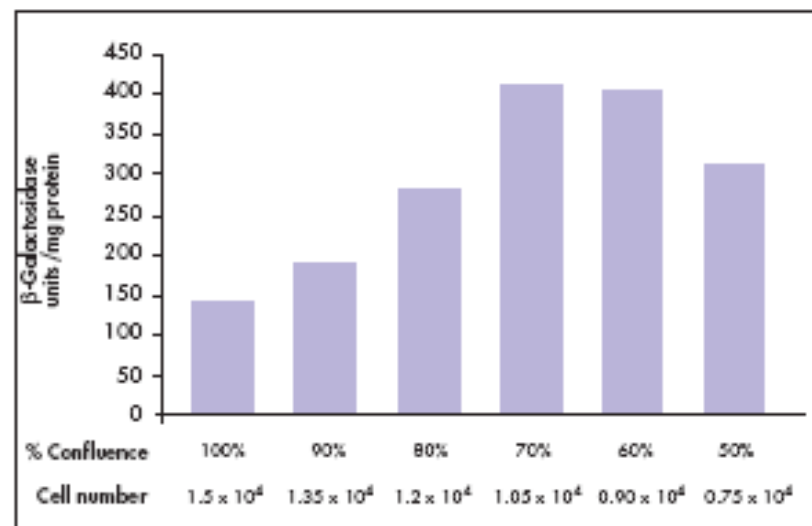


Figure 23.11 (A) Hydrolysis and condensation of unmodified particles. (B) Aminoalkylsilanes. (C) Modification scheme.

# Parameters

- Cell density
- Amount of DNA
- Transfection reagent to DNA ratio
- Incubation period with DNA complex
- Incubation time following transfection

### Transfection Efficiency vs. Cell Density



**Figure 16.** Transfections were performed in 96-well format using 0.1  $\mu\text{g}$  of a  $\beta$ -galactosidase reporter plasmid, 0.8  $\mu\text{g}$  Enhancer, and 1  $\mu\text{l}$  Effectene Reagent per well. The indicated numbers of HeLa-S3 cells were seeded one day prior to transfection to provide cell densities of approximately 50–100% at the time of transfection. Transfection efficiencies and protein content were measured from four replicates 48 h after transfection.

### Serum and DNA Quantity vs. Transfection Efficiency

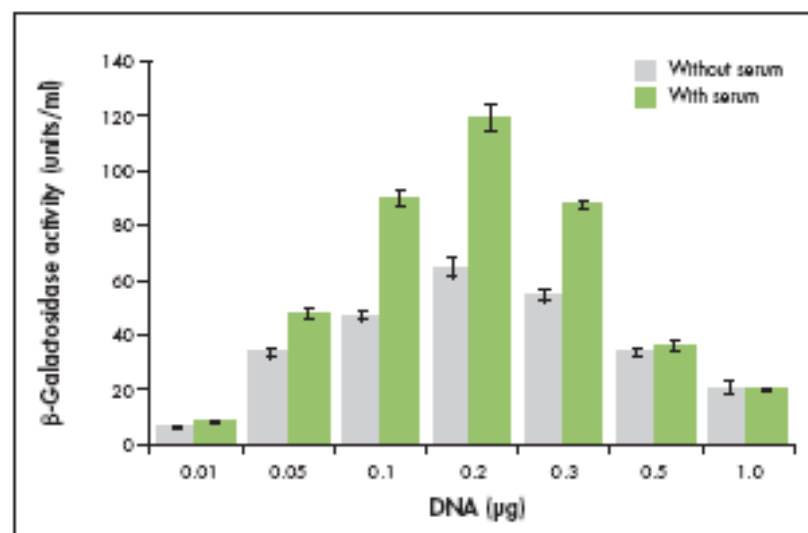
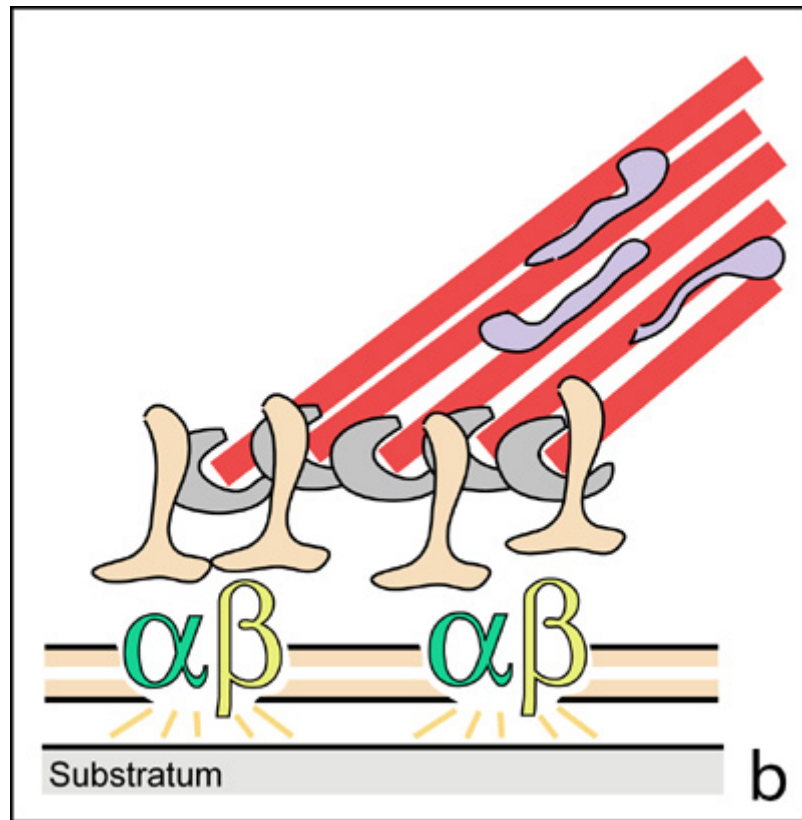


**Figure 13.** Influence of serum and DNA quantity on transfection using Effectene Reagent.  $2 \times 10^4$  COS-7 cells were seeded per well in 96-well plates one day before transfection. Cells were transfected using 0.01–1.0  $\mu\text{g}$  of a  $\beta$ -galactosidase reporter plasmid and 0.08–8.0  $\mu\text{g}$  Enhancer (DNA: Enhancer ratio of 1:8) and 2  $\mu\text{l}$  Effectene Reagent, in either the presence or absence of serum. Each bar represents the average efficiency from four replicates 48 h post-transfection.

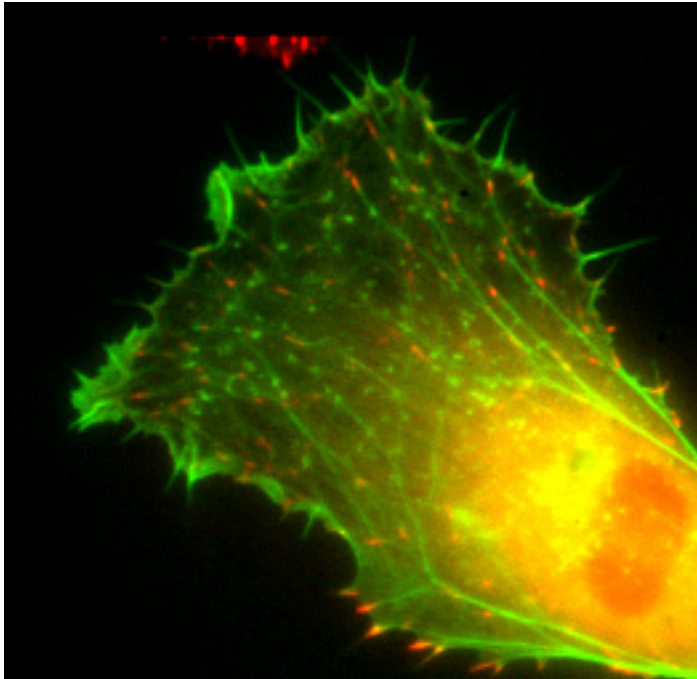
# Cell-Surface Interaction

For a cell to move, it must adhere to a substrate and exert traction. Adhesion occurs at specific foci at which the actin cytoskeleton on the inside of the cell is linked via transmembrane receptors (integrins) to the extracellular matrix on the outside. These adhesion sites are composed of complexes of more than 50 different proteins

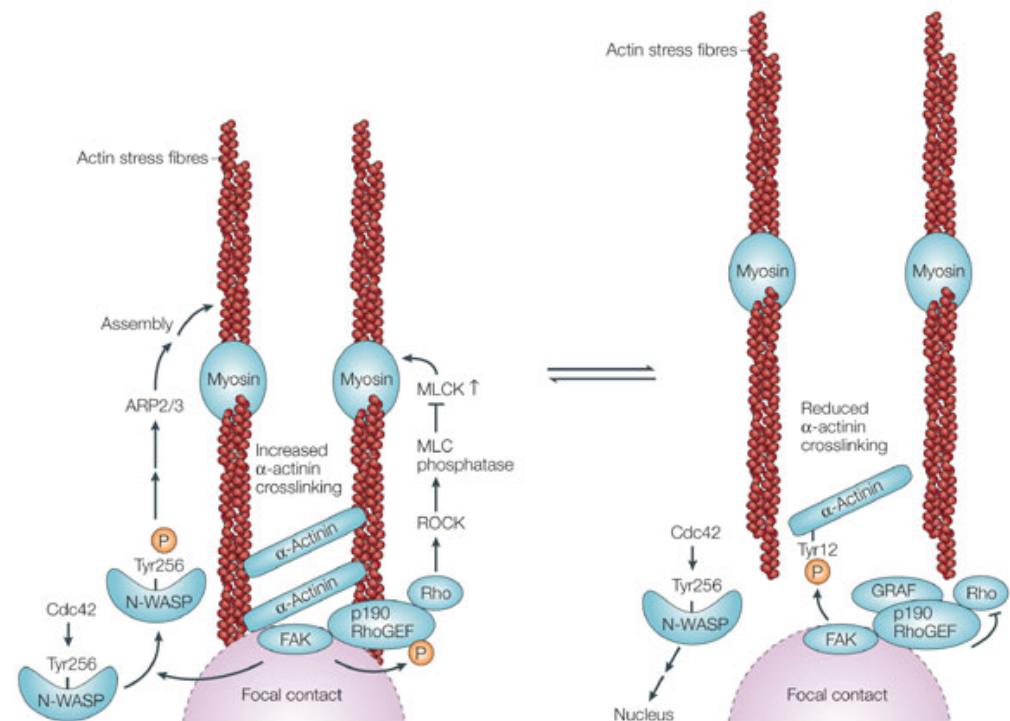


Highly simplified schematic illustration of the organisation of a focal adhesion. Transmembrane integrins (alpha/beta) bind to matrix ligands on the outside of the cell, and to a complex of molecules inside the cell that link to actin filaments. At focal adhesions, the actin filaments are bundled by actin filament cross-linkers, including the contractile protein myosin. Tension in the bundle, generated by myosin, is required to maintain the clustering of integrins and the integrity of focal adhesions





The formation of substrate adhesion sites in a migrating goldfish fibroblast. The cell was transfected with GFP-actin (green) and microinjected with rhodamine-tagged vinculin (an adhesion component; red). The protruding cell front is marked by a diffuse band of actin filaments (the lamellipodium), which contains radial filament bundles (filopodia) that project beyond the cell edge. Different types of adhesion foci (red) can be distinguished: small foci in association with lamellipodia and filopodia (focal complexes) and, behind the lamellipodium, larger foci associated with actin filament bundles (focal adhesions). Focal adhesions are also observed at the periphery of retracting cell edges (bottom region of figure). Focal complexes and focal adhesions in the advancing front remain stationary, relative to the substrate, whereas, focal adhesions at the retracting edges can slide.



Nature Reviews | Molecular Cell Biology

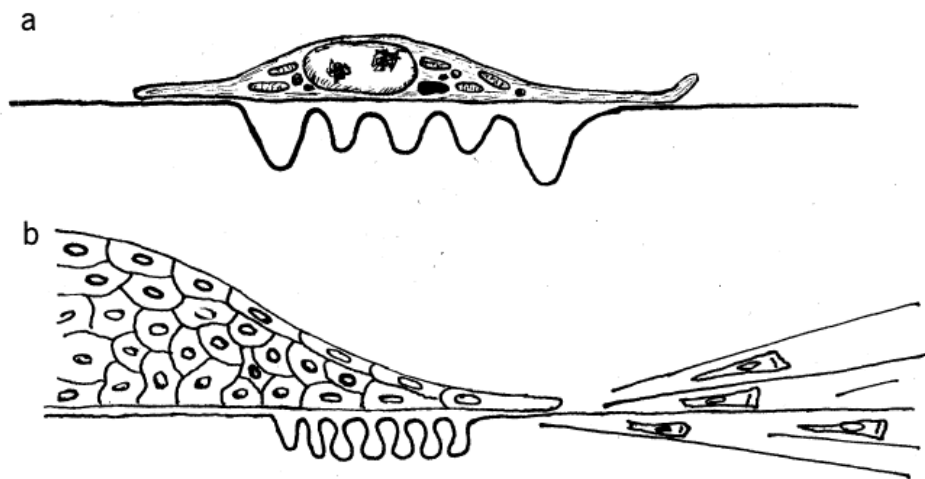


Fig. 1. (a) Diagrammatic side view of an individual cultured fibroblast distorting and wrinkling the elastic silicone substratum upon which it has spread and is crawling. (b) Diagrammatic side view of the margin of an explant whose cells are spreading outward on a silicone rubber substratum. The traction forces exerted by the outgrowing cells compress the rubber sheet beneath the explant and stretch it into long radial wrinkles in the surrounding area.

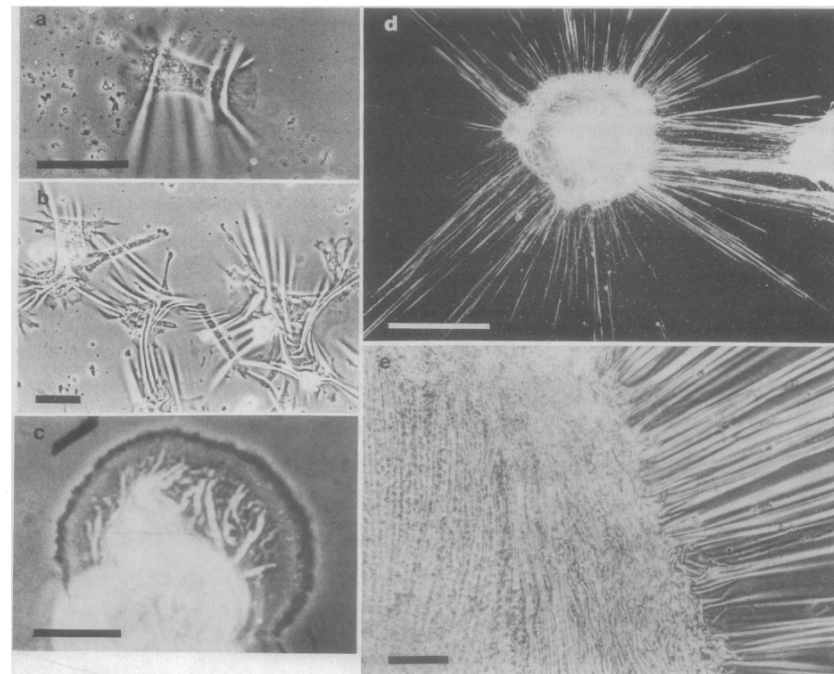
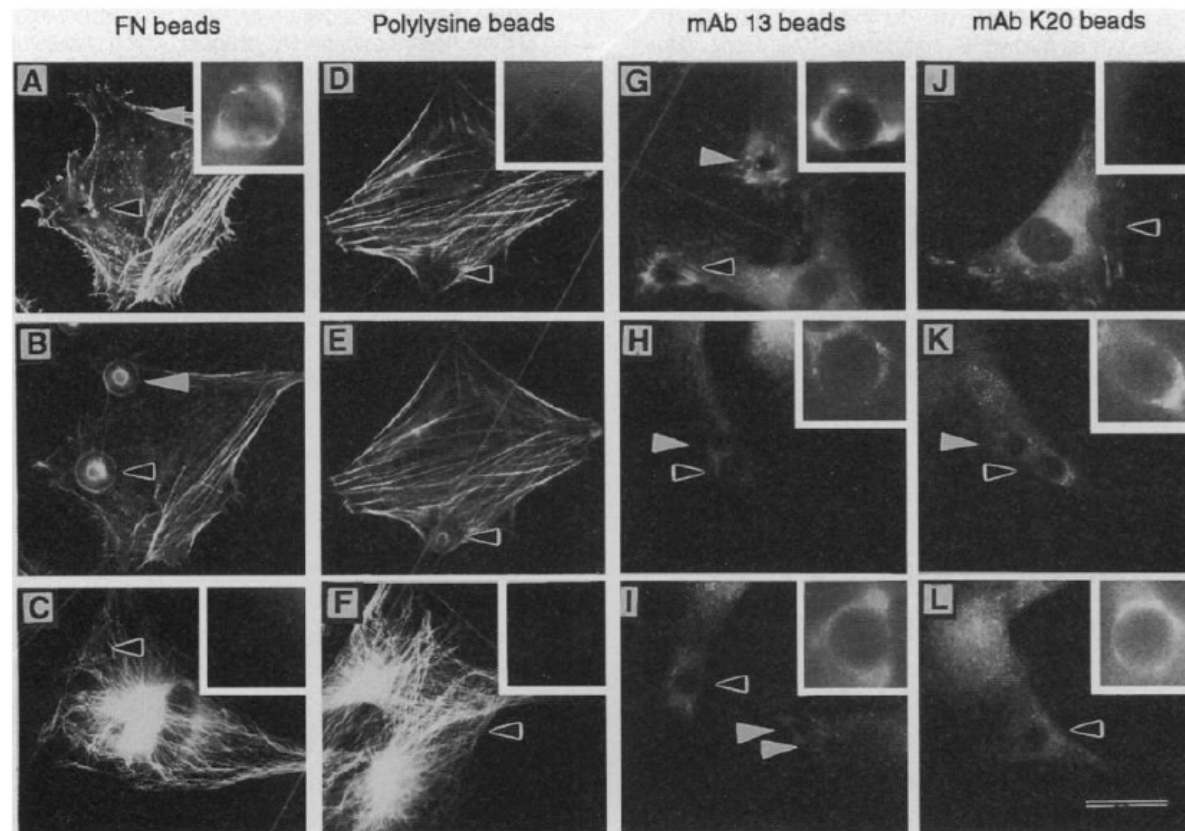
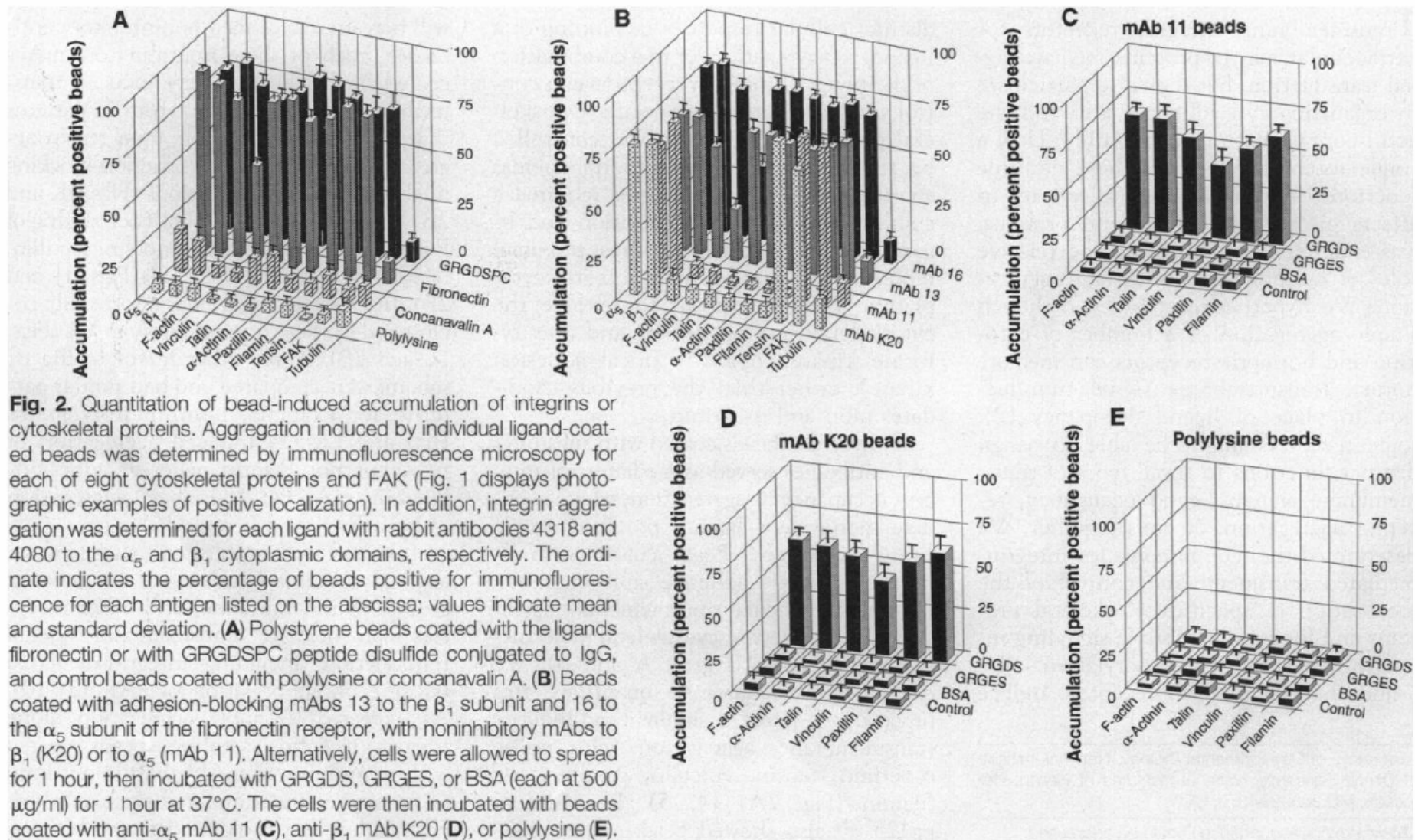


Fig. 2. (a) An individual chick heart fibroblast whose locomotion and contractility have visibly wrinkled the silicone rubber substratum upon which it is crawling (the bar is  $50\text{ }\mu\text{m}$  long). (b) Lower magnification view of about a dozen chick heart fibroblasts and the complex pattern of distortions produced in the rubber substratum by their locomotory traction (the bar is  $100\text{ }\mu\text{m}$ ). (c) Higher magnification view of an individual PTK-1 cell just beginning to spread onto a silicone rubber sheet after trypsinization. Ruffling activity is seen as a dark band around the periphery, while the wrinkles being generated in the substratum are seen as irregular white bands beneath the cell body (from an individual frame of a 16-mm time-lapse film; the bar is  $20\text{ }\mu\text{m}$  long). (d) Very low magnification, dark-field illumination view of a chick heart explant that had been spreading on a silicone rubber substratum for 48 hours. The bright radiating lines are stress wrinkles. Notice the "two-center effect" of wrinkles running between the large central explant and the smaller one at the edge of the photograph at the right (the bar is  $1\text{ mm}$  long). (e) Higher magnification, phase-contrast view of the marginal outgrowth zone of the same explant as shown in (d). The compression folds beneath the explant are seen on the left and the radial stress wrinkles around it are on the right (the bar is  $100\text{ }\mu\text{m}$  long).

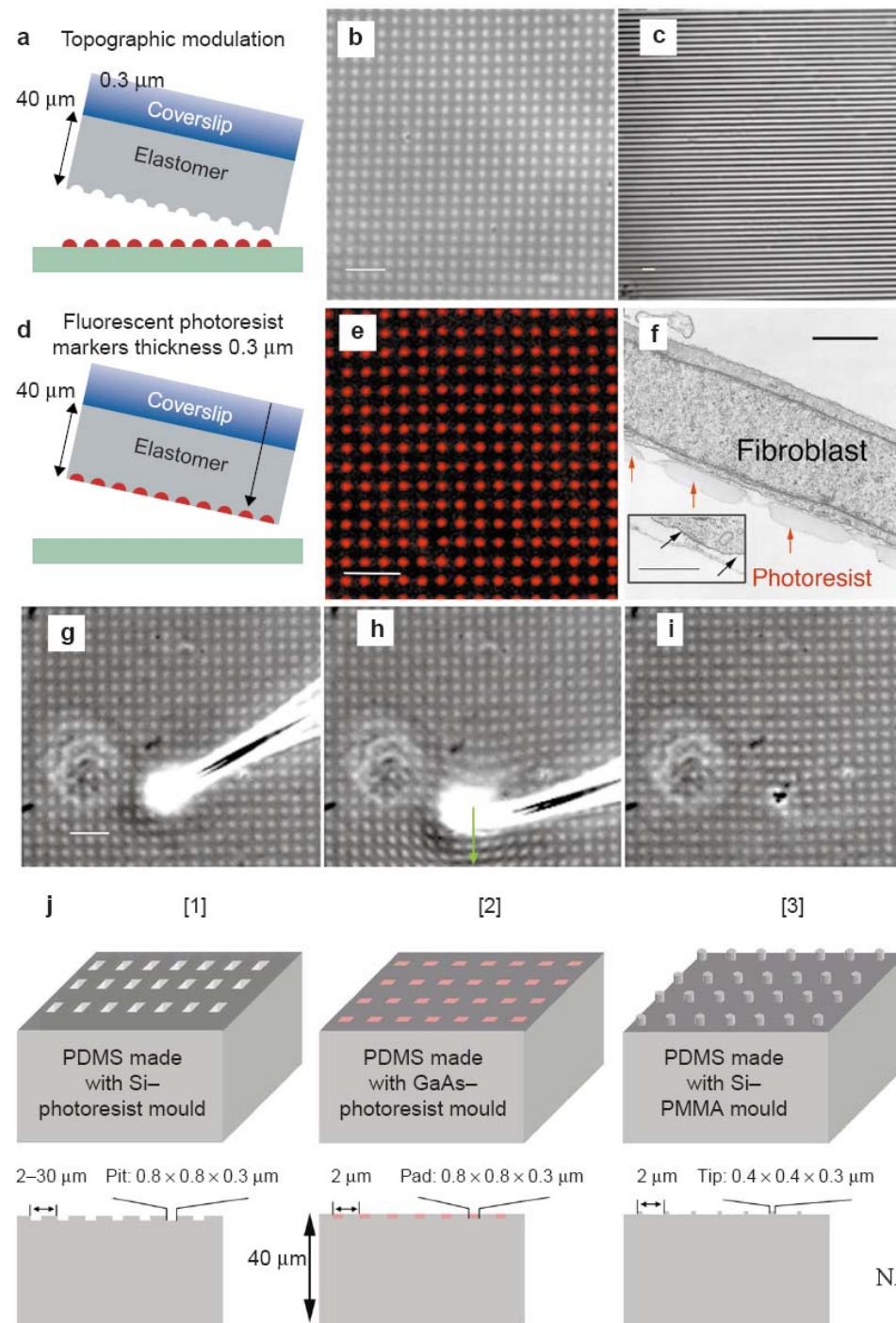


**Fig. 1.** Immunofluorescence for juxtamembrane accumulation of cytoskeletal proteins and FAK induced by beads coated with ligands or antibodies to integrin (4). Each inset shows a higher-magnification view, focusing on the equator of the bead marked by a highlighted black arrowhead; white arrowhead indicates a second bead bound to the cell. (**A** to **C**) Fibronectin-coated beads. Localization of F-actin as detected by rhodamine-labeled phalloidin (**A**), compared with combined transmitted light and fluorescence to illuminate the bead (**B**); no tubulin immunolocalization was detected adjacent to these beads (**C**). Lack of F-actin adjacent to polylysine-coated beads (**D**), and transmitted light to illuminate the bead (**E**); absence of tubulin immunolocalization (**F**). Effects of beads coated with adhesion-blocking mAb 13 (**G** to **I**) or noninhibitory mAb K20 (**J** to **L**) (both mAbs bind the  $\beta_1$  subunit) on immunolocalization of paxillin (**G** and **J**), tensin (**H** and **K**), and FAK (**I** and **L**). Scale bar, 20  $\mu$ m.









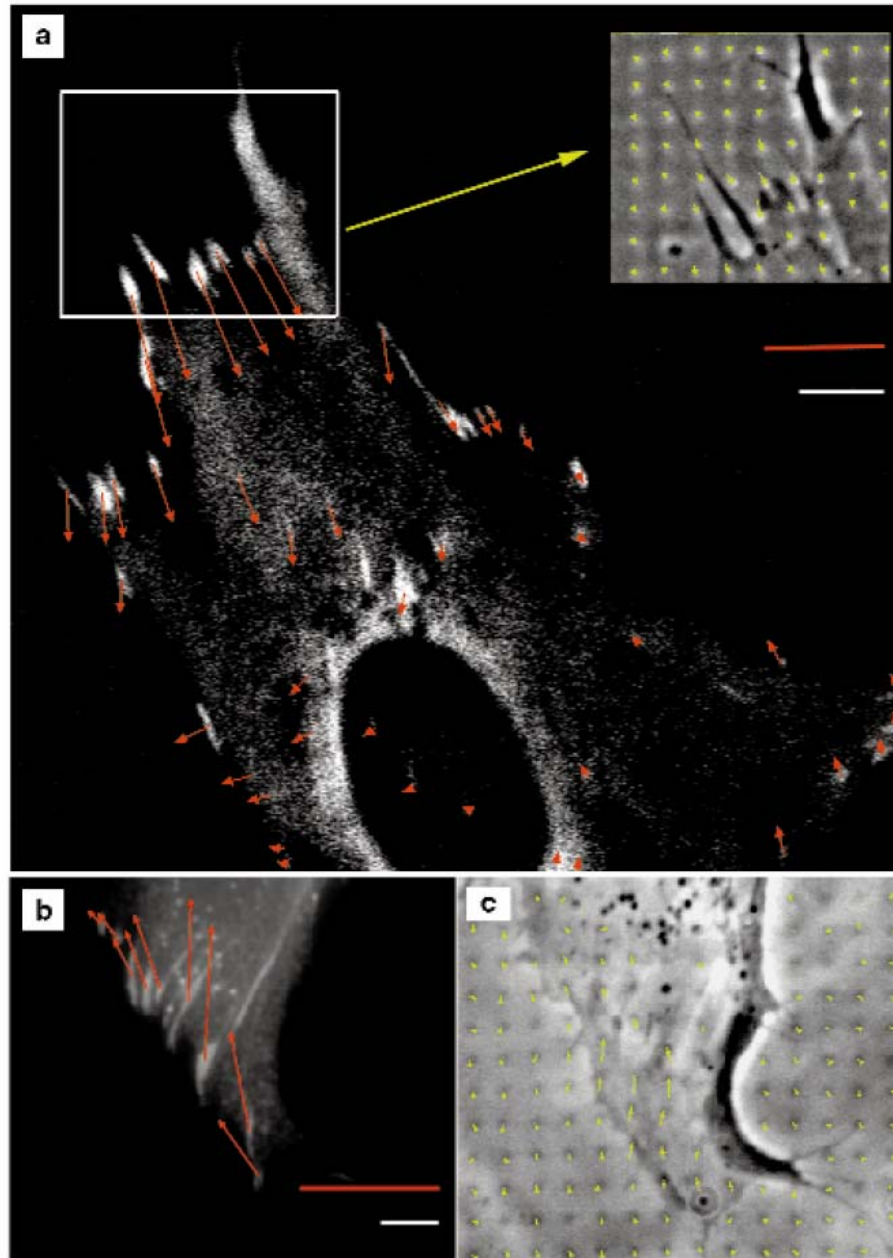


**Figure 3 Visualization of forces and focal adhesions.** **a**, Fluorescence image of a human foreskin fibroblast expressing GFP-vinculin, which localizes to focal adhesions. Red arrows correspond to forces extracted from the displacements of the patterned elastomer (Young's modulus = 18 kPa). Note the alignment of force with the direction of elongation of large focal adhesions. Inset, phase-contrast image of the upper part of the cell (white rectangle), showing displacements of the dots (green arrows); the pattern consists of small square pits (see Fig. 1j, 1). **b**, Fluorescence image of a human foreskin fibroblast stained with antibodies against paxillin, which also localizes at focal adhesions. Red arrows correspond to forces extracted from the displacements of the patterned elastomer (Young's modulus = 21 kPa); the pattern consists of small tips formed by electron-beam lithography (see Fig. 1j, 3). **c**, Phase-contrast image of the same cell immediately before fixation. White scale bars represent 4  $\mu\text{m}$ ; red scale bars represent 30 nN.



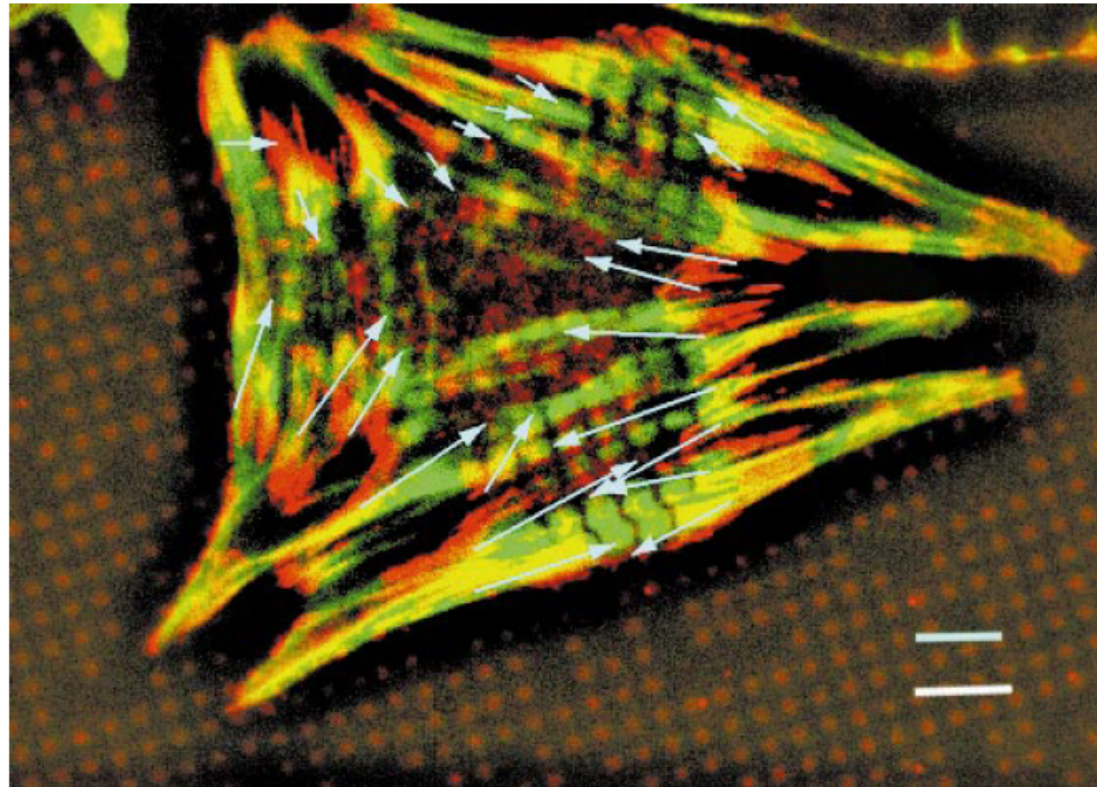
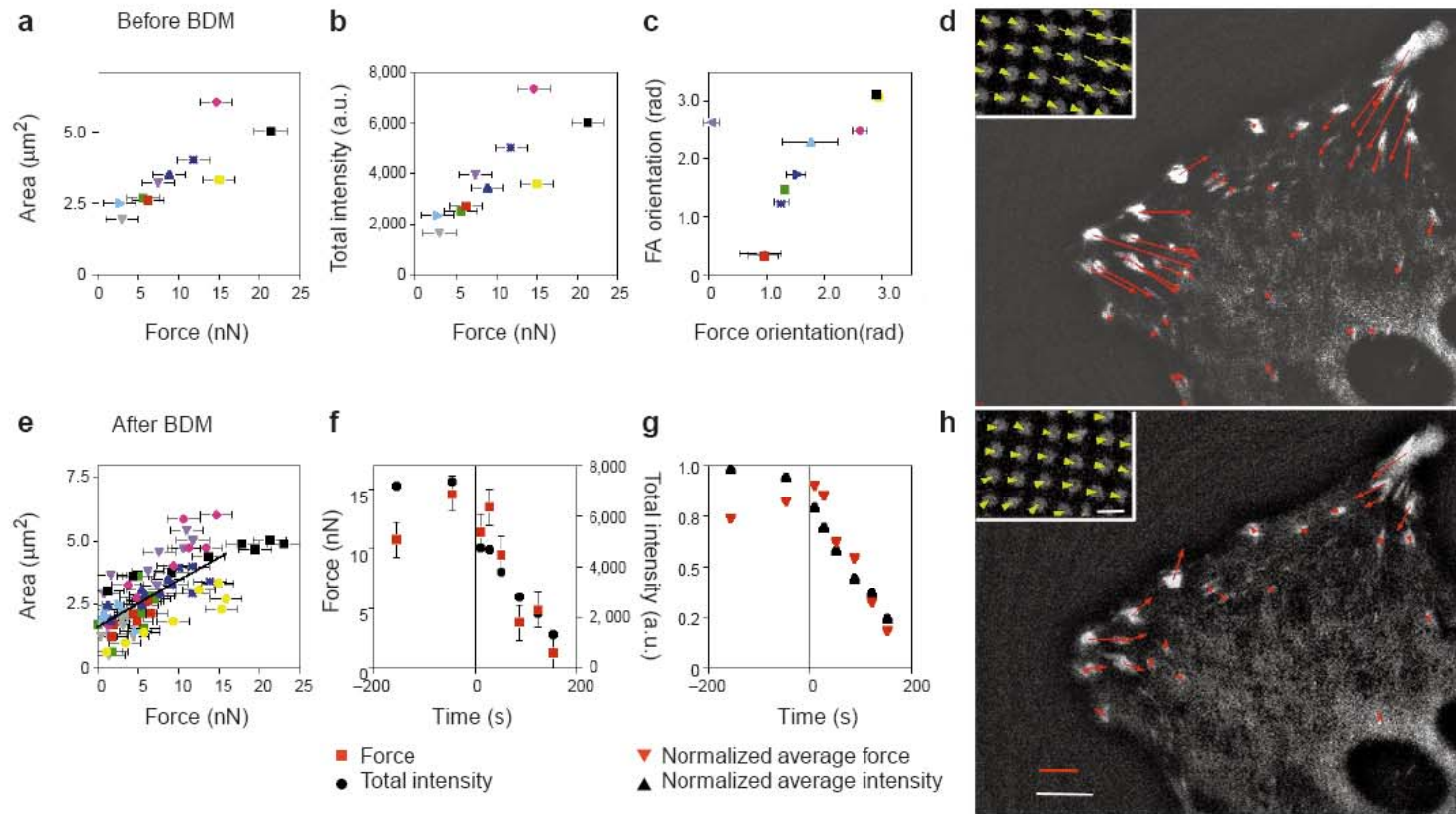
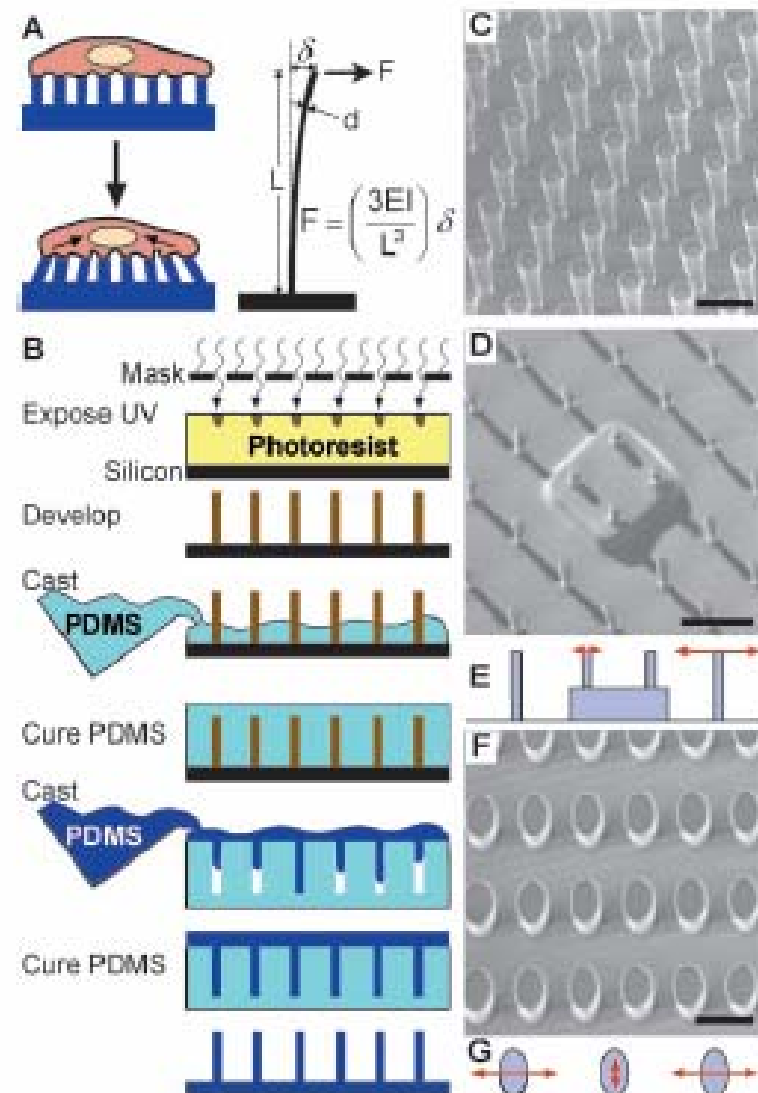


Figure 4 **Distribution of forces in a cardiac myocyte.** After recording the displacements of the pattern caused by beating (Fig. 2c, d), the cardiac myocytes are stained for vinculin (red) to visualize the sites of force transmission, and for actin (green). Yellow regions correspond to overlap of actin and vinculin. The light-blue arrows denote the forces applied to the substrate at the vinculin-rich areas. White bar = 6  $\mu\text{m}$ ; blue bar = 70 nN.



**Figure 5 Correlation between force and focal adhesion structure. a-d**, Before the addition of BDM. **a**, Correlation between force and area of single focal adhesions. **b**, Correlation between force and total fluorescence intensity of single focal adhesions. **c**, Correlation between the direction of the force and the elongation of the focal adhesion. The angles (in radians) were measured relatively to the x axis of the pictures. Each point represents a single focal adhesion from Fig. 5d. Absence of error bars indicates an error below the size of the symbol. **d**, Fluorescence image of a human foreskin fibroblast expressing GFP-vinculin, which localizes to the focal adhesions. The red arrows show the forces transmitted at the focal adhesions. Inset: fluorescence image of the pattern of dots below the left-hand side of the cell; green arrows denote displacements. **e-h**, After the addition of 15 mM 2,3-

butanedione monoxime (BDM). **e**, Correlation between the area and force of the focal adhesions of the cell shown in Fig. 5d, at all time points. Each different symbol represents a different focal adhesion. The black line is the correlation line of the linear part of the plot. Its slope defines a stress of  $5.5 \pm 2 \text{ nN } \mu\text{m}^{-2}$  at the focal adhesions. **f**, Time dependence of the relaxation of force (red squares) and total GFP-vinculin intensity (black dots) of a single focal adhesion. **g**, Time dependence of the relaxation of force and total intensity as a normalized average over all focal adhesions. Notice the close correlation between force and total intensity, as both decrease with time. **h**, Same cell as in **d** 2 min after BDM treatment. White bar = 4  $\mu\text{m}$ ; red bar = 10 nN; Young's modulus = 12 kPa.



$$F = \left( \frac{3EI}{L^3} \right) \delta,$$

and  $\delta$  are the bending force.  $V_0$



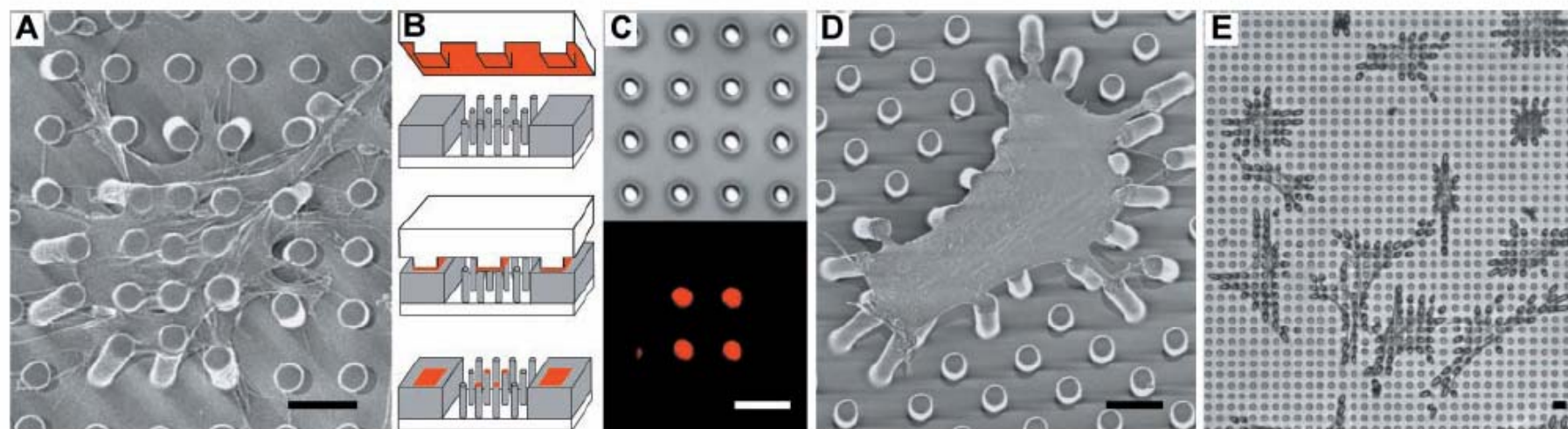


**Fig. 2.** Cell culture on arrays of posts. (A) Scanning electron micrograph of a representative smooth muscle cell attached to an array of posts that was uniformly coated with fibronectin. Cells attached at multiple points along the posts as well as the base of the substrates. (B) Schematic of microcontact printing of protein (red), precoated on a PDMS stamp, onto the tips of the posts (gray). (C) Differential interference contrast (*Upper*) and Immunofluorescence (*Lower*) micrographs of the same region of posts where a  $2 \times 2$  array of posts has been printed with fibronectin. (D and E) Scanning electron micrograph (D) and phase-contrast micrograph (E) of representative smooth muscle cells attached to posts where only the tips of the posts have been printed with fibronectin by using a flat PDMS stamp. Cells deflected posts maximally during the 1- to 2-h period after plating, were fully spread after 2 h, and were fixed and critical point dried 4 h after plating. (Scale bars indicate  $10 \mu\text{m}$ .)

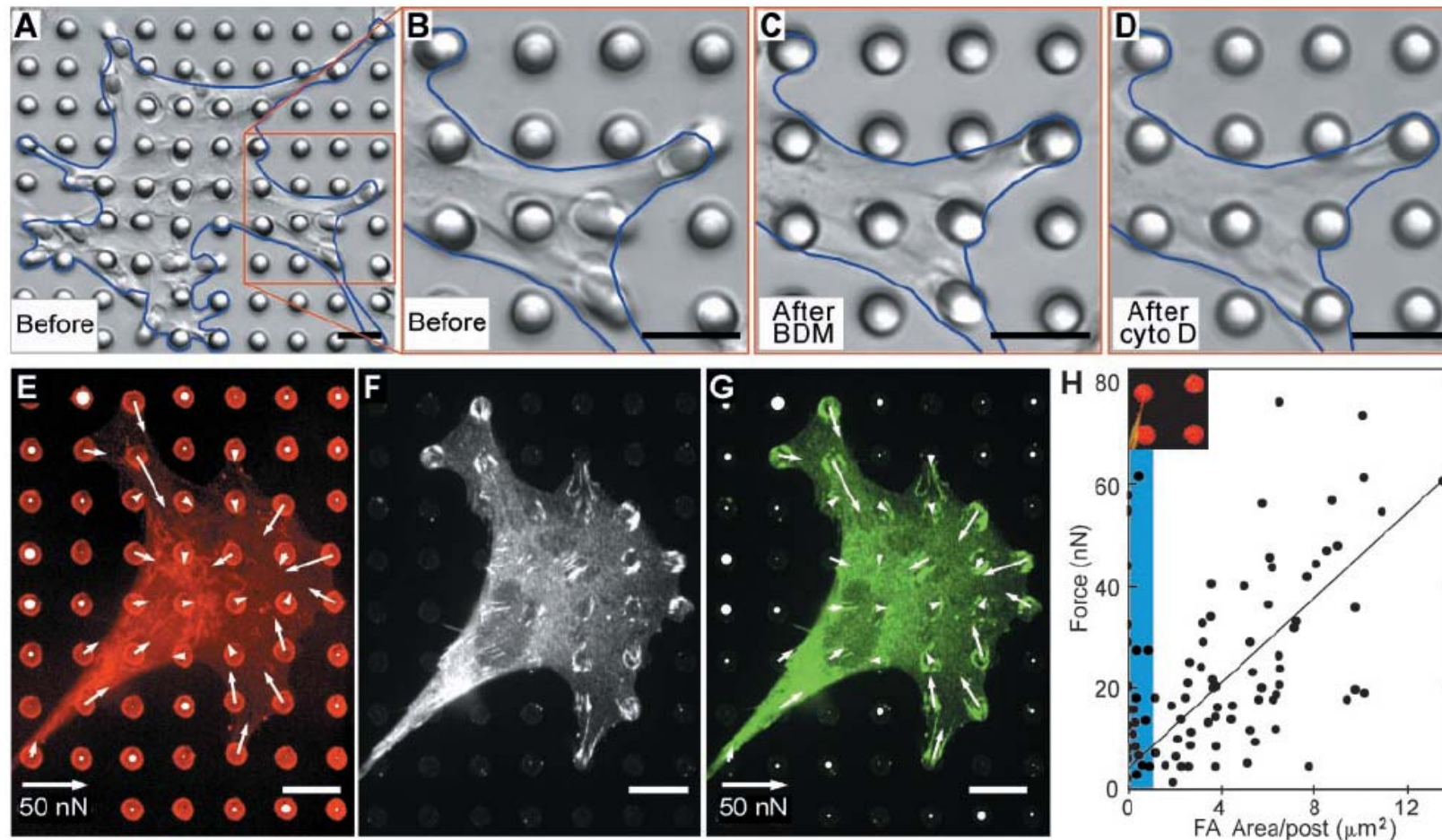


**Fig. 3.** Measurement of contractile forces in cells. (A–D) Differential interference contrast micrographs of a smooth muscle cell (outlined in blue) cultured for 2 h on an array of posts in 10% serum (A and B), 20 min after 20 mM 2,3-butanedione monoxime (BDM) was added to the culture to inhibit myosin contractility (C), and after 2  $\mu$ g/ml cytochalasin D (cyto D) was added to the same culture for an additional 10 min to disrupt the actin cytoskeleton (D). In each case, longer treatments did not result in additional loss of contractility. (E–G) Confocal images of immunofluorescence staining of a smooth muscle cell on posts. Position of fibronectin (E, red) on the tips of the posts was used to calculate force exerted by cells (white arrows). The force map was spatially correlated to immunofluorescence localization of the focal adhesion protein vinculin (F, white; G, green). A similar correlation in the orientation and the quantity of focal adhesion with the traction forces was observed in all cells examined ( $n > 10$ ). The lengths of arrows indicate the magnitude of the calculated force (top right arrow indicates 50 nN); white circles on undeflected posts depict the background error in the force measurement, where the diameter of the circle (same length scale as the arrows) indicates the magnitude of calculated force on each post not attached to a cell. (Scale bars indicate 10  $\mu$ m.) (H) Plot of the force generated on each post as a function of total area of focal adhesion staining per post. Each point represents the force and area of vinculin staining associated with each post; focal adhesions from five cells were analyzed. The shaded region (blue) indicates the adhesions smaller than 1  $\mu$ m<sup>2</sup>. (Inset) Image of a typical small adhesion (<1  $\mu$ m<sup>2</sup>) formed by a cell (green) generating substantial force on a post (red).



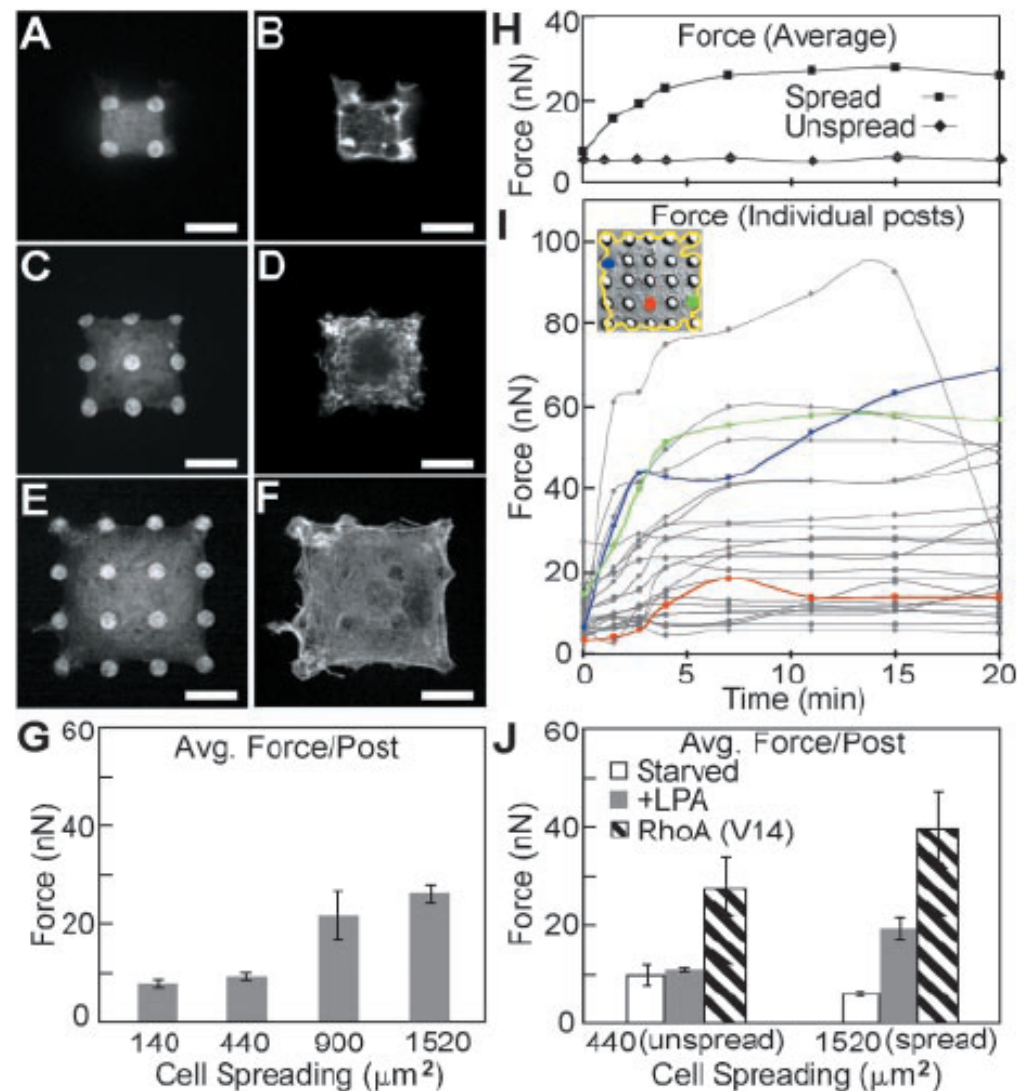


**Fig. 4.** Role of cell spreading in regulating contractile forces. (A–F) Confocal micrographs of smooth muscle cells attached onto different-sized sets of fibronectin-coated posts. Cells attached to  $2 \times 2$  (A and B),  $3 \times 3$  (C and D), or  $4 \times 4$  (E and F) sets of posts were costained for fibronectin (A, C, and E) and filamentous actin (B, D, and F). (Scale bars indicate  $10 \mu\text{m}$ .) (G) Plot of average force generated per post for cells spread to different degrees ( $140$ ,  $440$ ,  $900$ , or  $1,520 \mu\text{m}^2$ ) on arrays of posts ( $2 \times 2$ ,  $3 \times 3$ ,  $4 \times 4$ , or  $5 \times 5$ , respectively) for 20 h in standard culture media. (H) Plot of average force generated per post over time for a cell cultured on either a  $5 \times 5$  ("spread") or  $3 \times 3$  ("unspread") set of posts. Cells were serum-starved for 12 h on the posts and were exposed to LPA ( $10 \mu\text{g}/\text{ml}$ ) at time 0. (I) Plot of force exerted on each of the 25 posts over time for the spread cell plotted in H and shown as the *Inset*. The forces exerted on the posts colored in the *Inset* are indicated by line plots of the same color. (J) Plot of average force exerted per post for cells cultured on  $5 \times 5$  (spread) or  $3 \times 3$  (unspread) posts and were serum-starved, exposed to LPA for 12 min, or transfected with constitutively active RhoA. A total of 18 cells in G and 25 cells in J were analyzed across three independent experiments; error bars indicate standard error of the mean.

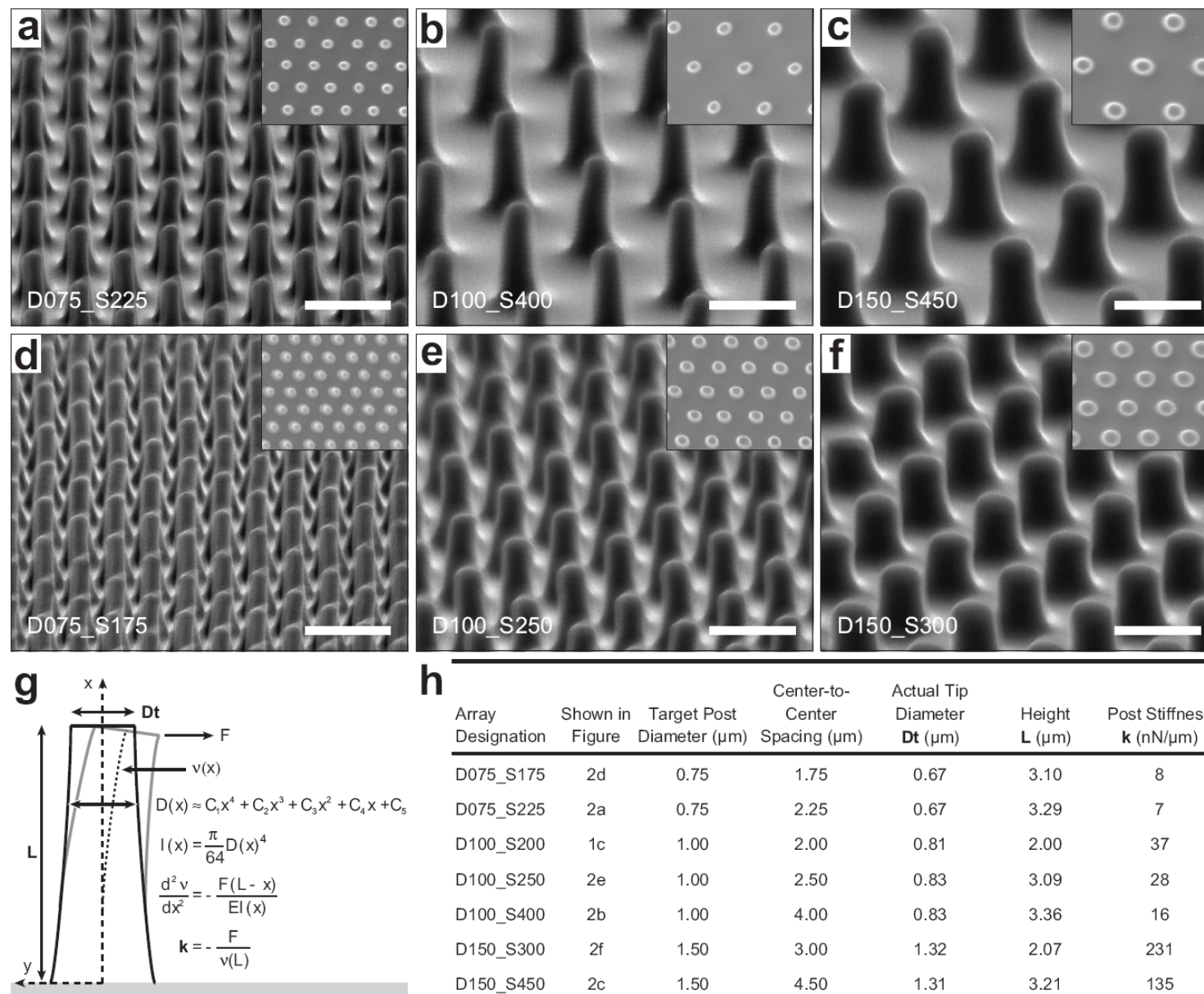


**Figure 2.** Characterization of elastomeric nanopost arrays. a–f) SEM images of PDMS nanopost arrays. Insets show top-down images of arrays. Scale bar is 3  $\mu\text{m}$ . g) Calculation of post stiffness for a post with varying cross-sectional diameter. h) Table summarizing post measurements and calculated stiffness for different post array geometries.

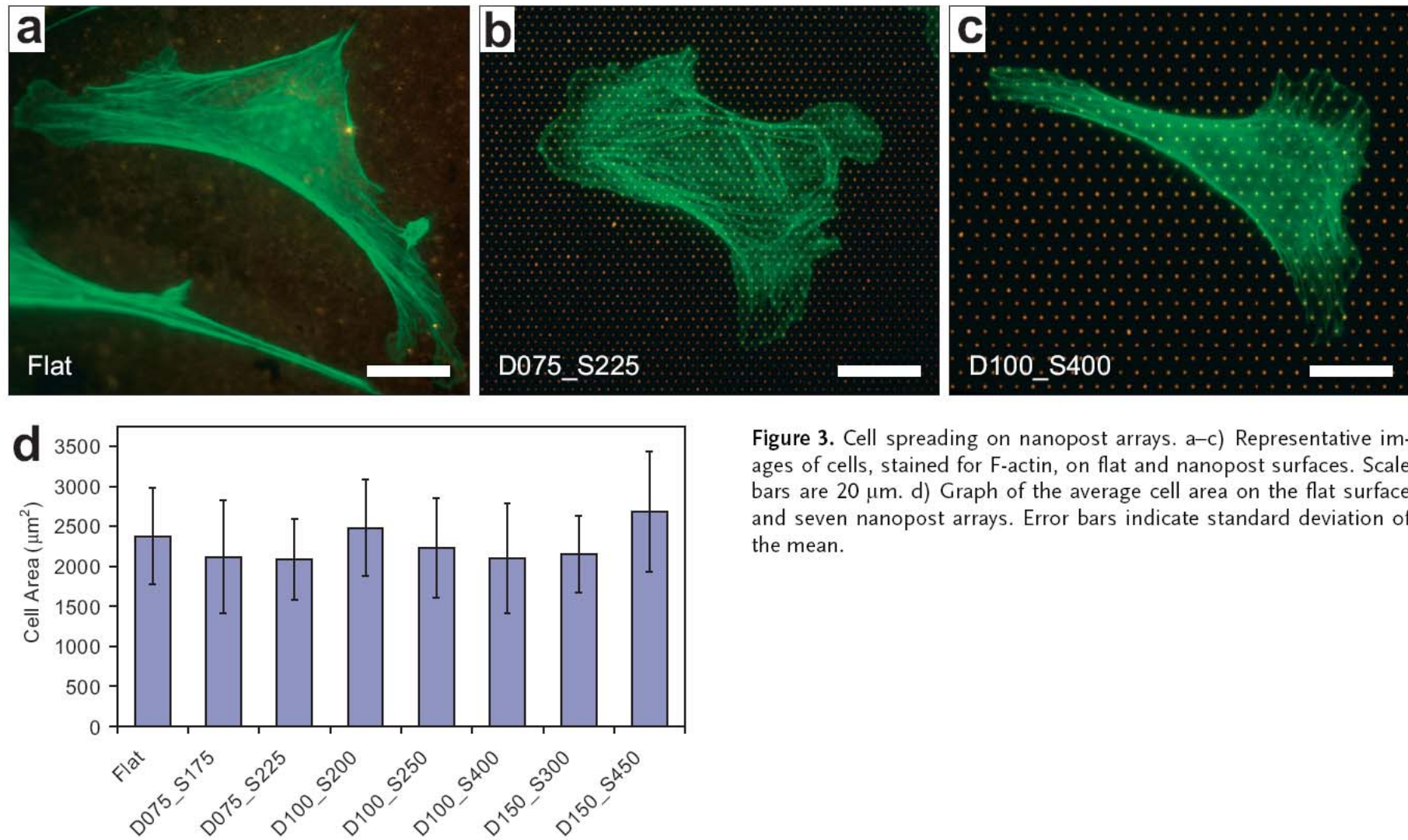


**Figure 3.** Cell spreading on nanopost arrays. a–c) Representative images of cells, stained for F-actin, on flat and nanopost surfaces. Scale bars are 20  $\mu\text{m}$ . d) Graph of the average cell area on the flat surface and seven nanopost arrays. Error bars indicate standard deviation of the mean.



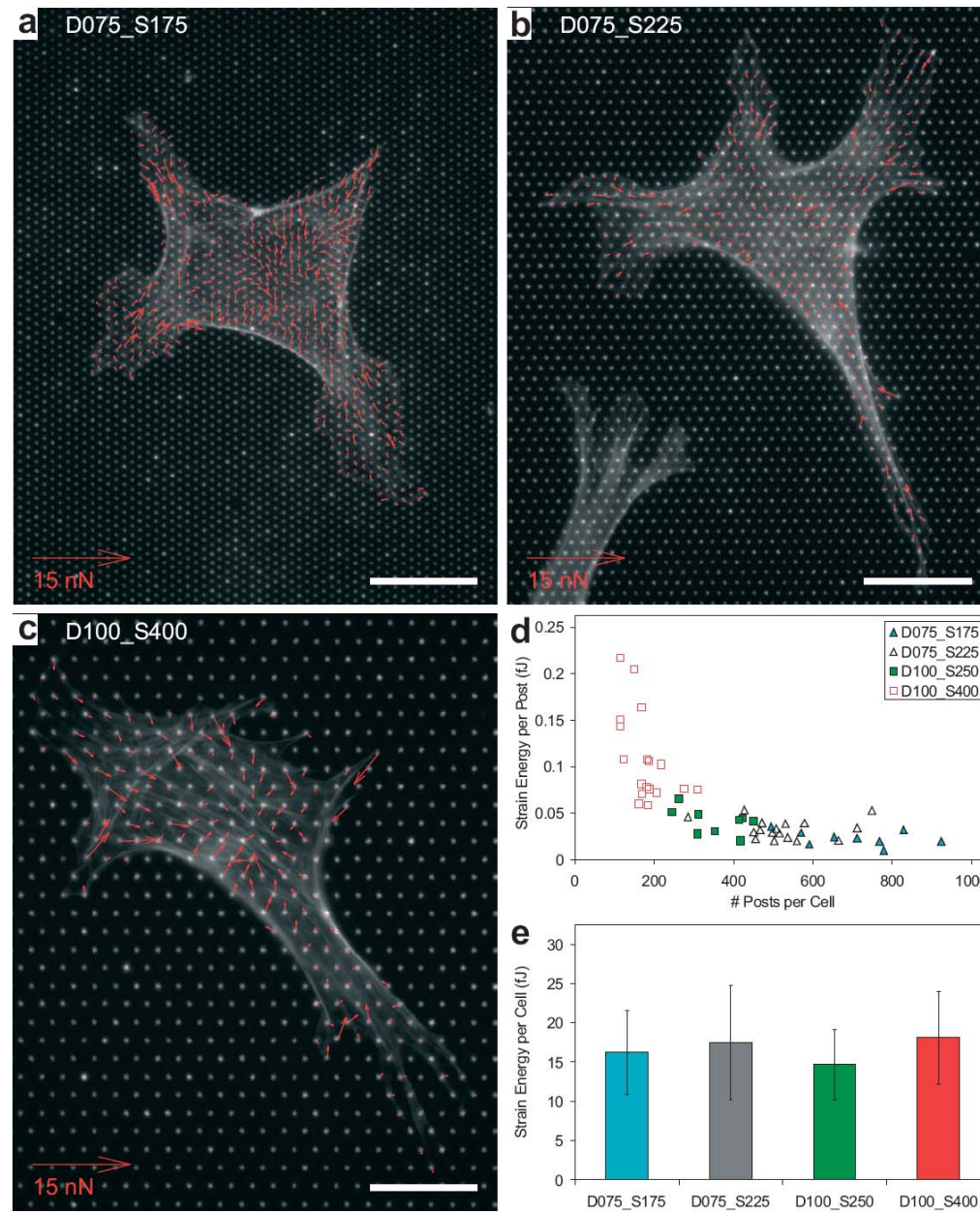


**figure 4.** Traction force measurement on nanopost arrays. a–c) Representative force vector plots overlayed on cells spread on different nanopost array geometries. White scale bars are 20  $\mu$ m. d) Graph of the strain energy per post versus the number of posts per cell. e) Graph of the average strain energy per cell on four nanopost arrays. Error bars indicate standard deviation of the mean.



Fig. 2. Molecular strategy for creating substrates that can be electrically switched to permit cell attachment. A monolayer presenting a mixture of hydroquinone groups and penta(ethylene glycol) groups (Left) is converted to a monolayer presenting the corresponding quinone groups (Center) by application of a potential to the underlying gold (500 mV versus Ag/AgCl). Both monolayers are inert to the attachment of cells. Addition of a conjugate of cyclopentadiene and the peptide Gly-Arg-Gly-Asp-Ser-NH<sub>2</sub> (RGD-Cp) to the monolayer presenting the quinone group results in the Diels-Alder-mediated immobilization of peptide (Right). 3T3 fibroblasts attach and spread on the resulting surface. Monolayers presenting the hydroquinone group are unaffected by the treatment with RGD-Cp and remain inert to cell attachment.



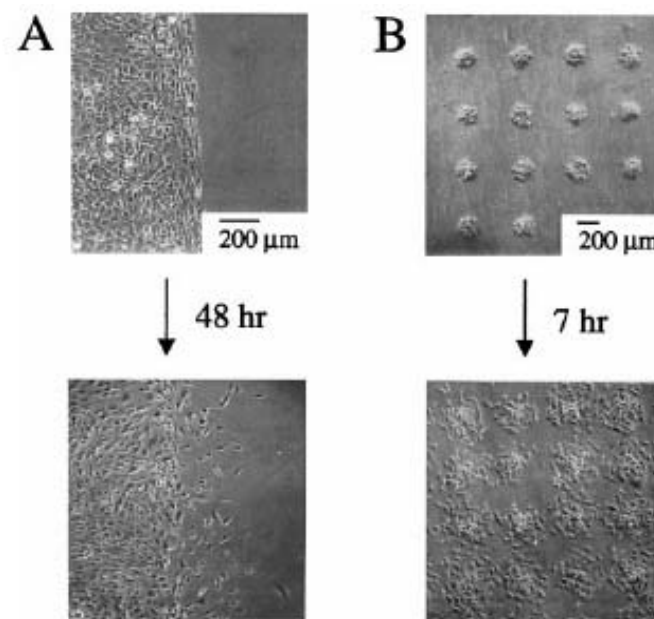
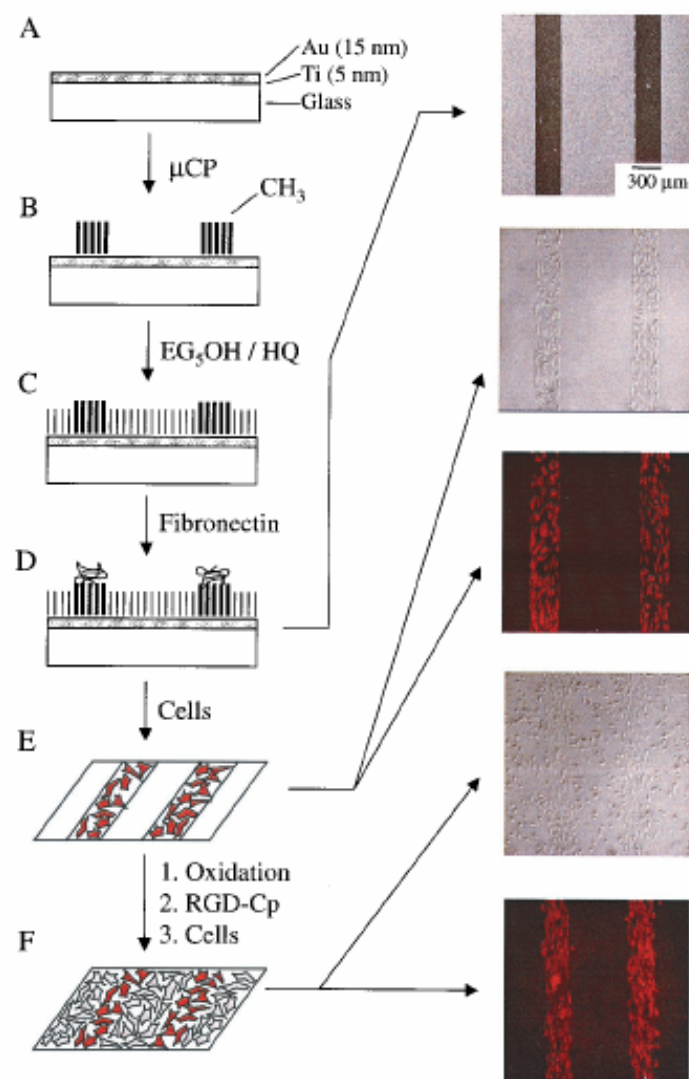


Fig. 4. The onset of migration into the second set of regions after electrochemical activation and peptide immobilization depends on the geometric features of the pattern. Cells patterned along a straight edge (A) showed little migration after 48 h, whereas cells patterned to 200-μm circles showed extensive migration after only 7 h (B). All micrographs were taken at  $\times 5$  magnification.

Fig. 3. Use of an electroactive substrate to pattern two cell populations into a coculture. (A) Substrates were prepared by evaporating titanium (5 nm) and then gold (15 nm) onto glass coverslips. (B) Microcontact printing was used to pattern hexadecanethiolate into lines that are 300 μm wide and separated by 800 μm. (C) A second monolayer was assembled on the remaining regions of gold by immersing the substrate into a solution of hydroquinone-terminated alkanethiol (HQ) and penta(ethylene glycol)-terminated alkanethiol (EG<sub>5</sub>OH). (D) The substrate then was immersed in a solution of fibronectin in PBS for 4 h. A scanning electron micrograph shows that protein adsorbed only to the methyl-terminated regions of the monolayer. (E) 3T3 fibroblasts attached only to the regions presenting fibronectin, and when cultured in serum-containing media, divided to fill these regions entirely. The surrounding inert monolayer strictly confined the cell to the rectangular regions. (F) Electrochemical oxidation of the monolayer in the presence of media containing RGD-Cp (2 nM) led to the immobilization of the peptide. Fluorescence microscopy shows that the two cell populations are patterned on the substrate. All micrographs were taken by  $\times 5$  magnification.

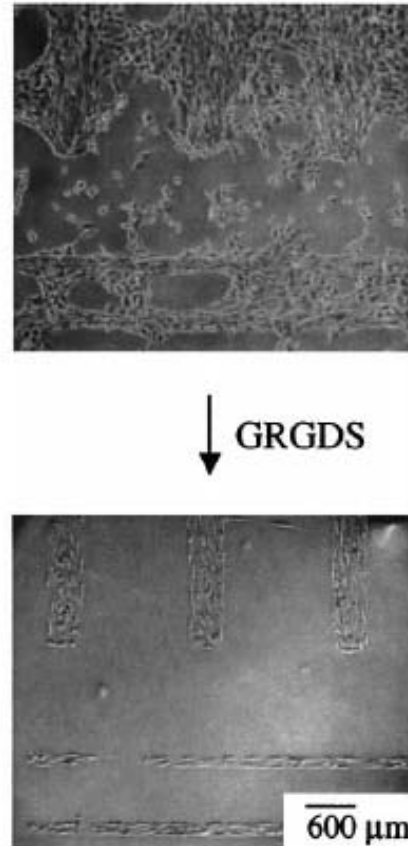
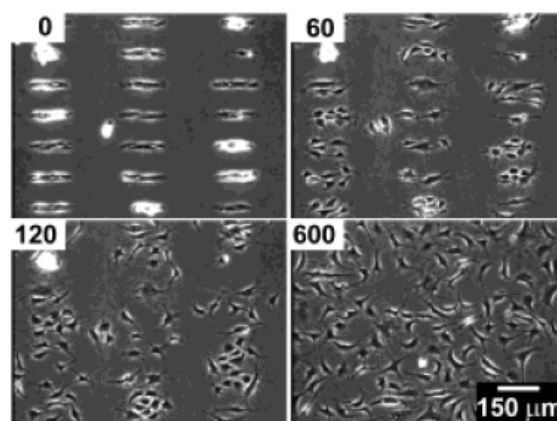


Fig. 5. Selective detachment of cells adhered to regions of the substrate presenting the RGD peptide among penta(ethylene glycol) groups. A patterned coculture was prepared as described in Fig. 3 *Left*. Addition of soluble peptide (GRGDS, 2 mM for 1 h) resulted in the detachment of cells only from the regions of the monolayer presenting peptide conjugates, indicating the specificity of the cell-substrate interaction. Micrographs were taken at  $\times 5$  magnification.

## Electrochemical Desorption of Self-Assembled Monolayers Noninvasively Releases Patterned Cells from Geometrical Confinements

procedure uses microcontact printing ( $\mu$ CP) and readily available thiols— $\text{HS}(\text{CH}_2)_{11}(\text{OCH}_2\text{OCH}_2)_3\text{OH}$  ( $\text{C}_{11}\text{EG}_3$ ) and  $\text{HS}(\text{CH}_2)_{17}\text{CH}_3$  ( $\text{C}_{18}$ )—to confine cells into patterns; these methods are well established.<sup>1,2</sup>  $\text{EG}_3$ -terminated SAMs resist the adsorption of



**Figure 1.** BCE cells were allowed to attach to a surface patterned with  $\text{C}_{11}\text{EG}_3$  and  $\text{C}_{18}$ . Application of a cathodic voltage pulse ( $-1.2$  V for 30 s in this case) released the cells from the microislands. The numbers indicate the time elapsed (in minutes) after the voltage pulse.

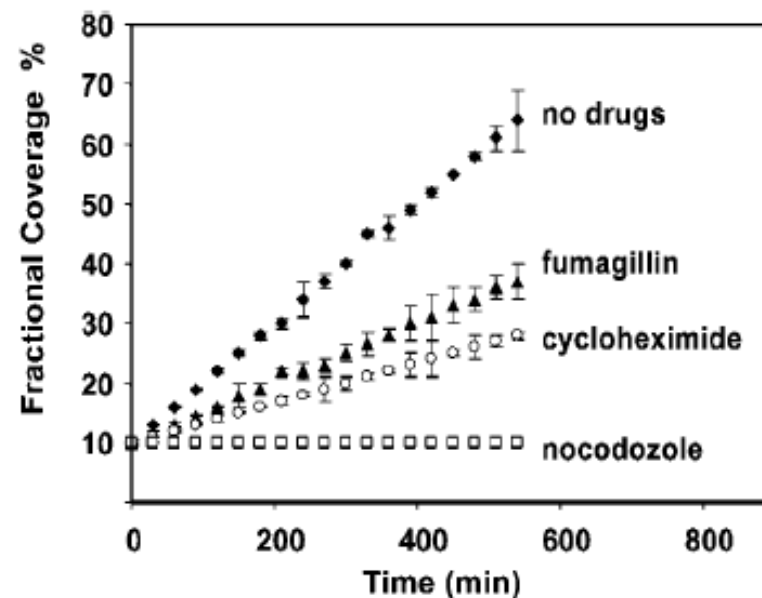


**Figure 3.** A cell-based screening assay. A summary of the influence of drugs on the motility of BCE cells after application of a voltage pulse ( $-1.2$  V, 30 s). Each datum represents the average of eight fields of cells. Error bars represent one standard deviation from the mean. See Supporting Information for the calculation of the Fractional Coverage.

# Electrically Driven Conformational Switching

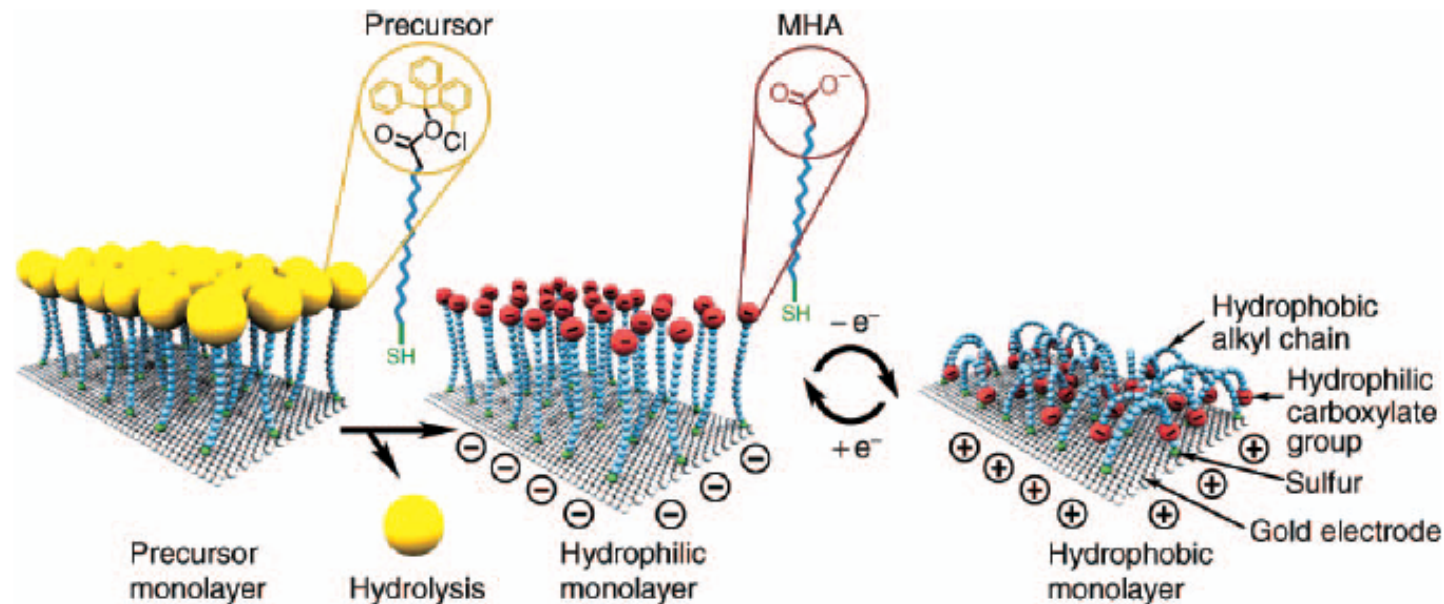


Figure 1. Idealized representation of the transition between straight (hydrophilic) and bent (hydrophobic) molecular conformations. Ions and solvent molecules are not shown. MHA is 16-mercapto-hexadecanoic acid. (Reproduced with permission from Reference 38.)



# Temperature Responsive Surface

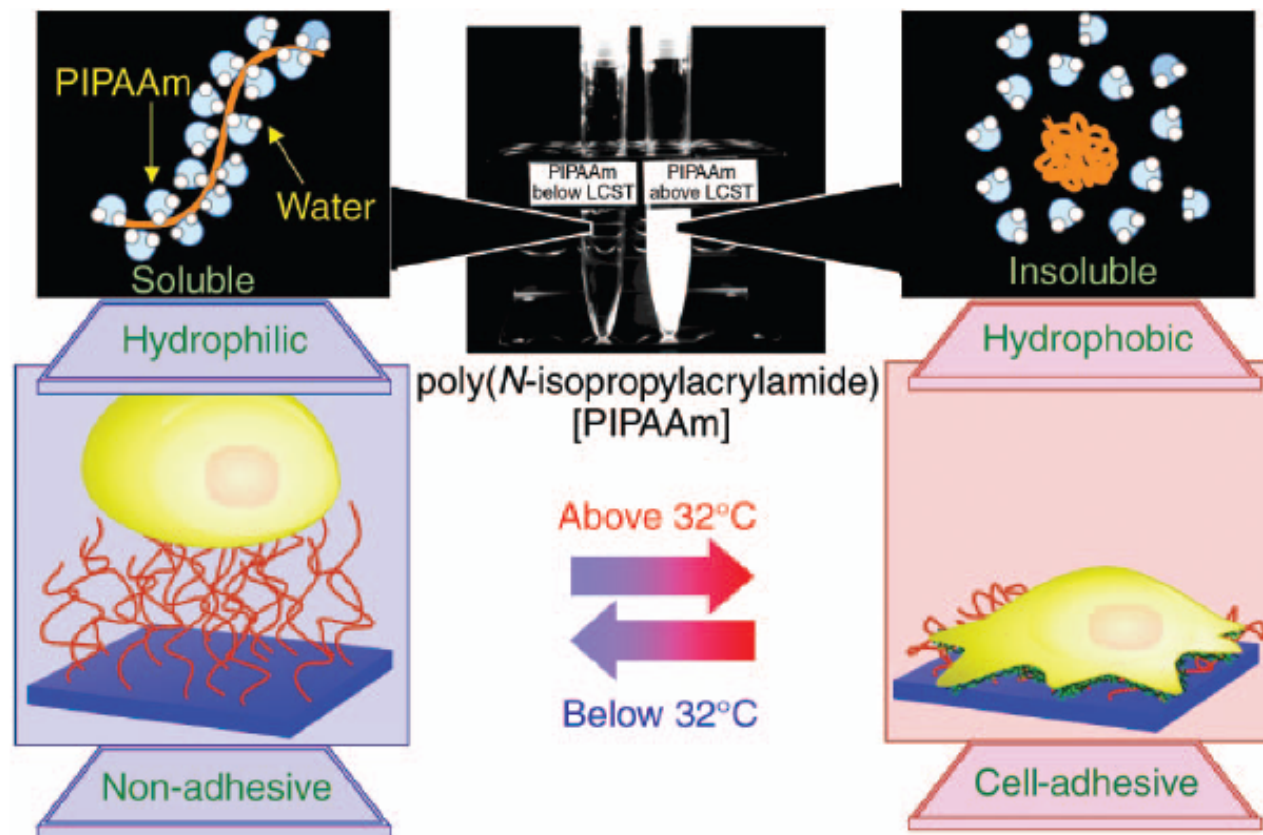
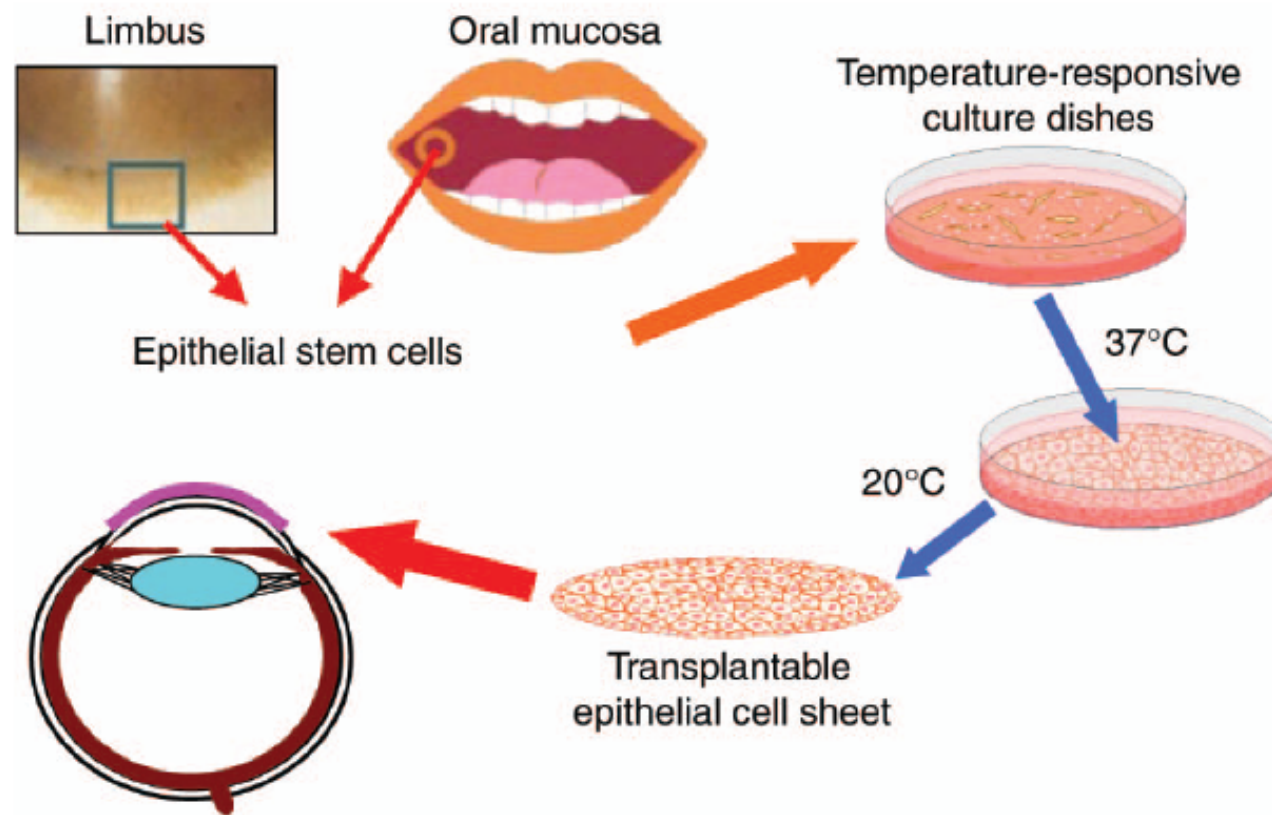
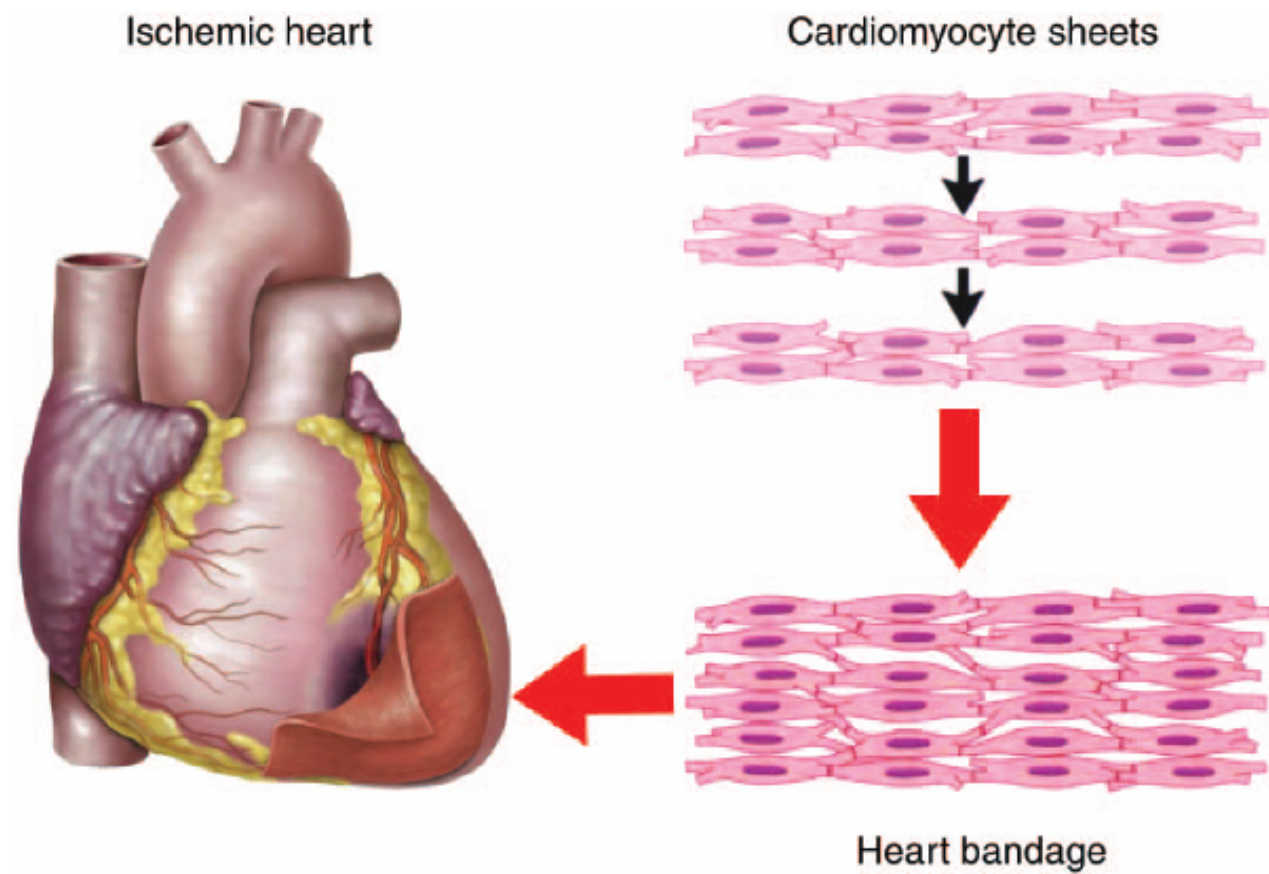


Figure 1. Temperature-responsive culture dishes. The temperature-responsive polymer poly(*N*-isopropylacrylamide) (PIPAAm) exhibits a transition from hydrophobic to hydrophilic across its lower-critical solution temperature (LCST) of 32°C. After electron-beam polymerization and grafting to normal tissue-culture polystyrene (TCPS) dishes, temperature-responsive culture surfaces can be produced. The non-invasive harvest of various cell types as intact sheets, along with deposited extracellular matrix, can be achieved by reducing the culture temperature.



*Figure 2. Corneal surface reconstruction. Small biopsies from the limbus (the border between the cornea and neighboring conjunctiva) or from oral mucosa provide for the isolation of epithelial stem cells. Cell sheets fabricated on temperature-responsive culture dishes can be harvested and transplanted directly to the ocular surface without the need for carrier substrates or sutures.*



*Figure 3. Myocardial cell-sheet engineering. Cardiomyocyte sheets harvested from temperature-responsive culture surfaces can be layered to form three-dimensional tissues that beat synchronously and simultaneously. We believe that layered cardiomyocyte sheets can act as a "heart bandage" for the recovery of ischemic cardiac tissue.*

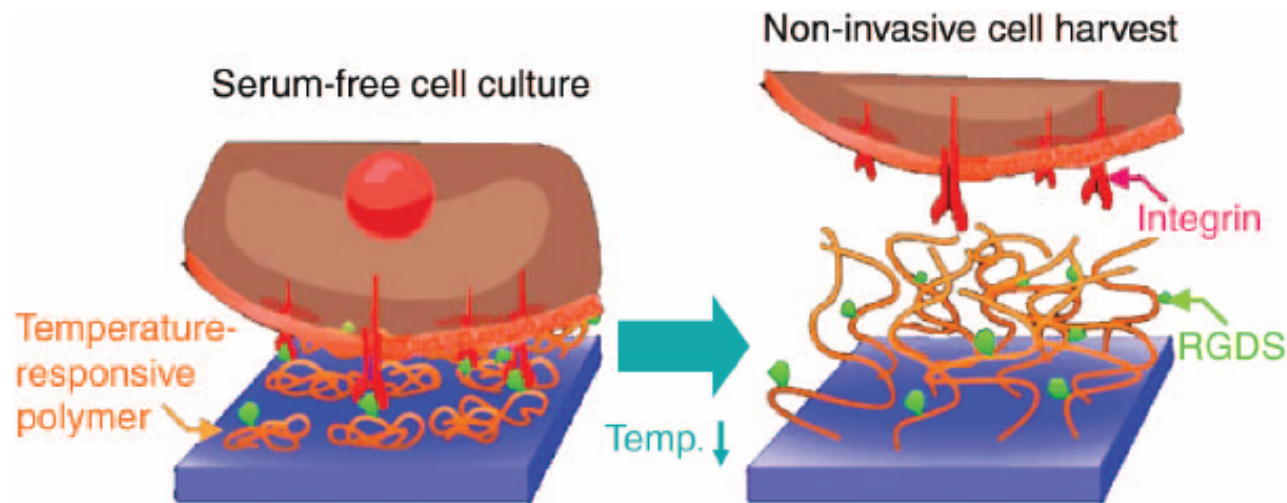


Figure 4. Immobilization of Arg-Gly-Asp-Ser (RGDS) peptides to temperature-responsive surfaces. Cells can be cultured in serum-free conditions by immobilizing the synthetic cell-adhesive RGDS peptide to temperature-responsive culture dishes. By decreasing the culture temperature, cells can still be non-invasively harvested, while the RGDS peptides remain attached to the temperature-responsive polymer surface.

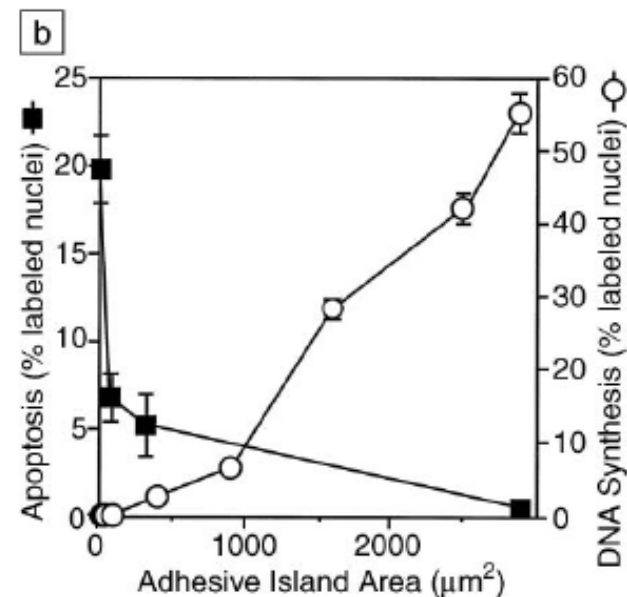
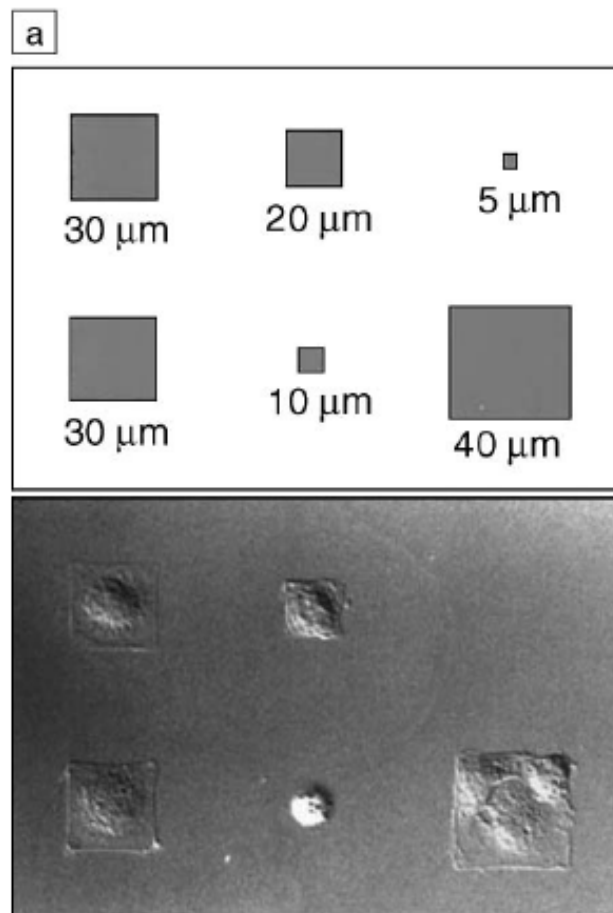


Figure 2. The influence of the footprint of a cell on its choice between growth and apoptosis. (a) (top) Schematic diagram showing the pattern: square islands of self-assembled monolayers (SAMs) to which proteins stick, surrounded by a different SAM to which proteins do not adsorb; (bottom) Nomarski microscopic image of the shapes of bovine adrenal capillary endothelial cells confined to the patterns. Scale labels indicate lengths of the sides of the squares. (b) Changes in cell shape as cells attach, spread, and flatten on an adhesive surface can regulate cell growth and death: apoptotic (cell death) index versus DNA synthesis (cell growth) index after 24 h, plotted as a function of the area of the spread cell.



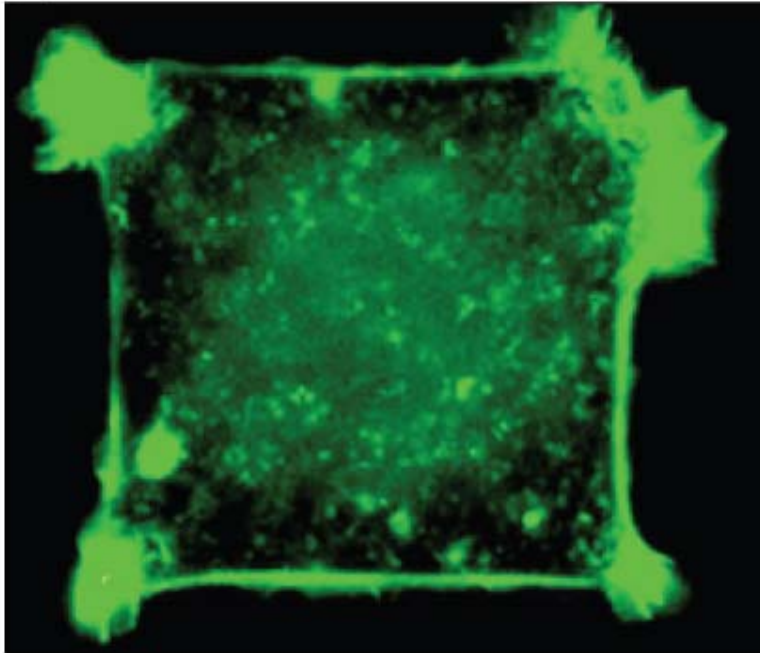
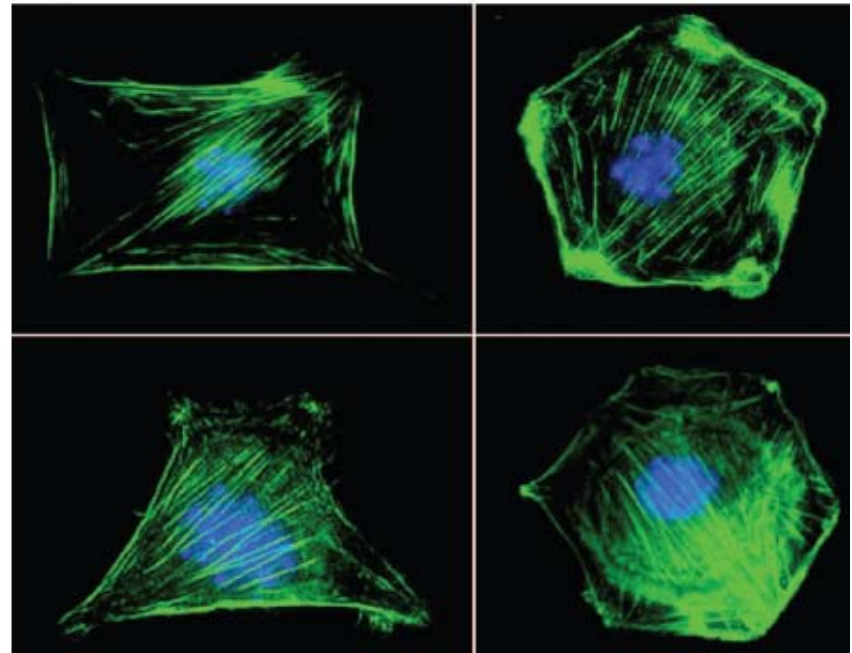
**a****b**

Figure 3. (a) A cell spread on a square  $30\ \mu\text{m} \times 30\ \mu\text{m}$  island; the cell was stimulated with platelet-derived growth factor (PDGF) and stained for F-actin with fluorophore-labeled phalloidin. (b) Cells confined to various shapes (all with areas of  $900\ \mu\text{m}^2$ ) were stimulated with PDGF and stained with phalloidin and 4'-6-diamidino-2-phenylindole to visualize F-actin (green) and nuclei (blue). Images obtained by fluorescence microscopy.

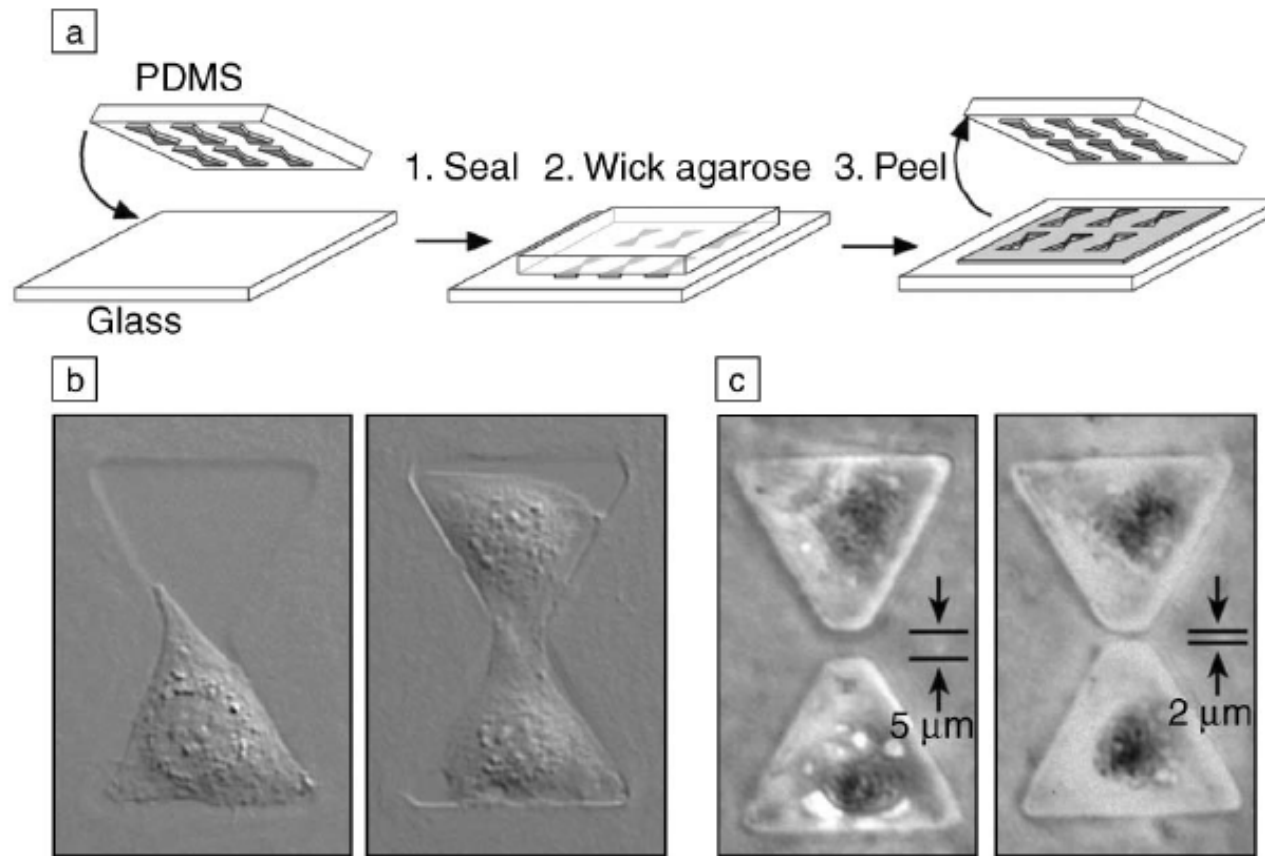
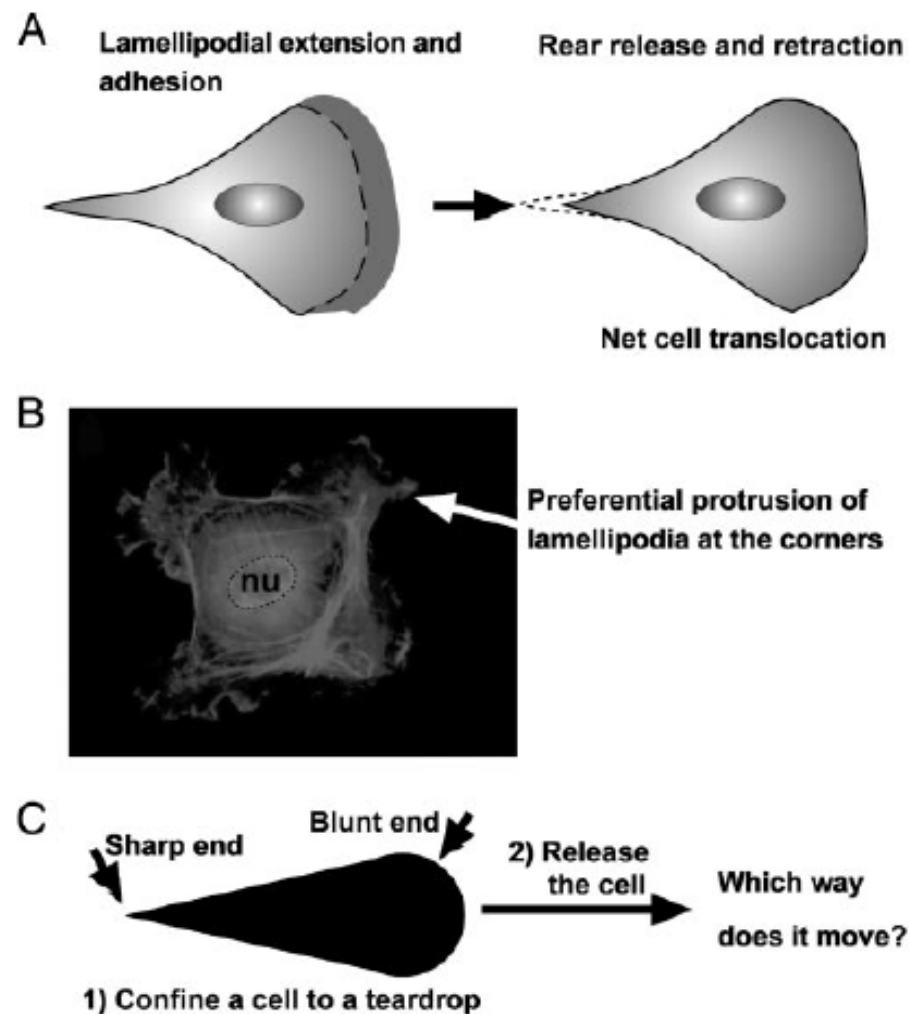
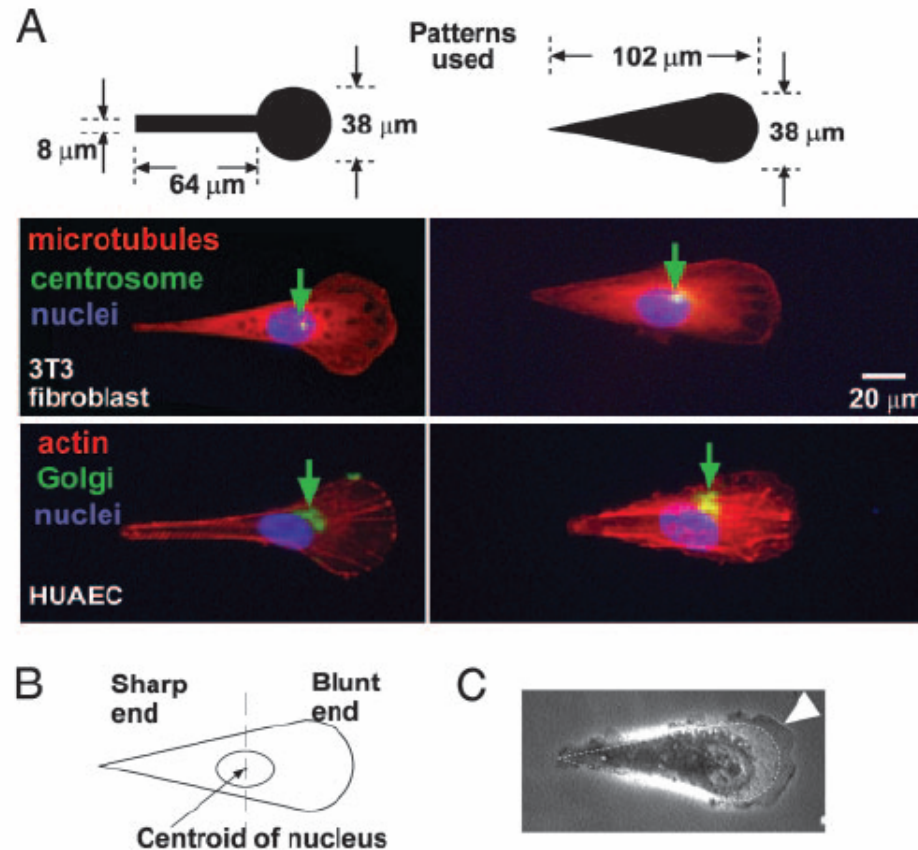


Figure 6. Method to induce cells to culture in pairs with control over the contact between them. (a) Agarose is wicked into channels formed by a poly(dimethylsiloxane) stamp sealed against a glass coverslip and allowed to gel before the stamp is peeled off. (b) When cells are seeded onto these substrates containing bowtie-shaped wells, cells attach and culture as either single cells or pairs. (c) The single cell-to-cell contact formed in these pairs can be blocked by fabricating substrates in which the agarose forms a thin wall, cutting the bowtie-shaped wells into separate, although closely spaced, wells.

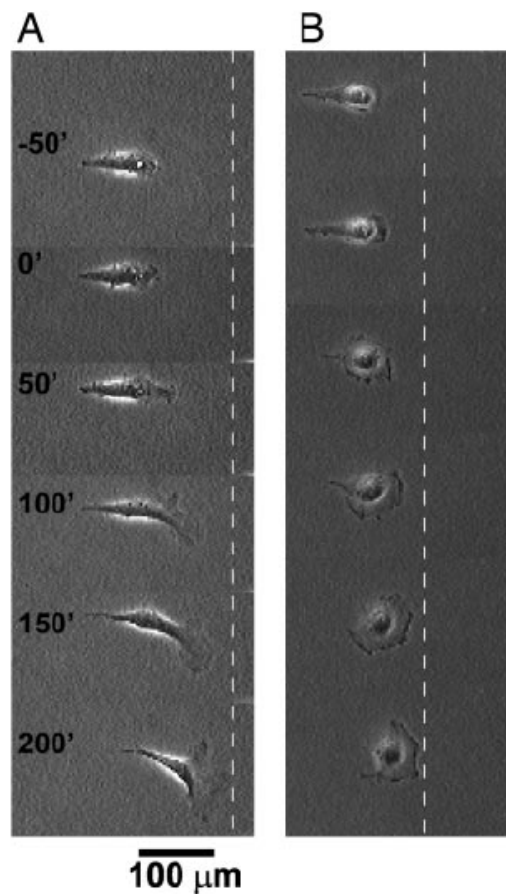


**Fig. 1.** A problem on cell motility. (A) A cartoon illustration of the migration of a typical mammalian cell on a flat surface. This teardrop shape is found in many types of cells. (B) Cells confined to squares preferentially extend their lamellipodia from the corners. nu, nucleus. (C) If a cell is confined to a shape of teardrop, will the cell preferentially extend its lamellipodia from the sharp end or from the blunt end? If released from confinement, in which direction will it likely move?

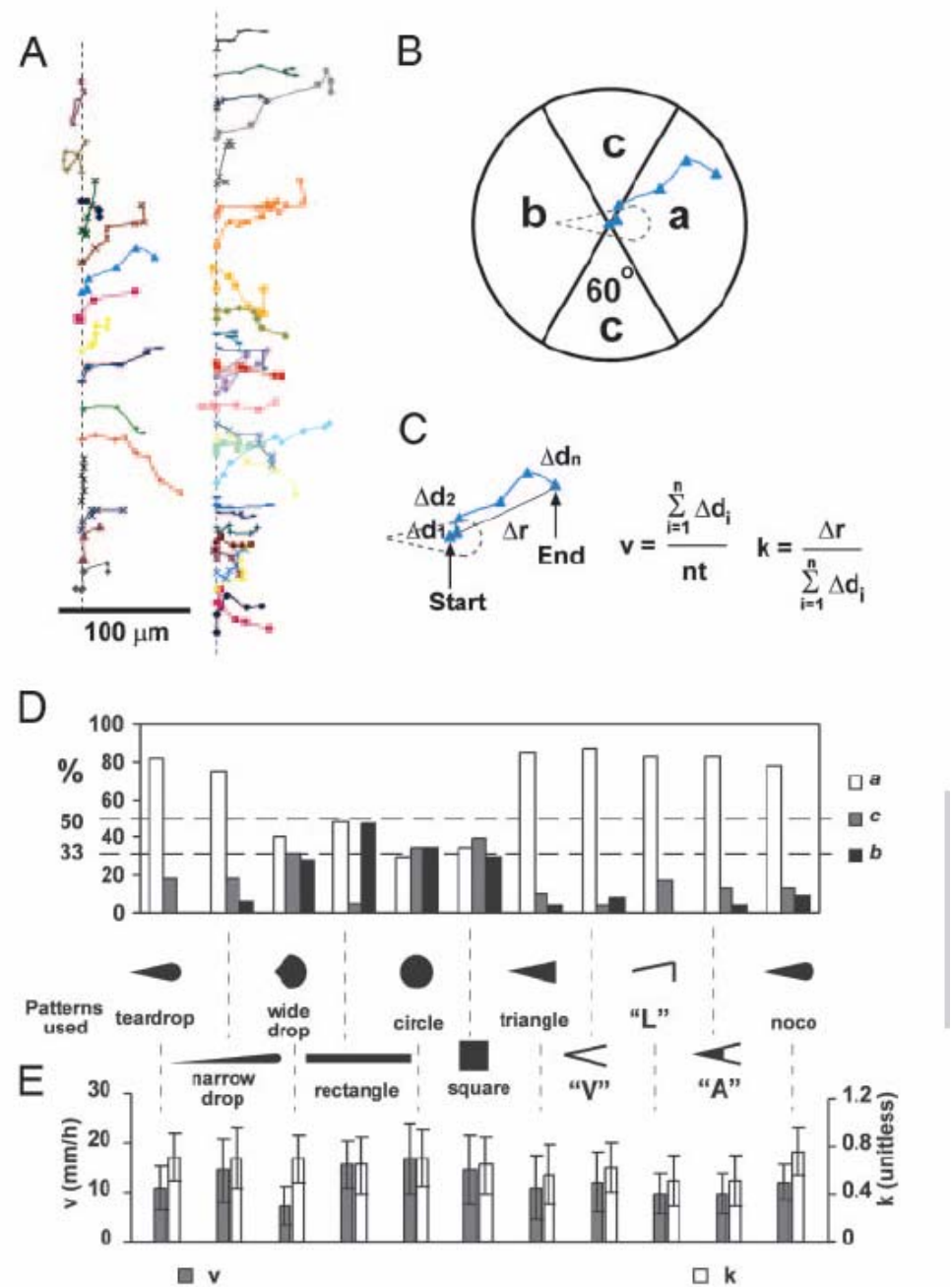




**Fig. 2.** Asymmetric patterns polarize immobilized cells. (A) The Golgi and the centrosome are located closer to the half of a cell with the blunt end. We used phalloidin, antigolgin, DAPI, antitubulin, and antipericentrin to identify actin (red), the Golgi (green), the nucleus (blue), microtubules (red), and the centrosome (green), respectively. The green arrows indicate the location of centrosomes in 3T3 cells and Golgi in human umbilical artery endothelial cells (HUAEC). (B) We divided the cell into a half with the sharp end and a half with the blunt end by a vertical line drawn at the centroid of the nucleus; >80% ( $n = 30$ ) of the centrosomes and Golgi were localized in the region of the wide end. (C) The lamellipodia of immobilized 3T3 cells tended to extend more from the blunt end as well (arrowhead). The dotted line indicates the edges of the adhesive pattern.



**Fig. 3.** Time-lapse images (in minutes) show the motility of an initially polarized 3T3 fibroblast after its constraint is released. (A) We applied the voltage pulse at time  $t = 0$ . The dotted line serves as a reference for the location of the cell. (B) Another type of cell, COS-7, shows similar behavior.



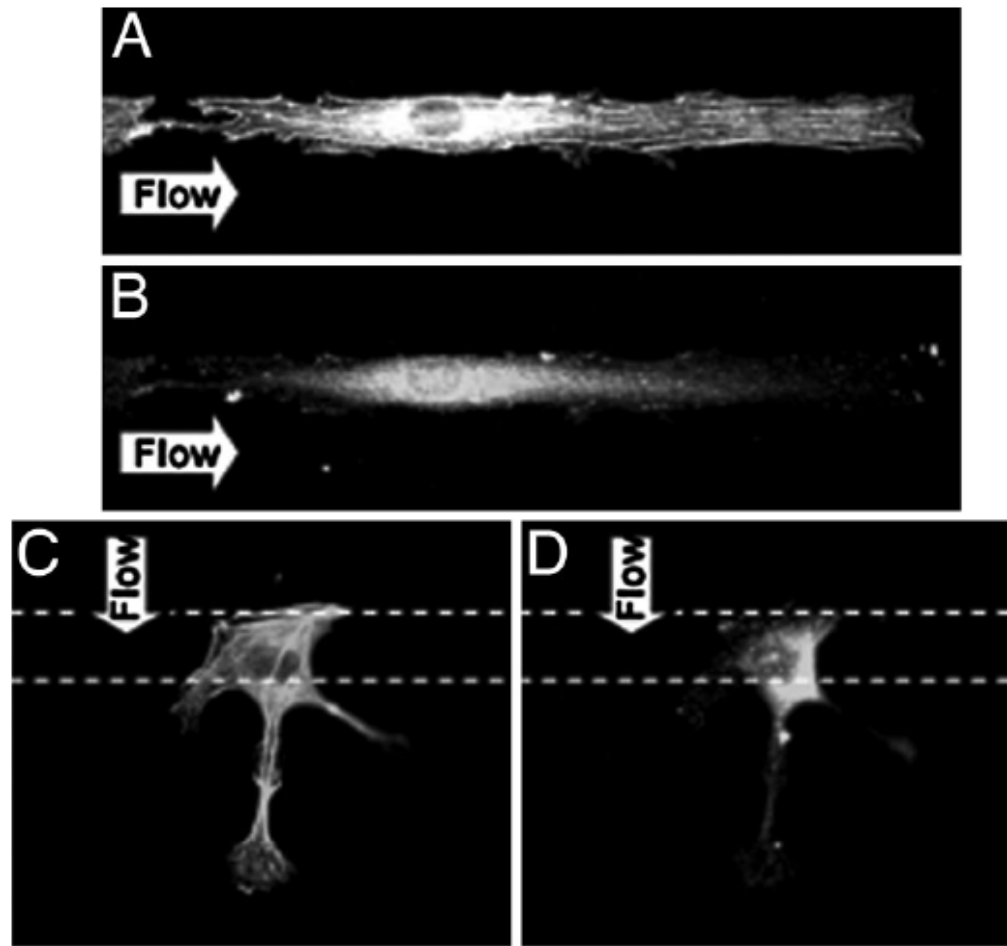


**Fig. 3.** HUVEC remodeling on MP strips under flow in different directions. Parallel flow increased the stress fiber formation for cytoskeleton remodeling (A) and *p*-FAK for the anchoring points at the ends of stress fibers (B). In contrast, the perpendicular flow increased the stress fibers (C) and *p*-FAK (D) in the ineffective NP surface and therefore mitigated the effectiveness of these inductions.

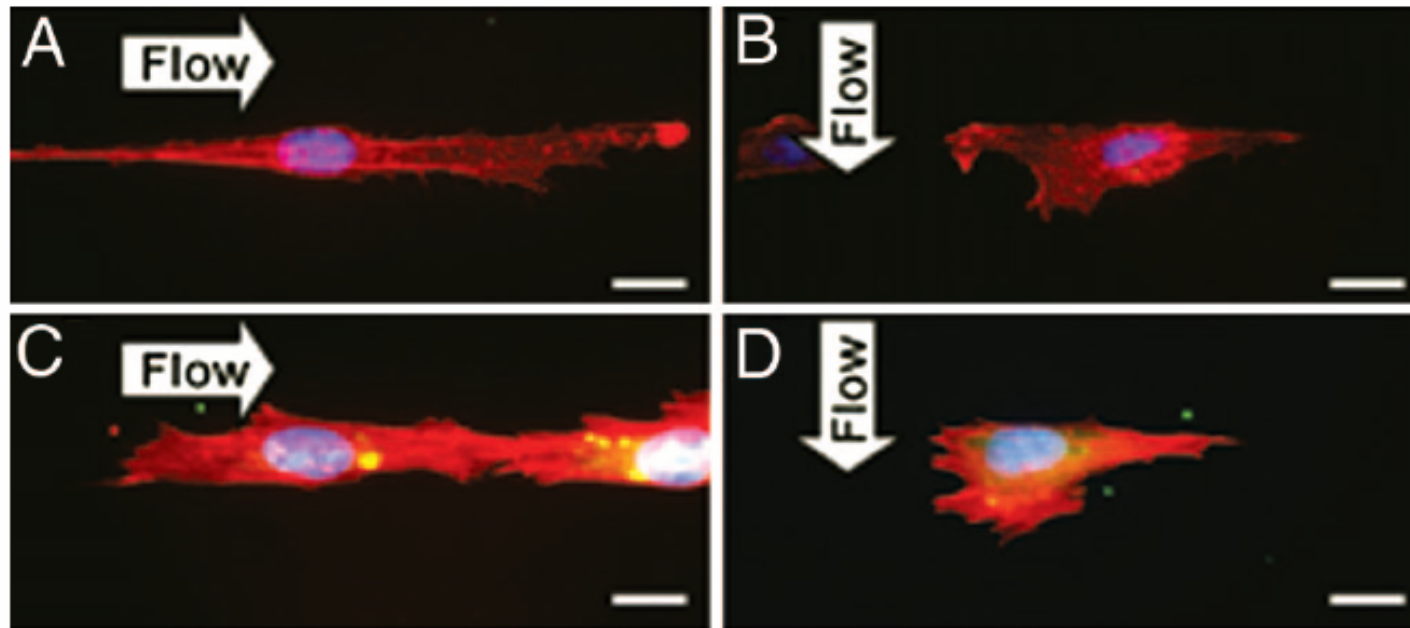


**Fig. 6.** Rho activities attenuate constraint-induced apoptosis and enable cytoskeleton remodeling independent of flow direction. Shown are images for HUVECs transfected with C3 exoenzyme (*A* and *B*) or RhoV14 (*C* and *D*) on 15- $\mu\text{m}$  strips, and then subjected to parallel (*A* and *C*) or perpendicular (*B* and *D*) flow. The inhibition of Rho activities abolished the antiapoptotic effect of parallel flow and blocked the formation of stress fibers (*A*); RhoV14 attenuated constraint-induced cell apoptosis and restored the actin cytoskeleton under both flow directions (*C* and *D*). Cells were immunostained in the same method as Fig. 4. (Scale bar: 15  $\mu\text{m}$ .)